**Ministry of Higher Education and Scientific Research**

**University of Babylon / College of Science**

**Department of Physics**

# Preparation and characterizations of PMMA - $P_3HT$ films for solar cell applications

**A thesis**

**Submitted to the Council of College of Science, University of Babylon in Partial Fulfillment of the Requirements of the Degree of Doctor of Philosophy of Science in Physics.**

**By**

## Lamis Faaz Nassir Muthanna

**B.Sc. in Physics / 2002**

**M.Sc. in Physics / 2016**

**Supervised by**

**Prof. Dr. Mohammed Hadi Shinen**

**2022 A.D.** **1444 A.H.**

بِسْمِ اللَّهِ الرَّحْمَٰنِ الرَّحِيمِ

﴿ نَرْفَعُ دَرَجَٰتٍ مَّن نَّشَآءُ ۗ وَفَوْقَ كُلِّ ذِى عِلْمٍ عَلِيمٌ ﴾

صدق الله العليّ العظيم

سُورَة يُوسف (٧٦)

# DEDICATION

***I dedicate this effort to***

***Dears***

***Father, God have mercy on him,***

***My mother,***

***My brothers, my sisters,***

***my son (Ali),***

***and my daughter(Maryam)***

***with all my gratitude***

*Lamis*

# ACKNOWLEDGMENTS

In the name of Allah (the Almighty) Great is the most gracious and the most merciful. I praise Allah (the Almighty), the lord of earth and heaven for completing my thesis.

Many thanks to the Deanery of the College of Science in Babylon University and the Department of Physics for offering me the opportunity to complete my study.

I would like to extend my thanks and gratitude to my supervisor, **Prof. Dr. Mohammed Hadi Shinen** for having suggested this topic for me and for his extinguished efforts, sound advice and directions that have helped in smoothing out every difficulty encountered during my work.

Last but not least I am very grateful to my family for their consistent encouragement support during my study, them have guided and changed my life with brighter and prosperous future. Without them, I will not be what I am today. I love them all.

*Lamis*

# Summary

In this study, poly(methyl methacrylate) doped with Poly(3-hexylthiophene) with ratios ( 0.02 , 0.04 and 0.06 ) %, and thin films were prepared by spin coating technique on glass substrates at room temperature.

The polymers (PMMA, $P_3HT$) powder of were analyzed by (FT-IR) to determine the active groups of the chemical bonds. The results of the analysis showed that the polymer is PMMA, $P_3HT$ and the results were compared and identical to the original material.

The X- Ray diffraction (XRD) results showed that the prepared PMMA films is amorphous in nature, and PMMA: $P_3HT$ films studied investigated films are polycrystalline in nature the and the doping did not effect on the synthetic properties of PMMA.

The surface morphology of thin films was examined using the atomic force microscope technique (AFM). The results showed that the prepared films were homogeneous. The average roughness, root mean square (RMS) values and the average grain diameter increased with the increasing of $P_3HT$ concentration.

The optical properties of the prepared films were investigated by obtaining the absorbance spectrums in the UV- VIS regions as a function of wavelength from(200 - 600) nm. The values of absorbance , refractive index and absorption coefficient for the of un-doped and doped films increasing with increasing of doping ratio. The energy gap decreasing with the increasing of the doped ratio, makes the material suitable for using application of solar cells .

Electrical properties including D.C conductivity measurement of thin films were studied .The results showed that the electrical conductivity

increased with the increasing dopant rate and that the material has one activation energy decreased with the increasing of doping ratio.

PMMA:$P_3$HT/Si heterojunctions have been prepared at different concentrations(0.02, 0.04 and 0.06) %, (J-V) characteristics show that the $P_3$HT- doping increases the energy conversion efficiency by retarding the electron-hole recombination and the improved device performance is caused by the high short-circuit current (Isc) and open circuit voltage (Voc) and found that the highest efficiency (η) at doping ratio 0.06% is 6.1% .

The efficiency of the solar cell was also studied with the change of time factor to knowing the efficiency of the prepared solar cell . Where the efficiency was measured for two months (November and March) in 2021, 2022 for ten days, and it was found that a change in the time factor does not effect on the efficiency of the cell.

# Contents

# List of Symbols

| Symbol | Physical meaning |
|---|---|
| A | Absorptance |
| $I_o$ | Incident Intensity of Light |
| $I_A$ | Absorbed Light Intensity |
| T | Transmittance |
| $I_T$ | Intensity of the Transmitting Rays |
| $I_o$ | Intensity of the Incident Rays |
| R | Reflectance |
| $\alpha$ | Absorption Coefficient |
| I | Intensity of Light |
| t | Thickness of Thin Film |
| $\upsilon$ | Frequency |
| h | Plank Constant |

| *Symbol* | *Physical meaning* |
|---|---|
| n | The Real Part of Refractive Index |
| c | Velocity of Light in Space |
| v | Velocity of Light in Thin Film |
| n* | Complex Refractive Index |
| $\lambda$ | The Wavelength of Incident Photon Rays |
| $\varepsilon_1$ | The Real Part of the Complex Dielectric Constant |
| $\varepsilon_2$ | The Imaginary Part of the Complex Dielectric Constant |
| $\Delta K$ | Wave Vector |
| $E_g^{opt.}$ | Energy Gap Between Direct Transition |
| J | The Current Density |
| $E_e$ | The Electric Field |
| B | constant depended on type of material |
| $\sigma$ | Electrical Conductivity |
| $\mu$ | The Mobility of the Carriers |
| $\tau$ | The Carrier's Lifetime |
| $n_e$ | The Carrier's Concentration |
| m* | The Effective Mass of the Carrier |
| q | The Electron Charge |
| $V_d$ | The Drift Velocity |
| $E_a$ | Electric Activation Energy |
| T | Absolute Temperature |
| $k_B$ | Boltzmann Constant |
| $\sigma_o$ | The Minimum Electrical Conductivity at 0K |
| $\sigma_{D.C}$ | The Conductivity of the Thin Film |
| $I_{sc}$ | Short Circuit Current |
| $I_s$ | The Saturation Current |

| *Symbol* | *Physical meaning* |
|---|---|
| $R_{sh}$ | The Shunt Resistance |
| $V_{oc}$ | Open Circuit Voltage |
| $I_m$ | The Maximum Value of the Current |
| $V_m$ | The Maximum Value of the Voltage |
| $\eta$ | The Efficiency |
| $P_m$ | The Maximum Power |
| $P_{in}$ | The Incident Power |

# *List of Abbreviations*

| *Symbol* | *Physical meaning* |
|---|---|
| AMMA | Poly (methyl methacrylate) |
| $P_3HT$ | Poly (3-hexylthiophene) |
| AFM | Atomic Force Microscope |
| C.B | Conduction Band |
| FT-IR | Fourier Transforms Infrared Spectrometer |
| F.F | Filling Factor |
| PVD | Physical Vapor Deposition |
| RMS | Root Mean Square |
| $TiO_2$ | Titanium dioxide |
| V.B | Valence Band |
| VIS | Visible Spectrum |
| UV | Ultra Violet Spectrum |
| XRD | X-Ray Diffraction |
| D.C | Electrical Conductivity |
| HJ | Heterojunction |

# List of Figures

## Chapter Four

# List of Tables

# CHAPTER ONE

# Introduction and Literature Review

## 1.1 Introduction

A thin film is a layer of material ranging from fractions of a nanometer (monolayer) to several micrometers in thickness [1]. The controlled synthesis of materials as thin films (a process referred to as deposition) is a fundamental step in many applications [2]. Thin film technology has made a significant contribution to the study of semiconductors and the determination of a number of physical and chemical properties it has an aim to determine its use in various applications [3]. Advances in thin film deposition techniques during the 20th century have enabled a wide range of technological breakthroughs in areas such as magnetic recording media, electronic semiconductor devices, Integrated passive devices, LEDs, optical coatings (such as antireflective coatings), hard coatings on cutting tools, and for both energy generation (e.g. thin-film solar cells) and storage (thin-film batteries) [4].

The properties of the material in the form of thin films have attracted the attention of physicists since the second half of the seventeenth century, where many theoretical researches was conducted in this area, and then developed the study of the practical side at the beginning of the nineteenth century when the semiconductor entered into practice[5]. Due to the thickness of these films, they are deposited on substrates of different materials depending on the nature of the use and study, such as glass, quartz, silicon, aluminum, etc [6]. Thin films are generally used to improve the surface properties of solids. Transmittance, reflection, absorption, hardness, abrasion resistance, corrosion, permeation and electrical behavior are only some of the properties of a bulk material surface that can be improved by using a thin film. Thin films are very important because they differentiate the properties and reactions of the material surface from its bulk [7]. Overall, thin films are used to enhance the properties of bulk materials by depositing a layer with the desired physical and

chemical characteristics to improve their functionality. Thin films have a wide range of properties that can be used in a variety of applications. Types of thin films can be categorized as follows [7]:

- **Optical thin films:** Used to create reflective coatings, anti-reflective coatings, solar cells, Monitors, waveguides and optical detector arrays.
- **Electrical or electronic thin films:** Used to make insulators, conductors, semiconductor devices, integrated circuits and piezoelectric devices.
- **Magnetic thin films:** Usually used to make memory disks.
- **Chemical thin films:** They are used to create resistance to alloying, diffusion, corrosion and oxidation, as well as to make gas and liquid sensors.
- **Mechanical thin films:** Tribological coatings to protect against abrasion, increase hardness and adhesion and use of micro-mechanical properties.
- **Thermal thin films:** They are used to create insulation layers and heat sinks.

It is formed of large organic molecules linked together by chains of different lengths and built these molecules from small units called monomers joined by the covalent bonds [٨]. In the recent years polymers have gained considerable famous due to extensive applications in various fields of life as, medical, engineering, and industrial fields. The reason for this is that polymer has unique properties. Ensure ease of treatment with polymer industrially, it also possesses a wide range of optical, electrical, and mechanical properties which can be controlled by performing some physical or chemical

process [9]. There are several methods for preparation of polymer films [10]:

- Casting Method.
- Spin Coating Method.
- Dip Coating Method.
- Sol-Gel Method.
- Langmuir- Blodgett (LB) Method.

We use in this study Spin Coating method, to prepare the films.

## 1.2 Properties of PMMA

Poly (methyl methacrylate) (PMMA), also known as acrylic or acrylic glass, is a transparent and rigid thermoplastic material widely used as a shatterproof replacement for glass. PMMA has many technical advantages over other transparent polymer (PC, polystyrene etc.), Its most important features them include [10,11]:

- High resistance to UV light and weathering,
- Excellent light transmission
- Unlimited coloring options
- Good tensile strength and hardness
- High transparency in the visible wavelength range
- High surface resistivity
- Good insulation properties, and thermal stability

PMMA is an important polymer for mechanical and optical applications due to high rigidity [11]. It is produced from monomer methyl methacrylate. PMMA polymer exhibits glass-like qualities– clarity, brilliance, transparency, translucence – at half the weight with up to 10 times the impact resistance. It is more robust and has less risk of damage [12]. PMMA is a high purity and

easy-to-clean material and hence used to fabricate incubators, drug testing devices, storage cabinets in hospitals and research labs. Also, due to its high bio-compatibility, PMMA is also applied as dental cavity fillings and bone cement [13]. Table (1.1) shows some properties of poly (methyl methacrylate) and Figure (1) shows the chemical composition of this PMMA [14].

**Table (1.1) Properties of poly (methyl methacrylate) PMMA [14].**

| **Molecular formula** | **$(C_5O_2H_8)_n$** |
|---|---|
| Molecular weight | 100.1 g/mol |
| Color | White crystalline powder |
| Density | 1.18 g/ $cm^3$ |
| Melting point | 160 °C (320 °F; 433 K) |
| boiling point | 200 °C |
| Energy gap | (2.6 -2.9) eV |
| Solubility | Chloroform, chlorobenzene |

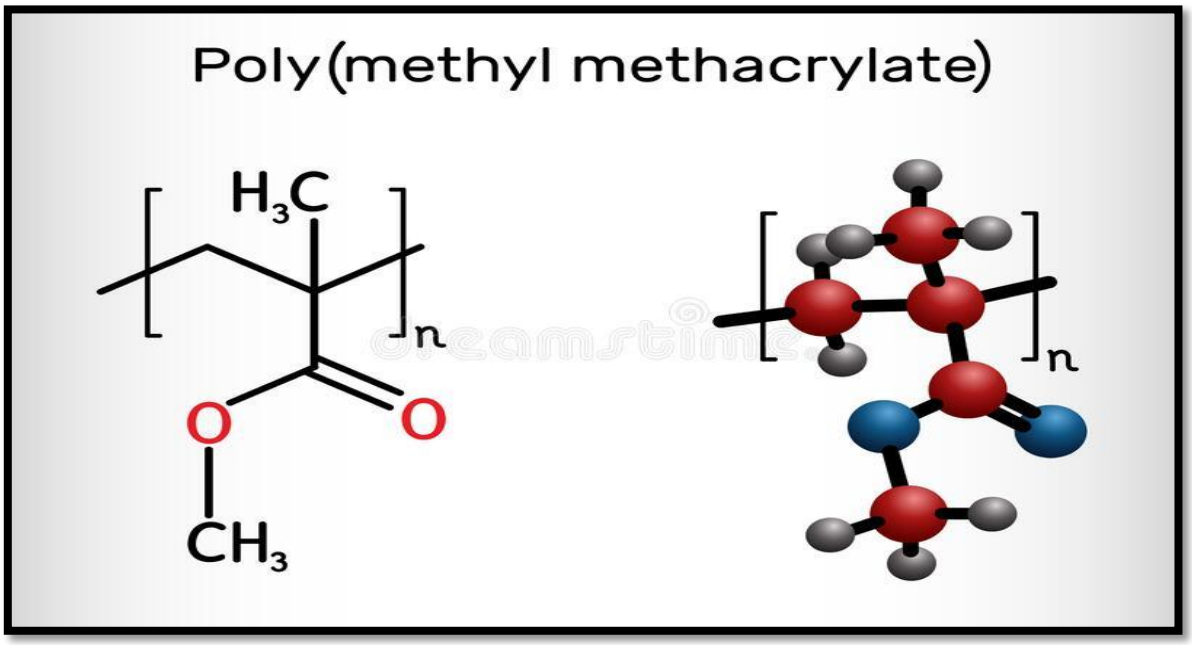


**Figure (1.1): The chemical structure of poly (methyl methacrylate)[12].**

## 1.3 Properties of $P_3HT$

$P_3HT$ is a Semiconducting polymer that can be used in the fabrication of a variety of devices which include solar cells, field effect transistors (FETs), light emitting diodes (LEDs) and photovoltaic cells. Semiconducting polymers have attracted a great deal of attention in the last decades because of their remarkable optoelectronic properties combined with low-cost solution processability. It could be said that poly (3-hexylthiophene) $P_3HT$ is one of the well-known π-conjugated polymers [15].Where attracted significant attention due to, excellent electronic properties; relatively high charge mobility ($10^{-4}$-$10^{-1}$) $cm^2V^{-1}s^{-1}$, excellent environmental stability [16]. Most of the fascinating properties of semiconducting polymers such as $P_3HT$ derive from their strong tendency to crystallize, because strong intermolecular interactions in well-ordered crystalline domains offer efficient charge transport pathways through the polymer layer on a macroscopic scale [17]. The rigidity and planar conformation of the conjugated backbone of many semiconducting polymers such as regioregular $P_3HT$ allows efficient packing and crystallization. However, due to the difficulty of forming ordered crystalline structures from interpenetrating and entangled polymer chains of high rigidity, there are very few publications on single crystals of polymeric semiconductors [18]. As a result of different processing conditions, there is a great diversity of morphologies for these polymers, which have been widely explored and reviewed during the last 50 years [19]. Table (1.2) shows some properties of poly (3-hexylthiophene) and Figure (2) shows the chemical composition of this $P_3HT$ [20].

**Table (1.2) Properties of poly (3-hexylthiophene) $P_3HT$ [20].**

| **Molecular formula** | **$(C_{10}H_{14}S)_n$** |
|---|---|
| Molecular weight | (54000 – 75000) g / mol |
| Color | Red |
| Density | 1.33 g/cm$^3$ |
| Melting point | 238 °C |
| boiling point | (211-226) °C |
| Energy gap | (1.9 -2) eV |
| Solubility | Chloroform, chlorobenzene |

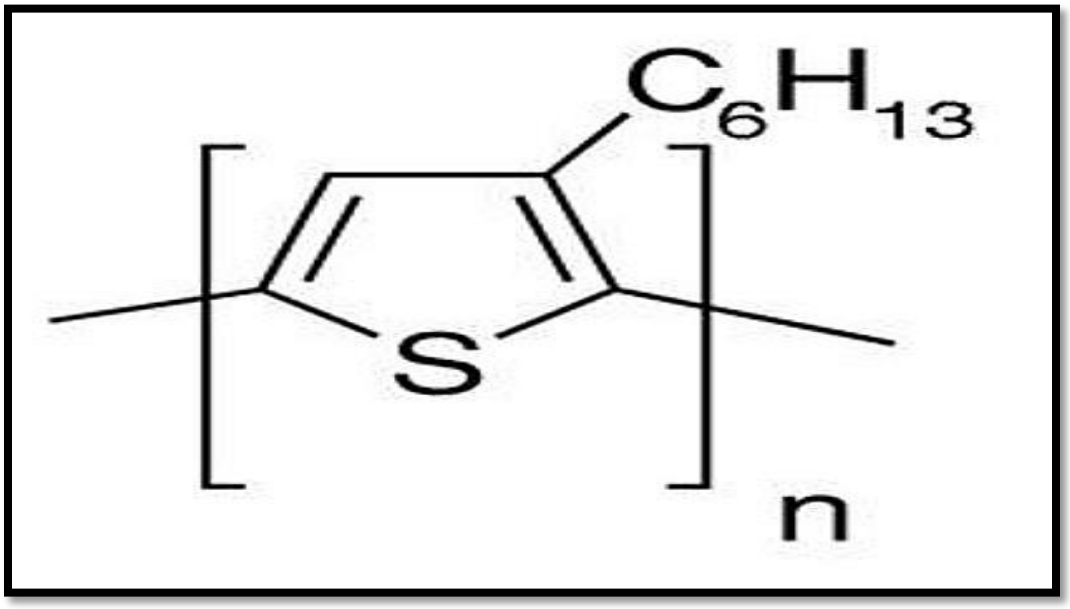


**Figure(1.2): The chemical structure of poly (3-hexylthiophene) [19].**

## 1.4 Working Principle of Solar Cell

solar cell, also called photovoltaic cell, device that directly converts the energy of light into electrical energy through the photovoltaic effect. The overwhelming majority of solar cells are fabricated from silicon-with increasing efficiency and lowering cost as the materials range from

amorphous (noncrystalline) to polycrystalline to crystalline (single crystal) silicon forms. Unlike batteries or fuel cells, solar cells do not utilize chemical reactions or require fuel to produce electric power, and, unlike electric generators, they do not have any moving parts [20].

When light reaches the p-n junction, the light photons can easily enter in the junction, through very thin p-type layer. The light energy, in the form of photons, supplies sufficient energy to the junction to create a number of electron-hole pairs. The incident light breaks the thermal equilibrium condition of the junction. The free electrons in the depletion region can quickly come to the n-type side of the junction[21]. Similarly, the holes in the depletion can quickly come to the p-type side of the junction. Once, the newly created free electrons come to the n-type side, cannot further cross the junction because of barrier potential of the junction.

Similarly, the newly created holes once come to the p-type side cannot further cross the junction became of same barrier potential of the junction. As the concentration of electrons becomes higher in one side, i.e. n-type side of the junction and concentration of holes becomes more in another side, i.e. the p-type side of the junction, the p-n junction will behave like a small battery cell. A voltage is set up which is known as photo voltage. If we connect a small load across the junction, there will be a tiny current flowing through it [21].

### 1.4.1 Advantage of Solar Cell

The advantage of solar cell is [22]:

**1.** Solar energy is a clean and renewable energy source.

**2.** Once a solar panel is installed, solar energy can be produced free of charge.

**3.** Solar energy will last forever whereas it is estimated that the world's oil reserves will last for 30 to 40 years.

**4.** Solar energy causes no pollution.

**5.** Solar cells make absolutely no noise at all.

**6.** Very little maintenance is needed to keep solar cells running. There are no moving parts in a solar cell which makes it impossible to really damage them.

### 1.4.2 Disadvantage of Solar Cell

The disadvantage of solar cell is [22]:

**1.** Solar panels can be expensive to install resulting in a time-lag of many years for savings on energy bills to match initial investments.

**2.** Solar power stations do not match the power output of similar sized conventional power stations; they can also be very expensive to build.

**3.** Solar power is used to charge batteries so that solar powered devices can be used at night. The batteries can often be large and heavy, taking up space and needing to be replaced from time to time.

## 1.5 Literature Survey

**In 2010, Bahaa Hussien and *el at*. [23],** the researchers studied the effect of the addition of $TiO_2$ on some electrical properties of poly-methyl methacrylate (PMMA) has been studied. Many samples have been prepared by adding $TiO_2$ on the poly-methyl methacrylate by different weight percentages of $TiO_2$ and with different thickness. The experimental results show that the D.C. electrical conductivity changes when the concentration of additional $TiO_2$ increases and when the temperature increases. Also the activation energy of D.C. electrical conductivity is decreases by increasing $TiO_2$ concentrations.

**In 2010, Assanee Jaipean and *el at*.[24],** researchers have fabricated thin films of poly (methyl methacrylate)by spin coating method, or

PMMA. The result shows for the spin-coating speed, it was observed that the transmittance of the film increased with the speed, but with a decreasing rate. For the baking temperature, the results showed that all the baked films provided roughly the same level of transmittance regardless of their baking temperatures after spin-coating, except the one baked at 130 °C. Where the sample baked at such temperature provided approximately 5% lower transmittance than those of the others. This effect was supposedly contributed to the glass transition temperature of the PMMA. The baking temperature of 130 °C was closed to the glass transition temperature of the material which is at 105 °C. This was suspected to result that such temperature is just above the glass transition temperature of the material. Thus the film baked at such temperature was a mixture of glassy state and complete solid state, leading to a lower transmittance. The results from this study could be used to help adjust the fabricating conditions of a spin-coated film of PMMA to provide a required optical transmittance.

**In 2011, L.N Ismail and *el at.*[25],** Poly (methyl-methacrylate) (PMMA) thin films were deposited by sol-gel spin coating method on glass substrates. PMMA powder was dissolved in 60ml Toluene with the concentration of the PMMA in the solution was varied from 30 ~ 120 mg. Besides the PMMA concentration, also studied the effect of the thin films thickness on the electrical properties. The results for electrical properties showed that there is a difference of the I-V, resistivity, conductivity and the dielectric constant with different thickness. Conductivity of the PMMA thin film was found to ~ $10^{-6}$ Ωcm and continue to decrease as the PMMA concentration increased. From AFM images, the surface morphology showed that there was no significant difference on the film morphology for

PMMA films having 5 and 10 layers when the PMMA concentration is being varied.

**In 2012, Lyly Nyl Ismail and *el at.*[26],** The researchers were deposited PMMA thin films by sol gel spin coating method on ITO substrates. Toluene was used as the solvent to dissolve the PMMA powder. The dielectric properties were measured for thin film. The dielectric permittivity was in the range of 7.3 to 7.5 which decreased as the PMMA concentration increased. The dielectric loss is in the range of 0.01 ~ – 0.01. All samples show dielectric characteristics which have dielectric loss is less than 0.05. The optical properties for thin films were measured at room temperature across 200 ~ 1000 nm wavelength region. All samples are highly transparent. The energy band gaps are in the range of 3.6 eV to 3.9 eV when the PMMA concentration increased. The morphologies of the samples show that all samples are uniform and the surface roughness increased as the concentration increased. From this study, it is known that, the dielectric, optical, and morphology properties were influenced by the amount of PMMA concentration in the solution.

**In 2013, A. Hassan Resen,[27],** where the researcher has studied the effect of doping on the optical constants of (PMMA) doping with phenolphthalein(8%)was studied. films were prepared by using casting technique with thickness(20μm), optical properties for this films were studied by recording the absorption and transmission spectra in the wavelength rang (190-1100)nm. And then the absorption, transmission, the reflectivity, extinction coefficient, refractive index, and real and imaginary parts of dielectric constant were studied. The results were shown that all properties that were studied increases by the ratio of doping except transmission which decreased at doping.

**In 2014, Hussein Neama N. and *el at.*[28],** The researchers studied optical characteristics of poly (methyl methacrylate) (PMMA) films doped with4-(5-{2-[5-(4-Cyanophenyl)-3-methylthiophen-2-yl]-3,3,4,4,5,5-hexafluorocyclopent -1-en-1-yl}-4-methylthiophen-2-yl) benzonitrile (I). Where the polymer films were prepared using casting method with different concentrations of the dopant (I) were used and the optical properties of the prepared films were investigated. where has been measure the optical absorption spectra of these films. The results showed that energy gap ($E_g^{opt}$) of the polymer films decreases with increasing I concentration. The absorbance, absorption coefficient, extinction coefficient, finesse coefficient, refractive index, parts dielectric constant (real and imaginary) and optical conductivity of the prepared PMMA films were found to be increased with increasing the concentration of I. The indirect optical band gap for the pure and doped PMMA films were evaluated to be about (2.6, 2.8, 3, and 3.2)eV for indirect allowed transition, while the indirect forbidden band gaps were determined as (2.5, 2.6, 2.7 and 3.2) eV with increase (I) contents, respectively.

**In 2015, Raheem G. Kadhim, [29],** studied the effect of nano$TiO_2$ particles on electrical properties of polymer PMMA. The samples of (PMMA-$TiO_2$) Nano composites were prepared by using casting method. The experimental results show that the D.C electrical conductivity for the(PMMA-$TiO_2$) Nano composite increase with the increasing temperature, the activation energy for D.C electrical conductivity for (PMMA-$TiO_2$) ) Nano composite decrease with the increasing of concentrations of the($TiO_2$) nanoparticles, while the dielectric constant, dielectric loss, and the A.C electrical conductivity for (PMMA-$TiO_2$) Nano composite are increasing with the increasing of concentrations of the (

$TiO_2$)nanoparticle, the dielectric constant and the dielectric loss of the (PMMA-$TiO_2$) Nano composite is decreasing with the increase of frequency of the applied electric field.

**In 2016, P. Maji and *el at.*[30],** where the researchers used a simplistic sol-casting technique was used to fabricate polymeric Nano composite film of PMMA-$ZrO_2$. Phase analysis, micro-structure and chemical composition were examined through X-ray diffraction (XRD) and Fourier transformed infra-red spectroscopy (FTIR). Where observed a significant enhancement in absorption coefficient of UV-VIS absorption profile with the increase in $ZrO_2$ content. The addition of $ZrO_2$ filler into PMMA markedly enhanced the dielectric constant (~26) and suppressed the loss (tanδ~0.06). The value of A.C conductivity was found around 7.75 $cm^{-1}$ at 373K and 3MHz. The Conducting behavior of the Nano composite film was ascribed to hopping mechanism. The researcher's conclusions that it is possible to use the synergistic combination of $ZrO_2$ and PMMA can be used as an appropriate candidate for high frequency capacitor application.

**In 2018, Zaiying Shi and *el at.*[31],** the researchers was prepared a thin film of pure PMMA polymer to study the optical and electrical characterization of broadband terahertz met material absorbers. The relative permittivity and reflectivity properties of the poly (methyl methacrylate) (PMMA) films prepared with a spin layer were examined and an excellent meta-terahertz absorbent (THz) was fabricated using PMMA film as the dielectric layer. The results of XRD and AFM showed that all PMMA films with thicknesses from (11 to 17) μm were amorphous and extremely smooth with a roughness of about 0.203 nm. The results showed an increase in the dielectric constants from 2.88 to 4.04 with an increase in the thickness from (9 to 14) μm. And the dielectric constants of

PMMA films of a certain thickness (8 μm) decreased. The UV-VIS spectrum showed that the thickness had little effect on the reflectance and transmittance in the visible region, resulting in the same Eg (energy gap) of about 3.7 eV.

**In 2019, Ömar Bahadır Mergen and *el at.*[32],** Researchers have studied the effects of graphene Nano platelet (GNP) doping on the optical parameters and the optical transition energies (optical band gap) of poly(methyl methacrylate)/graphene Nano platelet (PMMA/GNP) composite films were studied. In this study, were prepared the composite films by spin coating technique. The absorbance (A) changes of the prepared composites were measured by using UV–Vis technique. found the composites have high absorption properties in the low wavelength region (k<250 nm) and low absorption properties in the high wavelength region (k>250 nm). The extinction coefficient, k is increased with the increase of GNPs doping. $E_d$ and $E_i$ band gap energies were calculated, they found that the indirect transition energies ($E_i$) lower than the direct transition energies ($E_d$), where calculated as (4.7– 6.2) eV and (2.0–5.9) eV, respectively. the results obtained were interpreted as the increase in the conductivities of the GNP-doped composites. found too the conductive additives added to the insulating PMMA matrix increase the conductivity of the composites and composites become semi-conductive state.

**In 2019, Ahmed Shaker Hussein and *et al.* [33],** study the effect of thickness on the optical properties for polymer poly(methyl methacrylate),that the films were prepared by spin coating method. Some of optical properties of poly(methyl methacrylate)film have studied. This study shows that the values of optical properties that include (absorption,

refractive index, reflectance, real dielectric constant) decreasing with increasing of speed due to the difference in thickness. While the (transmittance, extinction coefficient, absorption coefficient, imaginary dielectric constant) increasing with increasing of speed due to the impact of thickness. The measurements were taken for different thickness (206,116, 87, 66, 47) nm and different number of rotation (1000, 2000, 3000, 4000, 5000) rpm respectively. They also found that the value of the energy gap is as high as possible and reaches to (3.08 eV) at 5000 rpm with thickness (47) nm. They also found that the highest value of refraction was at the thickness (206) nm.

**In 2020, A. A. Hasan and *el at.*[34],** Researchers have studied the optical and electrical properties of PMMA/CB, PMMA/G and PMMA/(CB+G) composites. They found that that transmittance of pure PMMA is very high, which shows drastic reduction as carbon black and graphene added separately to the host material in opposite to that the transmittance decreased the wavelength by addition of (G) or (CB) to PMMA. Minimum energy gap (1.0 eV) obtained for PMMA+0.04% G composite sample. And obtained Maximum refractive index for PMMA+0.06% G composite sample. As such that they found all the optical parameters of pure PMMA like n, k real and imaginary dielectric constant is lower than those of composites samples, while the energy gap of PMMA is higher than those of composites samples. as they noticed The values of ($\varepsilon_r$) and ($\varepsilon_i$) clearly affected by the increasing of graphene and CB content. Where the exponent s was very low for all composites samples. The Band Gap of the films was measured, showed the Optical Band Gap of the pure PMMA is 5 eV drastically, decreased to low energy especially for (PMMA doped with (CB)).

**In 2021, Qais M. Al-Bataineh and *el at.* [35],** In 2021, Qais M. Al-Bataineh and el at. [31], Researchers have synthesize and optically characterize pure PMMA and PMMA incorporated with metal oxides nanoparticles (MO NPs) such as ZnO, CuO, $TiO_2$ and $SiO_2$ NPs Nanocomposite . The optical parameters were determined by analyzing the transmittance and reflectance spectra. The transmittance of PMMA thin film was found to be around 92% in the visible region. And has been found that, as MONPs are introduced into PMMA thin films, the transmittance of thin films significantly decreases. Thus, relevant optical parameters are strongly influenced by this decrease. Calculated refractive indices (n) of PMMA thin film lie in the range (1.53–1.97) that increase as MONPs are introduced into PMMA matrices. . The $E_g$ value of un-doped PMMA thin films is found to be 4.273 eV. This value decreases as pre-selected MONPs are introduced into thin films. The FTIR technique has been used employed to elucidate the vibrational bands of the Nano composites and the intermolecular bonding between PMMA matrix and the MOs NPs. The obtained doped thin films show a great promise for fabricating high-efficient optoelectronic devices.

**In 2021, Angham Hazim and *el at.*[36],** Researchers have studied the fabrication of Novel (PMMA-$Al_2O_3$/Ag) Nano composites and its structural and optical properties for light weight and low cost electronics Applications. Where the results showed that the structural and optical properties of (PMMA-$Al_2O_3$-Ag) Nano composites are promising materials for different optoelectronics applications such as solar cells, sensors, electronics gates, transistors, lens, lasers .etc. The results showed that the optical absorbance of (PMMA-$Al_2O_3$) Nano composites increases with the increase in Ag nanoparticles concentration. The absorption coefficient,

extinction coefficient, refractive index, imaginary and real dielectric constants and optical conductivity of (PMMA-$Al_2O_3$) Nano composites increase with the increase of silver nanoparticles concentrations while the transmittance and energy band gap decrease with the increase of Ag nanoparticles concentrations. FTIR studies showed that there are no interactions between (PMMA-$Al_2O_3$) and Ag nanoparticles concentrations. And, the (PMMA-$Al_2O_3$-Ag) Nano composites have higher absorption at high energies photons and it have energy band gap 2.1 eV < $E_g$ < 4.22 eV; these behaviors make it suitable for modern optoelectronics applications.

**In 2021, Areen A.B.S. *et al*. [37]**, prepared thin films based on (PMMA) and (PS) doped with (1, 3, 5, and 7) % of cerium dioxide nanoparticles ($CeO_2$ NPs). The transmittance and reflectance are measured in the spectral range (250–700) nm. High transmittance of 87% is observed in the low energy regions. The optical band gap energy of (PMMA-PS) thin film is found to be 4.03 eV. FTIR analysis is identify the major vibrational modes of the Nano composite. The peak at 541.42 $cm^{-1}$ is assigned to Ce–O and indicates the incorporation of $CeO_2$ NPs into the copolymers matrices. There were drastic changes to the width and intensity of the vibrational bands of PMMA-PS upon addition of $CeO_2$ NPs.

## 1.6 Aim of the Work

The aims of this work can be summarized in the following points:

**I.** Study of structural, optical and electrical properties of prepared (PMMA: $P_3HT$) thin films on glass substrate by spin coating technique.

**II.** Studying the possibility preparation of (PMMA: $P_3HT$) as a solar cell and determination of the optimum conditions work for these devices such as, efficiency, and employing the proposed optimization parameters and combining them in one device in order to achieve highly efficient solar cell.

**III.** Investigate the stability of the prepared solar cells.

# CHAPTER TWO

# Theoretical Part

## 2.1 Introduction

This chapter includes a general description of the theoretical part of this study, physical concepts, scientific clarifications, relationships, and laws used to interpret the study results.

## 2.2 Structural Properties

The structural properties represent important tool to study the crystallographic structure of thin films.

### 2.2.1 Atomic Force Microscopy (AFM)

Atomic force microscopy (AFM) or scanning force microscopy (SFM) is a very high-resolution type of scanning probe microscopy, with demonstrated resolution on the order of fractions of a nanometer, more than 1000 times better than the optical diffraction limit. The AFM is a conceptually simple apparatus [38]. A micrometer-scale cantilever with a sharp tip (diameter ~ 10-50 nm) is scanned over a sample at distances on the order of a few nm. Interatomic forces between the tip and the sample are sensed by the cantilever, whose deflection is measured (usually) by a laser and a photodetector. The force experienced by the tip varies nonlinearly with the tip-sample separation[39].

### 2.2.2 Fourier Transform Infrared (FT-IR)

FT-IR is a technique that is used to obtain an infrared spectrum of absorption, emission, photoconductivity or Raman scattering of a solid, liquid or gas. FT-IR spectrometer simultaneously collects spectral data in a wide range of spectral range [40]. Spectra were recorded as a sample

dispersion in (potassium bromide) through IR disk as (sample 1 mg to 200 mg KBr) with a scanning range of (500-3500) $cm^{-1}$ and resolve (1 $cm^{-1}$).

### 2.2.3 The X-ray Diffraction (XRD)

X-ray diffraction is one of the widely used experimental techniques for determining lattice parameters, preferred orientation of the crystal [41]. The mechanism of XRD is simple. When a monochromatic X-ray beam incident onto a crystal sample, the constructive diffractions (or interference) from parallel planes of atoms with inter-planar spacing d occur if the Bragg's law is satisfied [42].

$$2d \sin\theta = n\lambda \qquad (2.1)$$

Where n is an integer that indicates the order of the reflection, θ is Bragg angle, and λ is the wavelength of the X-ray beam. By measuring the Bragg angle θ, the interplanar distance (d) can be obtained if the wavelength of the X-ray beam is known [43].

The particle size could be easily calculated by using the Debye Scherer formula given by the following equation [26]:

$$D = \frac{0.9\lambda}{\beta\cos\theta} \qquad (2.2)$$

Where, D is the particle size (crystallite size), $\lambda$ is the wavelength of the X-ray, $\beta$= FWHM of most stronger peak (highest intensity peak).

## 2.3 Optical Properties

The study of the optical properties of a material is interesting for many reasons. Firstly, the use of materials in optical applications such as interference filters, optical fibers, and a reflective coating requires accurate knowledge of their optical constants over a wide range of wavelengths [44]. Secondly, the optical properties of all materials may be related to their atomic structure, electronic band structure and electrical properties [45].

### 2.3.1 Absorptance (A)

Absorption can be defined as the ratio between absorbed light intensity ($I_A$) by material and the incident intensity of light ( $I_o$ ) [46].

$$A = \frac{I_A}{I_o} \qquad (2.3)$$

### 2.3.2 Transmittance ( T )

Transmittance is given by the ratio of the intensity of the transmitting rays ($I_T$) through the film to the intensity of the incident rays ($I_o$) on it as follows [47]:

$$T = \frac{I_T}{I_o} \qquad (2.4)$$

We can also find a transmittance as a function of wavelength through the exponential relationship for both absorbance and transmittance which [48]:

$$A = \log\left(\frac{1}{T}\right) \qquad (2.5)$$

### 2.3.3 Reflectance (R)

Reflectance can be obtained from absorption and transmission spectrum in accordance to the law of conservation of energy by the relation [49]:

$$R + T + A = 1 \qquad (2.6)$$

### 2.3.4 Absorption Coefficient (α)

Absorption coefficientα can be defined as the relative rate of decrease in light intensity (I) along it is propagation path. According to Beer Lambert low [50]:

$$\alpha = \frac{1}{I}\frac{d[I]}{dt} \qquad (2.7)$$

Where

I: is the intensity of light in ($W/cm^2$)

t: is the thickness of thin film in (cm).

α can be given by [51]:

$$\alpha = \frac{2.303 \, . A}{t} \qquad (2.8)$$

In semiconductors, the absorption coefficient is a strong function of the wavelength or photon energy. Photon energy is given by [51]:

$$E = h\upsilon \qquad (2.9)$$

Where:

υ: frequency in (Hz.)

h: Plank constant ($6.625\times10^{-34}$ J.s).

### 2.3.5 Extinction Coefficient ( $k_o$)

It represents the imaginary part of complex refractive index (n*) [52]:

$$n^* = n - ik_o \qquad (2.10)$$

Where :

n : the real part of refractive index , equal (c/v).

c : velocity of light in space

v : velocity of light in thin film

n*: complex refractive index which depends on the material type, crystal structure (grain size), crystal defects, stress in the crystal and extinction coefficient ($k_o$), is given by following equation [53]:

$$k_o = \frac{\alpha \lambda}{4 \pi} \qquad (2.11)$$

Where:

$\lambda$ : is the wavelength of incident photon rays.

$\alpha$ : absorption coefficient .

### 2.3.6 Refractive Index (n)

The refractive index can be defined as a ratio between velocity of light in vacuum (c), to its velocity inside the material. The value of refractive index (n) was calculated by using equation depending on the reflectance and extinction coefficient ($k_o$) as in the following equation [54] :

$$R = \frac{(n-1)^2 + k_o^2}{(n+1)^2 + k_o^2} \qquad (2.12)$$

The refractive index can be expressed through the following equation [54]:

$$n = \left[\left(\frac{1+R}{1-R}\right)^2 - (k_o^2 + 1)\right]^{\frac{1}{2}} + \frac{1+R}{1-R} \qquad (2.13)$$

### 2.3.7 Dielectric Constant

When a light incident on the atoms in the material, a reaction between incident radiation and the charges of the material will happen. This will lead to a polarization of the charges of the material [55]:

$$\varepsilon = \varepsilon_1 - i\varepsilon_2 \qquad (2.14)$$

Where:

$\varepsilon_1$ : is the real part of the complex dielectric constant,

$\varepsilon_2$ : is the imaginary part of it. For the calculation of the dielectric constant in its two parts, one can use the following expressions [55]:

$$\varepsilon_1 = n_o^2 - k_o^2 \qquad (2.15)$$

$$\varepsilon_2 = 2\, n_o\, k_o \qquad (2.16)$$

### 2.3.8 The Fundamental Absorption Edge

The fundamental absorption refers to band-to-band or to excitation transitions (i.e. the excitation of an electron from the valence band to the conduction band), it manifests itself by a rapid rise in absorption, which can be used to determine the energy gap of the semiconductor. Absorption regions can be classified into three regions [56].

**a) High Absorption Region**

This region is shown in Figure (2.1). In part (A), the magnitude of absorption coefficient ($\alpha$) is larger or equal to ($10^4$ $cm^{-1}$). From this region the magnitude of forbidden optical energy gap ($E_g^{opt.}$) can be introduced [57].

**b) Exponential Region**

This region is shown as in Figure (2.1). In part (B) the value of absorption coefficient ($\alpha$) is equal to ($1\ cm^{-1} < \alpha < 10^4\ cm^{-1}$). It refers to the transition between the extended levels from the (V.B ) to the local levels in the (C.B ) and from local levels in (V.B) to extend the levels in (C.B).

**c) Low Absorption Region**

The absorption coefficient ($\alpha$) in this region is very small. It is about ($\alpha < 1\ cm^{-1}$). The transition happens in this region because of density of state in mobility gap resulted from faults structural, as in Figure (2.1), the part (C) [58].

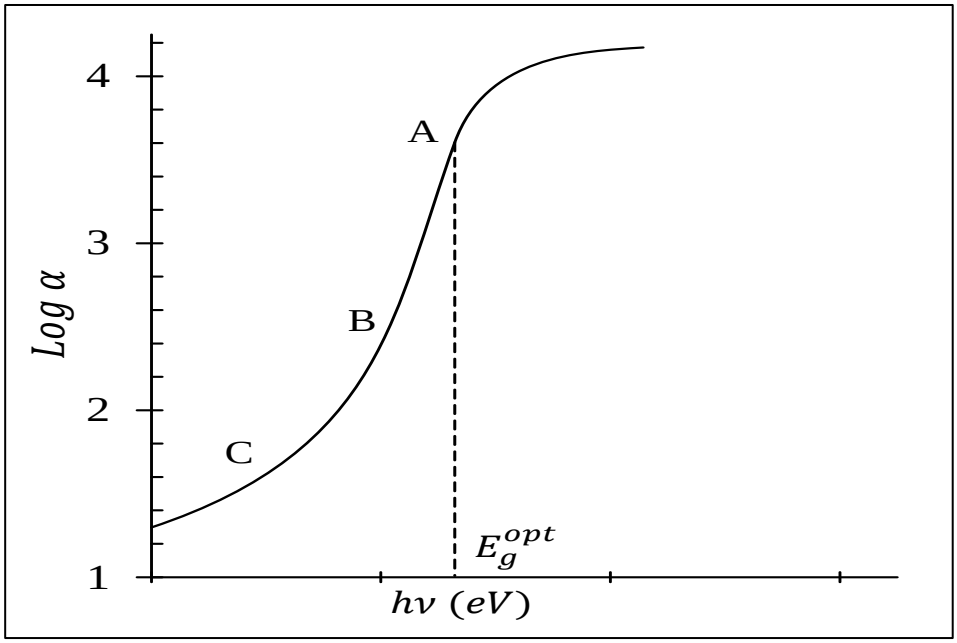


**Figure (2.1): The variation of absorption edge with absorption regions [56].**

### 2.3.9 Electronics Transition

The absorption of radiation, which leads to electronic transition between the valence and conduction bands, is split into direct and indirect transition as shown in Figure (2.5) [59].

The direct transition happens in semiconductors when the bottom of (C.B ) is exactly over the top of (V.B ). This means that they have the same value of wave vector, i.e. (ΔK=0) in this state the absorption appears when ($h\upsilon=E_g^{opt.}$). This transition type is required for the Law's of conservation of energy and momentum. These direct transitions have two types [60]:

**a) Direct Allowed Transitions**

The transition happens from the top points in the (V.B) and the bottom point in the (C.B), as shown in Figure (2.2.a).

**b) Direct Forbidden Transitions**

This transition happens from near top points of (V.B) and the bottom points of (C.B) [61], as shown in Figure (2.2.b).

The absorption coefficient for this transition type is given as relation:

$$(\alpha\, h\upsilon) = B\,(h\upsilon - E_g^{opt.})^r \qquad (2.17)$$

Where:

$E_g^{opt.}$ : energy gap between direct transition.

B: constant depended on type of material.

r: exponeat constant, its value depended on type of transition:

r =1/2 for the allowed direct transition.

r =3/2 for the forbidden direct transition.

For the indirect transition in this case the bottom of (C.B) is not over the top of (V.B), in curve (E-K). The electron transits from (V.B) to (C.B) is not perpendicularly where the value of the wave vector of electron before and after the transition is not equal ($\Delta K \neq 0$). This transition type happens with helpful of particle called "Phonon", for conservation of the energy and momentum law. There are two types of indirect transitions, they are [62]:

**c) Allowed Indirect Transitions**

These transitions happen between the top of (V.B) and the bottom of (C.B) which is found in the difference region of (K-space) as in Figure (2.2.c).

**d) Forbidden Indirect Transitions**

These transitions happen between the nearest points on the top of (V.B) and near points in the bottom of (C.B) [63], as shown in Figure (2.2.d). The absorption coefficient for transition with a photon absorption is given by:

$$\alpha\, h\upsilon = B\,(h\upsilon - E_g^{opt.} \pm E_{ph.})^r \qquad (2.18)$$

Where:

$E_{ph.}$: energy of the phonon, is (-) when phonon absorption, and (+) when photon emission.

r = 2 for the allowed indirect transition.

r = 3 for the forbidden indirect transition.

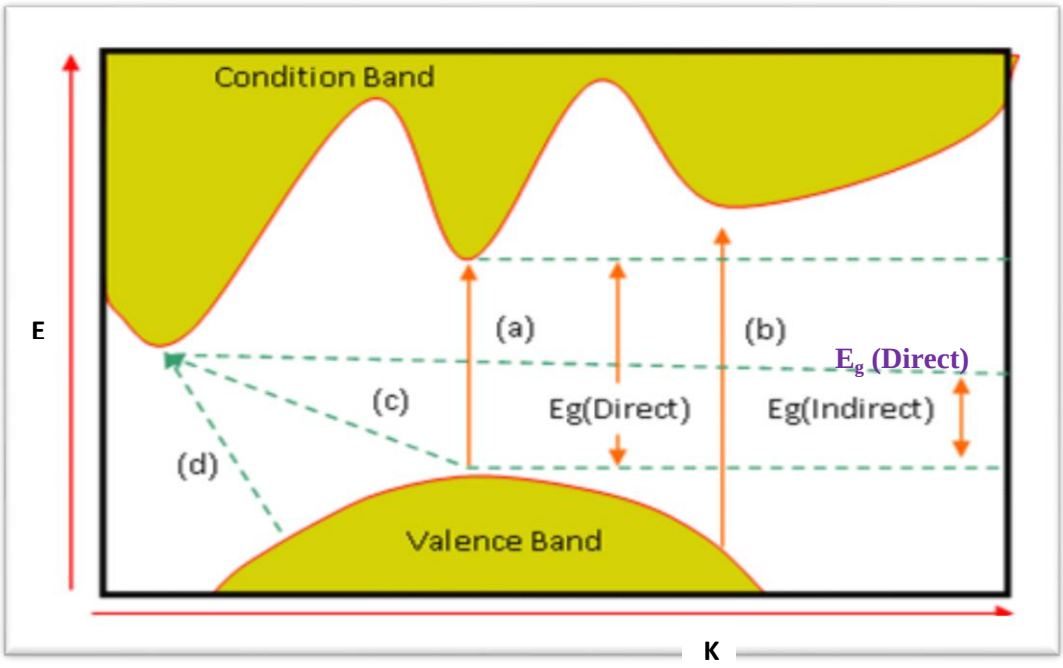


**Figure( 2.2 ): The transition types [63].**

**(a) Allowed direct transition.** **(c) Allowed indirect transition.**

**(b) Forbidden direct transition.** **(d) Forbidden indirect transition.**

## 2.4 The Electrical Properties

The unique electrical properties of semiconductors permit their use in devices to perform specific electronic functions. Advantages of semiconductor devices include: small size, low power consumption, and no warm up time, The invention of semiconductor devices, which has given rise to miniaturized circuitry and is responsible for the advent and extremely

rapid growth of a host of new industries in the past few years. The electrical properties of semiconductors depend upon the nature of semiconductors they being pure or doped , crystalline or amorphous.

The electrical properties of materials are determined not only by chemical composition, but also by the arrangement of atoms in the solid, and the existence of defects when gives rise to the electron states in the energy gap which effected on the electrical properties of material, this defect can be reduced by many processes such as the annealing process. Transport properties such as D.C electrical conductivity ($\sigma_{D.C}$) are important electrical properties [64,65].

### 2.4.1 D.C. Electrical Conductivity

The D.C conductivity in crystalline semiconductors depends on the presence of free electrons and free positive holes. At (0K), the valence band is regarded as filled and the conduction band is empty. As the temperature is raised bonds are broken and the effect is that free electrons are excited into the conduction band, and this leaves behind holes in the valence band. Electrical conductivity (σ) is defined as the proportional factor between the current density and the electric field, and it's given by the equation [66]:

$$J = \sigma E_e \qquad (2.19)$$

Where:

J: is the current density.

$E_e$: is the electric field.

and

$$\sigma = n_e q \mu \qquad (2.20)$$

or

$$\sigma = \frac{(n_e q\, 2\tau)}{m^*} \qquad (2.21)$$

Where

$\mu$: is the mobility of the carriers.

$\tau$: is the carrier's lifetime.

$n_e$: is the carrier's concentration.

m*: is the effective mass of the carrier.

q: is the electron charge.

In semiconductors, the relation between the current density and electric field is given by [67]:

$$J = q\left(n\mu_n + p\mu_p\right)E_e \qquad (2.22)$$

Where, n and p are the electron and hole concentration, respectively, and $\mu_n$ and $\mu_p$ are the mobility of electron and hole, respectively.

The mobility is related to drift velocity by the following equation [68]:

$$\mu = \frac{v_d}{Ee} \qquad (2.23)$$

Where:

$V_d$ is the drift velocity. So that we have [69]:

$$\sigma = q\left(n\mu_n + p\mu_p\right) \qquad (2.24)$$

This important relationship is connecting the conductivity with the electron and hole concentrations and motilities [70].

The change of electrical conductivity with temperature for most cases of intrinsic semiconductors is given by [70]:

$$\sigma = \sigma_o \exp\left(\frac{-E_a}{k_B T}\right) \qquad (2.25)$$

Where:

$E_a$: is the electric activation energy

T: is the absolute temperature

$k_B$: is the Boltzmann constant

$\sigma_o$: is the minimum electrical conductivity at 0K.

The electrical resistance of the prepared films was determined as a function of the substrate temperature and its value ($R_e$) is given for a rectangular shaped sample [71]:

$$\rho_{D.C} = R_e \frac{b.t}{l} \qquad (2.26)$$

Where:-

b: the width of electrodes.

l: the distance between two electrodes .

$$\sigma_{D.C} = \frac{1}{\rho_{D.C}} \qquad (2.27)$$

Where

$\sigma_{D.C}$ : is the conductivity of the thin film .

The activation energy ($E_a$) which can be calculated using the equation (2.25).

Then the exponential of the equation (2.25) is taken, it will be:

$$\ln \frac{\sigma_{D.C}}{\sigma_o} = -\frac{\Delta E_a}{k_B T} \qquad (2.28)$$

$$\ln \sigma_{D.C} = \ln \sigma_o - \frac{\Delta E_a}{k_B T} \qquad (2.29)$$

Since : $\ln \sigma_o - \frac{\Delta E_a}{k_B}$ is numerical constant.

## 2 .5 Heterojunction Solar Cells Photovoltaic

Heterojunction (HJ) it can be defined as the interface between two different materials in the electron affinities, work function and the energy band gap. Since two of the materials used to form the ( HJ) would be a different band gaps energy. Can be classified the (HJ) to the sharp and graded, depending on the distance by which the transition from one of the material to other, as well as classification depends on the type of conductivity on either side of the junction if two semiconductors have the same type of conductivity then the junction is called isotype heterojunction Such as (p-p),(n-n) otherwise it is called anisotype heterojunction Such as (p-n),(n-p) [72, 73].

Availability of conventional solar cells cheap and clean, which can help reduce the world's dependence on oil. Currently, silicon solar cells have the highest solar energy conversion efficiency of about 24%, however, the offset efficiency by the high cost of production [74,75].

## 2.6 Photoelectric Current-Voltage (J-V) Characteristic

Many of the parameters are used to determine the characteristics of solar cells, Figure (2.3) shows the J-V characteristics of solar cells in the dark and under light.

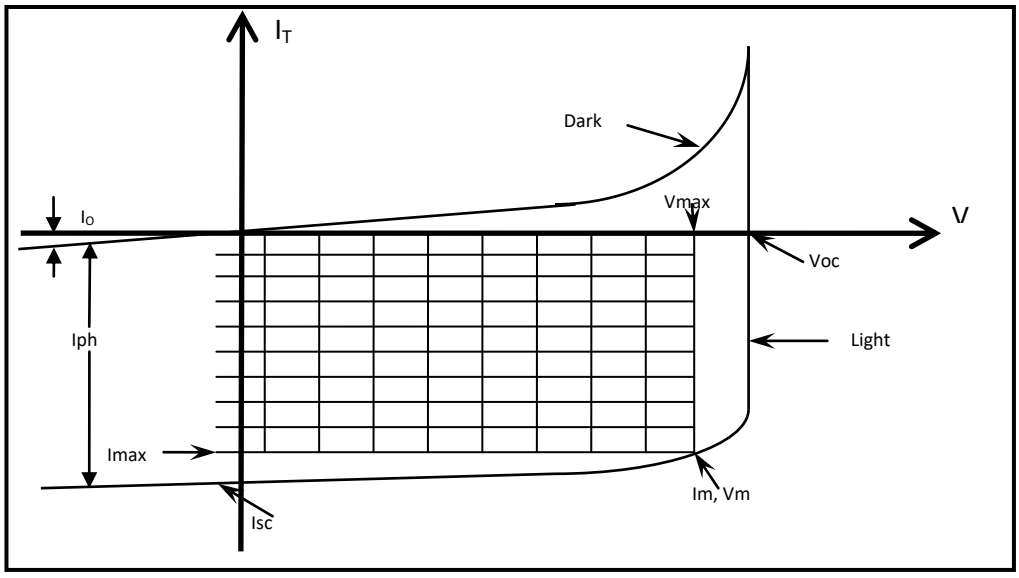


**Figure(2.3): J-V characteristics of solar cell in dark and illumination [75].**

The voltage and current in the fourth quarter are negative. This indicate that the cell put out power, this is the important region of the solar cells. One of the parameters is the short circuit current ($I_{SC}$), which is defined as the current flowing in the circuit when the load is shorted, is given by the equation [75, 76].

$$I_{sc} = I_s[\exp(qV_{oc}/k_BT) + V_{oc}/R_{sh}] \qquad (2.30)$$

Where:

$I_{sc}$ : is the short circuit current.

$I_s$ : is the saturation current.

$R_{sh}$ is the shunt resistance.

The open circuit voltage ($V_{oc}$), supplementary important parameter, is the voltage output of the cell when the attached load is infinite and is given by the relation [77]:

$$V_{oc} = A_\circ(k_BT/q)(I_{sc}/I_\circ + 1) \qquad (2.31)$$

where $I_o$ is the dark current at the junction or inverse saturation current.

The expression for the whole current is :

$$I = I_{\circ}\left(e^{qv/Ak_BT} - 1\right) - I_L \qquad (2.32)$$

where ($I_L$) is the light generated current. Each of ($I_o$) and ($A_o$) give us the essential information on the predominant current transport mechanism in a device.

There are a number of ways to get these standards, despite the fact that there a more consistent method it includes the use of dark J-V curves. The slope of the J-V curve gives the value of ($A_o$), whereas the (y-intercept) gives the value of ($J_o$) ($J_o$ is the current density) [78]. There are another parameter of interest is the fill factor (F.F) given by the relation [79].

$$F.F = V_m I_m / V_{oc} I_{sc} \qquad (2.33)$$

where ($I_m$ , $V_m$) represented the maximum value of the current and voltages respectively, they represent the maximum power point, (this is the point where maximum power can be generated by the device) [79,80]. The photoelectric conversion efficiency is also an important parameter. It is a measure of the amount of light energy that is converted into electrical energy and is given by :

$$\eta = \frac{P_m}{P_{in}} \times 100\% \qquad (2.34)$$

or:

$$\eta = \frac{V_{oc} \times J_{sc} \times F.F}{P_{in}} \qquad (2.35)$$

where ($P_m$) is the maximum power, and ($P_{in}$) is the incident power [80,81].

# CHAPTER THREE

# Experimental Part

## 3.1 Introduction

This chapter deals with the basic knowledge of PMMA and $P_3HT$ preparation and spin coating technology, their work, film formation, and factors leading to film growth. In the thin film deposition part, the procedure starts with substrate cleaning, solution preparation and formation of PMMA and polymer $P_3HT$ thin films. The spin-coating technology deposition on the glass substrate used in this work is discussed in detail. This chapter involves a description of all the instruments used in this work. Next is the discussion of the details of the experimental setup for testing and researching the performance of the solar cells developed in this chapter.

Considering new and improved optics, electronics, magnetic devices, solar cells, and photovoltaics, thin film technology has revolutionized the fields of optics, electronics, and magnetism. The advantages of thin-film devices are low material consumption and flexible substrates [82].

## 3.2 Solutions Preparation

To prepare the solution, 0.1g of the PMMA was dissolved in 15 mL of (Chlorophom), then the solution is placed on the magnetic mixer and stir well to dissolve the material. Then, $P_3HT$ added is to a solution for the purpose of mixing different proportions (0.02, 0.04 and 0.06) %, after that the films were prepared by spin coating method the chemical materials used in this work are listed in table (3.1).

**Table (3-1): The chemical materials used.**

| No. | Chemicals | Company supplied |
|---|---|---|
| 1 | Poly (methyl methacrylate) | Sigma Aldrich |
| 2 | Chlorophom | Bio solve |
| 3 | poly (3-hexylthiophene) | Sigma Aldrich |
| 4 | Ethanol (99.98%) | Bio solve |
| 5 | Si wafer | SEH America |
| 6 | Glass | Sigma Aldrich |
| 7 | Al (99.99%) | Bio solve |
| 8 | Hydrofluoric acid (HF) | Sigma Aldrich |

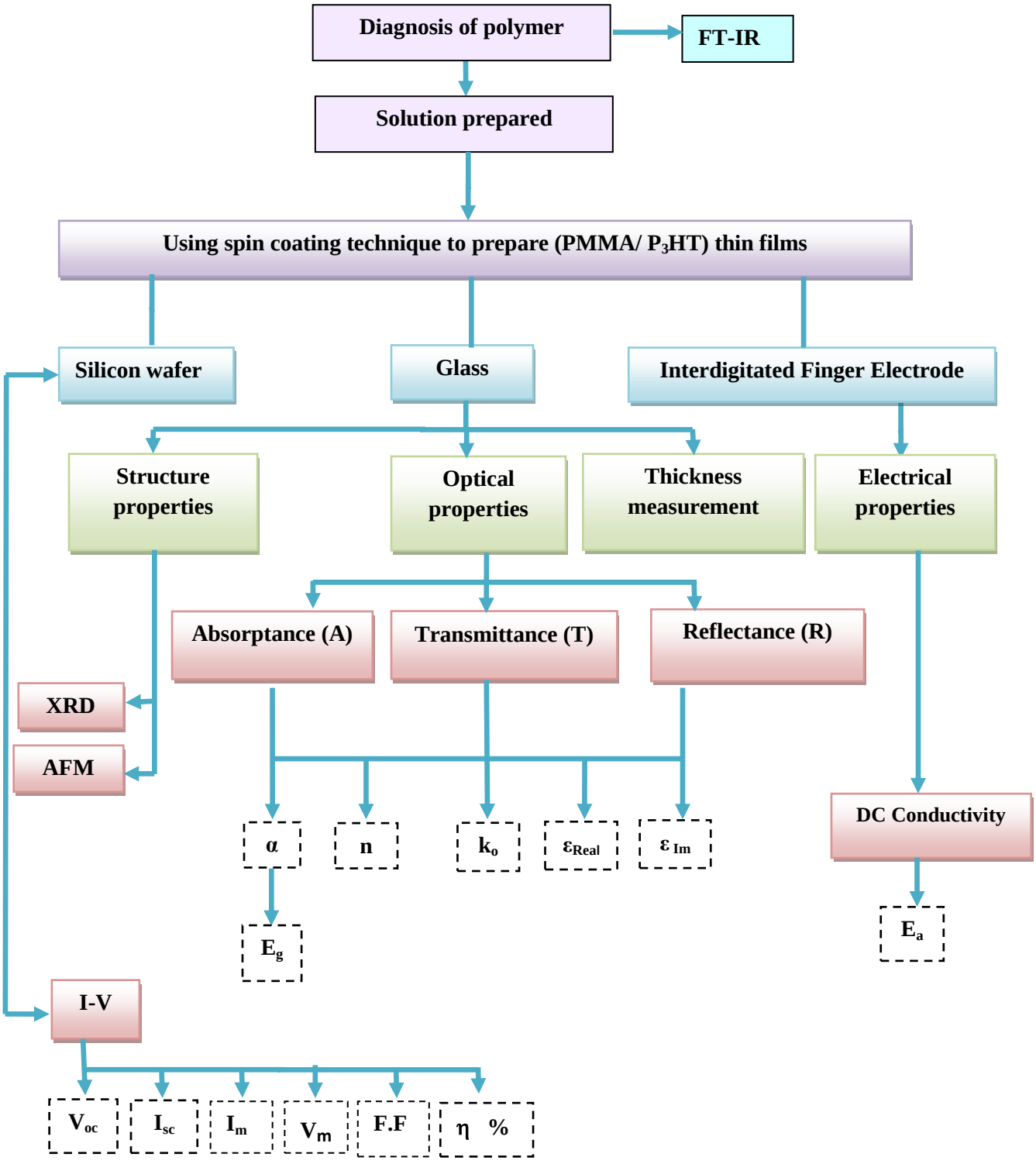


**Figure (3.1): Schematic diagram of the main steps of the procedure.**

## 3.3 Spin Coating Method

Spin coating is a versatile and effective technique to polymer film it is an attractive method to prepare a wide variety of powders and film materials for various industrial applications. Polymers films have been deposited using this technique. Spin coating opens up the possibility to control the film morphology. The quality and properties of the films depend heavily on the process parameters. A spin coating system, (model V T C-100) , this system is present in the laboratory of the Department of Physics, College of Science, University of Babylon, employed to prepare thin films. The system consists of several parts which have been arranged so as to make use of them in the preparation of various films on various substrates. In this system the thickness of the prepared films can be controlled by increasing or decreasing the rotation speed of the system, where the increasing of the speed rotation of the system the thickness of the films are decreasing and vice versa. Also the homogeneity of the prepared films depends on the speed of rotation and on the balance and stability of the system. Figure (3.2) shows the spin coating system [62].

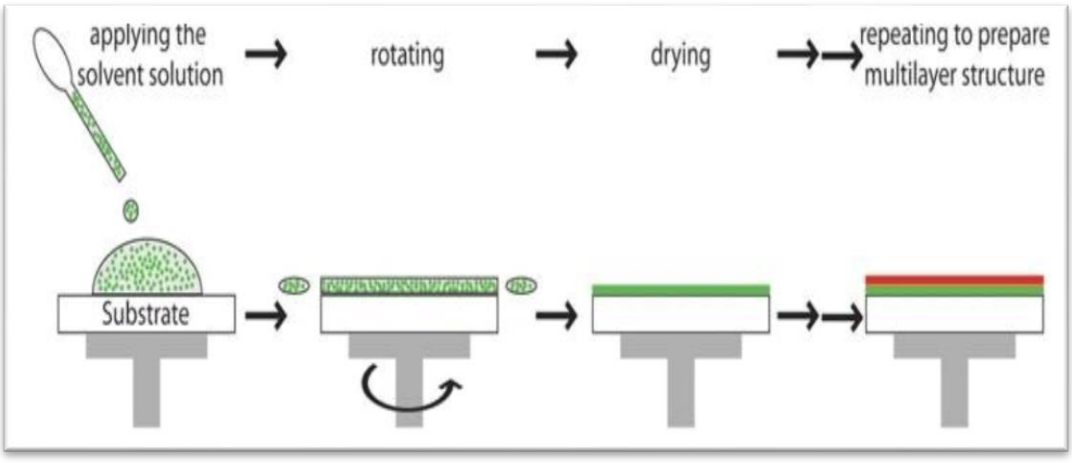


**Figure (3.2): Schematic of the spin-coating process [62].**

## 3.4 Substrates Cleaning

The cleaning of substrates is very important process because the influences like oil or dust affect the properties of thin films, clean substrate is also essential to achieve good film adhesion.

### 3.4.1 Glass Substrate

It can be summarized the glass substrate cleaning as follow:

1- using detergent with water to remove any oil or dust that can be attached to the substrate surface and then placed under distilled water and rub gently.

2- Put in a clean beaker containing distilled water and then rinsed in a unit of ultrasound for 15 minutes.

3- After this, step 2 is repeated by replacing the distilled water with pure alcohol, which reacts with contamination such as grease and some oxide.

4- Eventually, the slides are dried with blowing air, and then wiped with soft paper.

### 3.4.2 Silicon Wafer

The silicon wafers are used as substrates to prepare the film solar cells with area $1cm^2$ after cleaning it with the same way as above; these substrates were chemically etched in dilute hydrofluoric acid with water in a ratio of 1:10 to remove native oxide. That the silicon wafer used for the PMMA-$P_3HT$ / Si heterojunction from n-type with the orientation (100) and resistance (1-10) Ω can be obtained it commercially.

## 3.5 Solar Cell Manufacturing (Ohmic Contact)

The process is done by depositing a layer of aluminum with high purity on the non-shiny silicon, then pour polymer on the other side and then the deposition of gold poles with masks arranged in a circle.

## 3.6 Thin Films Characterization and Measurements

The measurements are listed below:

### 3.6.1 Thickness Measurement

Thickness is one of the most important thin film parameters since it largely determines the properties of the film. The thickness of the films is usually measured by monitoring the rate of the deposition during the coating process. In our work, the thickness of the thin films was measured by the optical method. This instrument is present to the University of Babylon / Faculty of Basic Education. As shown in the Figure (3.3).


**Figure (3.3): Optical thin film measurement system [61].**

## 3.6.2 Structural and Surface Morphological Properties

The structural properties of the films were study the morphology of surface thin films was study by atomic force microscope (AFM), Fourier Transforms Infrared Spectrometer (FTIR) and X- ray diffraction (XRD).

### 3.6.2.1 Atomic Force Microscope (AFM)

Atomic Force Microscope (AFM) micrographs with digital instruments (Inc. BY2000) are taken to observe the surface roughness and topography of deposited thin films. Typical data have been taken from AFM height images include root mean square (RMS) roughness and grain size. It has three main modes of mapping topography: contact, non-contact and intermittent contact or tapping. The most important part of an AFM is the tip with its Nano-scale radius of curvature. The tip is attached to a micro scale cantilever which reacts to the Van der Waals interaction and other forces between the tip and sample. This instrument is present in Islamic Republic Iran- Tehran University. The schematic of AFM microscope is showed in Figure (3.4).

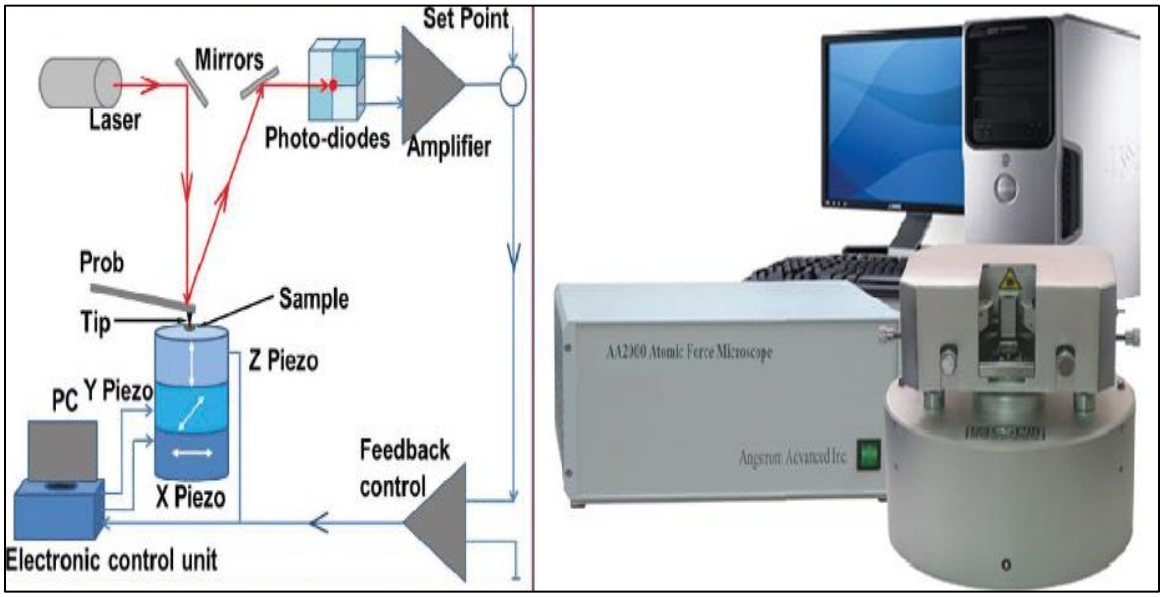


**Figure (3.4): Photograph illustrates the AFM [58].**

### 3.6.2.2 Fourier Transforms Infrared Spectrometer (FT-IR)

Samples of (PMMA-P3HT) films are studied by Fourier Transfer Infrared Spectroscopy (FT-IR), using Vertex 70 from broker company, (FT-IR) instrument that found in University of Kufa/ College of Science, Department of Chemical. The spectrums have recorded as a dispersion of the sample in (potassium bromide) by (IR) disk as (1mg sample in 200 mg KBr) with the scanning range from (500-4000) $cm^{-1}$ and the resolution of ($1cm^{-1}$). The schematic of FTIR Spectroscope is showed in Figure (3.5).

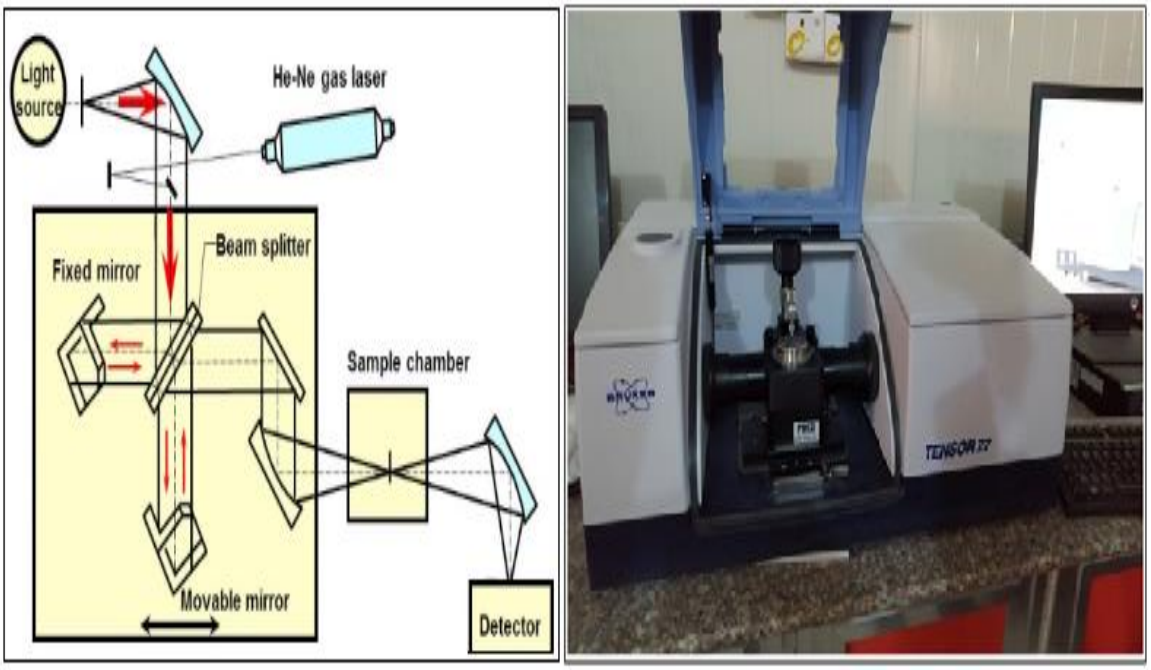


**Figure (3.5): Fourier transforms infrared spectrometer [58].**

### 3.6.2.3 X-ray Diffraction (XRD)

X-ray diffraction (XRD) analysis is used to recognize the crystal structure of thin films. When incident beam of (X-ray) diffracts from a mono wavelength on film surface this will exhibit peaks on limit angels for each material because of Bragg's reflection on parallel crystalline surface. Figure

(3.11) shows the (X-ray) diffractometer type (Shimadzu 6000) made in Japan, the source of radiation is Cu ($k_\alpha$) with wavelength ($\lambda$=1.54060) Å, current (30) mA and voltage (40) kV. The scanning angle 2θ is varied in the range of (20 – 80) degree with a speed of (7) deg/min. This instrument is present in Islamic Republic Iran- Tehran University. The schematic of X-ray diffractometer is showed in Figure (3.6).

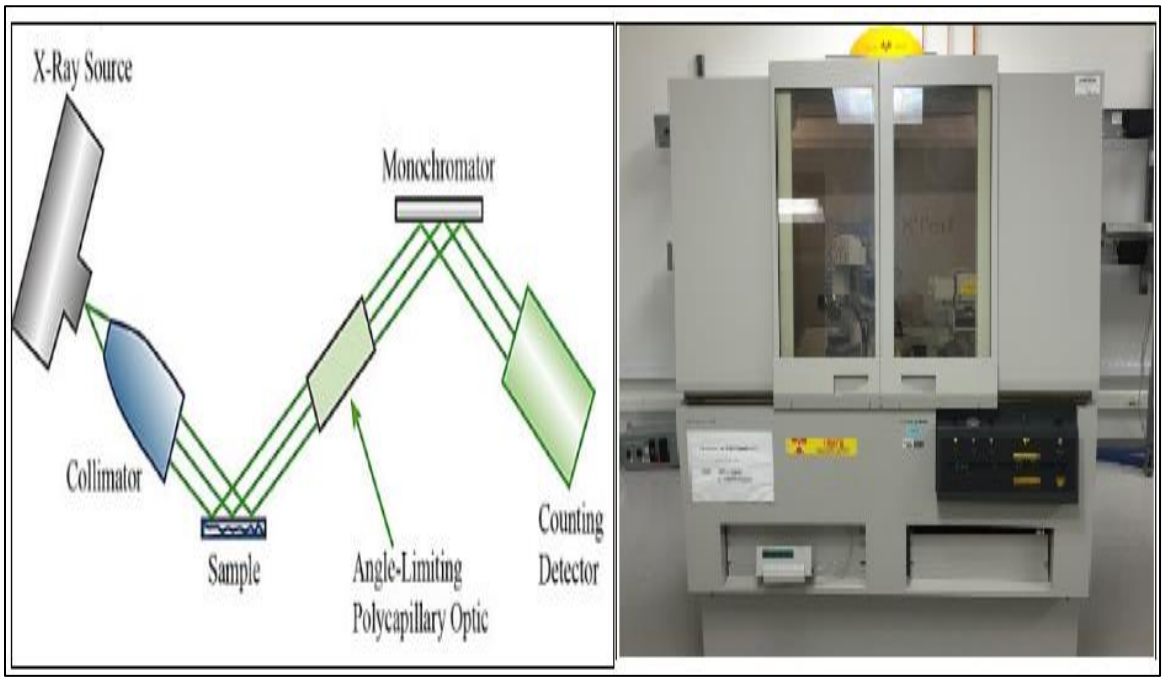


**Figure (3.6): X-ray diffraction system (XRD) [58].**

## 3.6.3 Optical Measurements

A double –beam UV-vis 1800 Shimadzu spectrophotometer was used to measure the absorption of PMMA-$P_3$HT thin films in the range (400-1200) nm. Where the sample is placed in front of the fallen rays, where they fall perpendicularly on the sample, also is used as a sample of the same type of glass as a reference to cancel the effect of the glass. The use of transmittance and reflectance data to calculate the absorption coefficients of

the films in different wavelength, which have been used to determine the band gap. This instrument is present in the laboratory at the University of Babylon / College of Science, Department of Physics. The schematic UV-VIS spectrophotometer is showed in Figure (3.7).

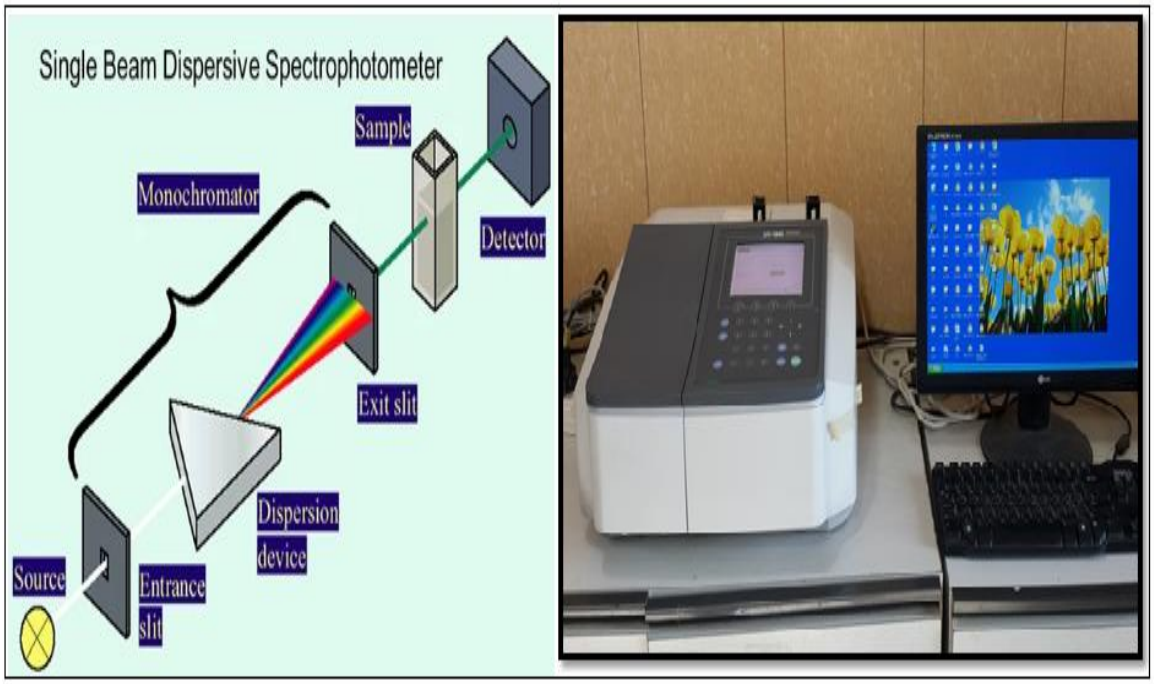


**Figure (3.7): UV-VIS 1800 spectrophotometer system [61].**

## 3.6.4 Electrical Properties

The electrical properties of the films were study by D.C electrical conductivity.

### 3.6.4.1 D.C Electrical Conductivity Measurements

The direct D.C electrical conductivity of the deposited films is measured in University of Babylon-College of Science- Department of Physics -Thin Films Laboratory by using the circuit for measuring D.C conductivity shown in Figure (3.8), which consists of electrical oven type (Memmert Lab Oven UFB 400,400W) and Keithly model 2400, the sample is placed inside the

oven and from oven control adjusted temperature to (373) K, the sample connecting with Keithly by wire and adjusted on resistant scale. The electrical resistivity of the prepared films was determined as a function of the temperature and resistance value ($R_e$) that is given for a rectangular shaped sample by equation (2.26)[83]:

The activation energy ($E_a$) which can be calculated using the reciprocal values of equation (2.2°) then taken the logarithm for each side of equation to get on activation energy [84]:

Thus, the activation energy is equal to the slope of the graphs relation between (lnσ) and inverted temperature ($10^3$/T) multiplied by Boltzmann constant in eV unit where [85]:

$k_B = 1.38 \times 10^{-23}$ J/K $= 0.086 \times 10^{-3}$ eV/K

$$\mathbf{E_a(eV) = Slope \times k_B(eV)} \qquad (\mathbf{3.1})$$

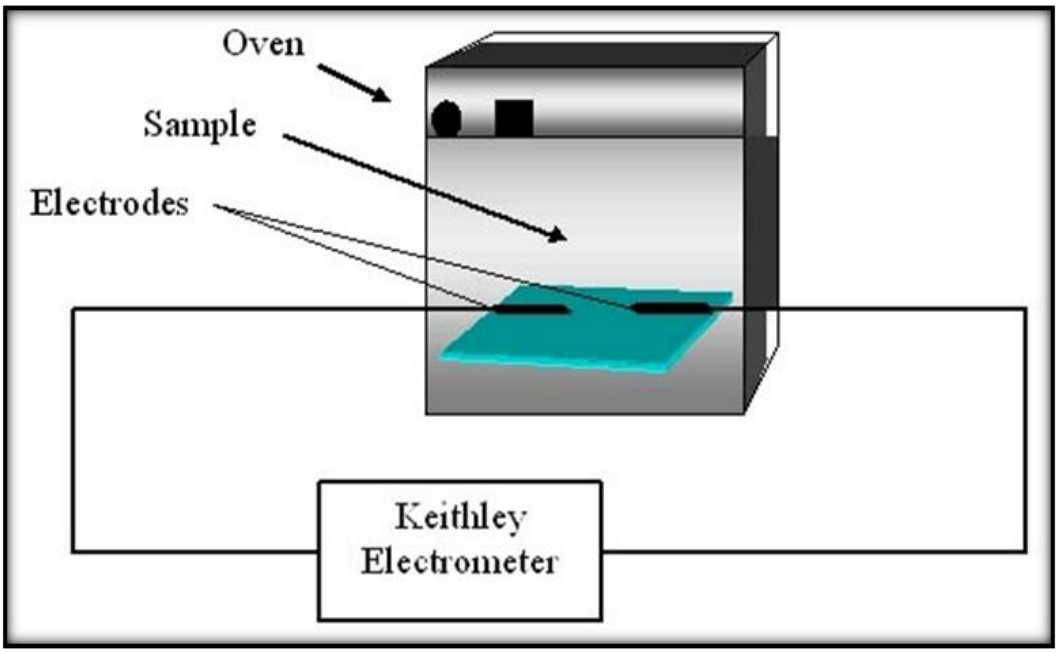


**Figure (3.8): Circuit for measuring D.C conductivity [86].**

## 3.7 Illumination Current-Voltage Characteristics

The study was conducted of electrical and photovoltaic properties of solar cells through an electrical circuit, which consists of the following instruments D.C. power supplied of type (6291A), Micrometer type Keithley 177, Micrometer Dmm, Voltmeter and Halogen light with power (120 W). This instrument is present in the laboratory at the University of Basra / College of Science.

## 3.8 The Short Circuit Current and Open Circuit Voltage Measurements

The short circuit current ($I_{sc}$) is measured when the resistance (R) is zero. The voltage are also (0), while the open circuit voltage ($V_{oc}$) is measured when the resistance value (R) is close to the infinity (∞), where the total current is zero. The short circuit current ($I_{sc}$) and voltages ($V_{oc}$) are measured under illumination as in the following circuit, figure (3.9).

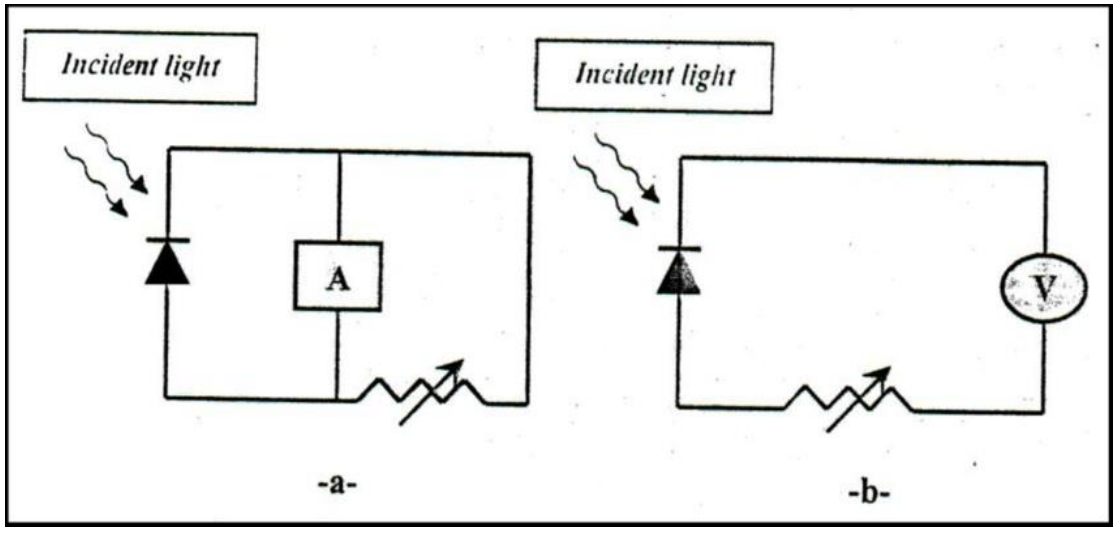


**Figure(3.9): Circuit diagram of (a) the short - circuit current (b) the open – circuit voltage[85].**

# CHAPTER FOUR

# Results, discussion, conclusions, and suggestions

## 4.1 Introduction

In this chapter, the results and the analysis of the experimental measurements and tests of structural, optical, electrical, solar cell properties of the deposited thin films are displayed in this chapter.

The structural properties of the PMMA and PMMA:$P_3$HTare covered by the study of optical microscope FT-IR, AFM and XRD. The optical properties are studied, the optical energy gap and some other parameter such as absorption coefficient, refractive index, extinction coefficient, both real and imaginary part of the dielectric constant as a function of wavelength are determined, and the electrical properties involve the D.C conductivity are also studied. Some important factors of solar cell characteristics will be investigate here, the find parameters of solar cell, short circuit current, open circuit voltage, and fill factor and conversion efficiency.

## 4.2 Structural Properties of PMMA-$P_3$HT

In this section, we studied the effect of $P_3$HT adding on the structured and surface morphology properties for PMMA thin film on glass substrate. The overall crystallinity and purity of the as-synthesized samples were investigated by X-ray powder diffraction (XRD) and morphological by atomic forces microscope (AFM).

### 4.2.1 Fourier Transformation Infrared (FT-IR) Analysis

The polymers (PMMA and $P_3$HT) powder of were analyzed using Fourier transform infrared spectroscopy (FTIR, Bruker IFS 66V/S). The FTIR spectra of PMMA reveals the functional groups that are present. In the PMMA that has been synthesized due to the presence of ester, a strong intensity peak at 1521$cm^{-1}$ developed. Vibration stretching of the carbonyl group C-O (ester bond) stretching vibration is responsible for the broad peak extending from (1400 to 1000) $cm^{-1}$.

C-H bending causes the wideband from (950 to 650)$cm^{-1}$. Because of stretching vibration's existence, the broad peak ranges from (3500 to 3800) $cm^{-1}$. The FTIR spectra of PMMA powder are essentially similar, with no notable alterations in line locations, suggesting a non-wetting polymer particle interfacial surface, as shown in Figure (4.1). The results showed that the active groups of the polymer match its chemical composition. This results is a good approximation with the results of the researcher[87].

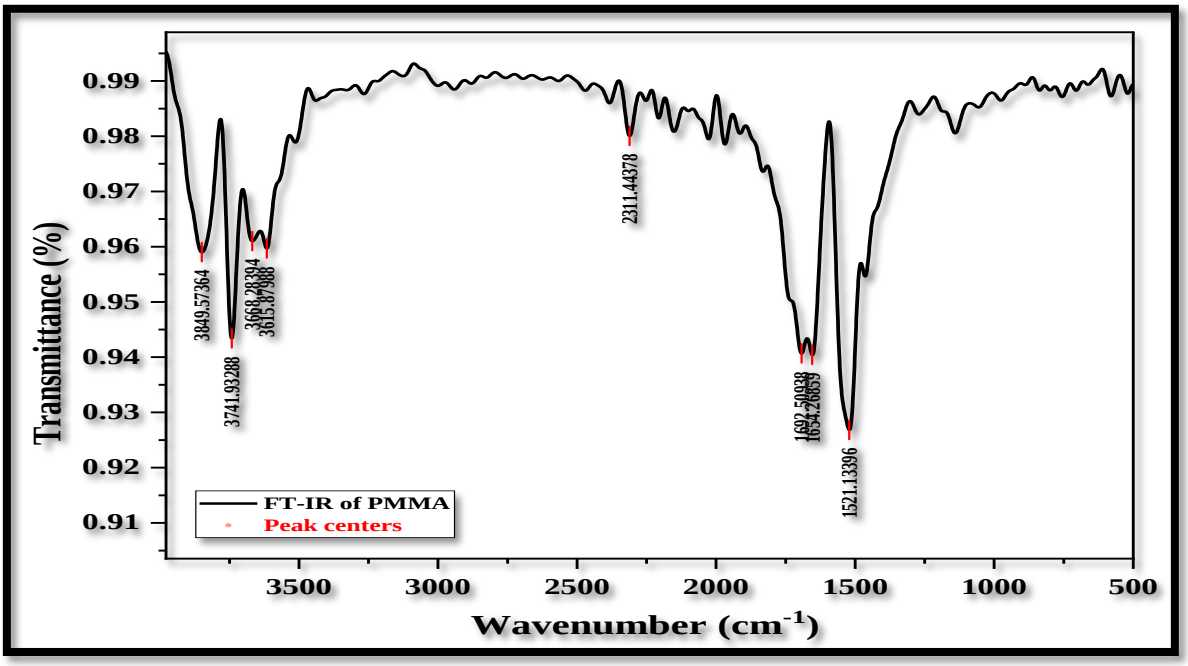


**Figure (4.1): FTIR spectra for PMMA.**

FTIR research confirms the molecular composition of the produced polymer. The FTIR spectrum revealed all of $P_3HT$ distinctive peaks Figure (4.2). C–H vibration in the aliphatic chain of hexyl groups causes peaks at 2800 $cm^{-1}$ and 3000$cm^{-1}$. The peak's intensity is vital due to the polymer's large concentration of carbon-hydrogen bonds. The signal at 1460.6 $cm^{-1}$ can be used to identify the thiophene ring. A peak at 1079.0 c confirms the presence of C–H

in the aromatic ring. This results is a good approximation with the results of the researcher [88,89].

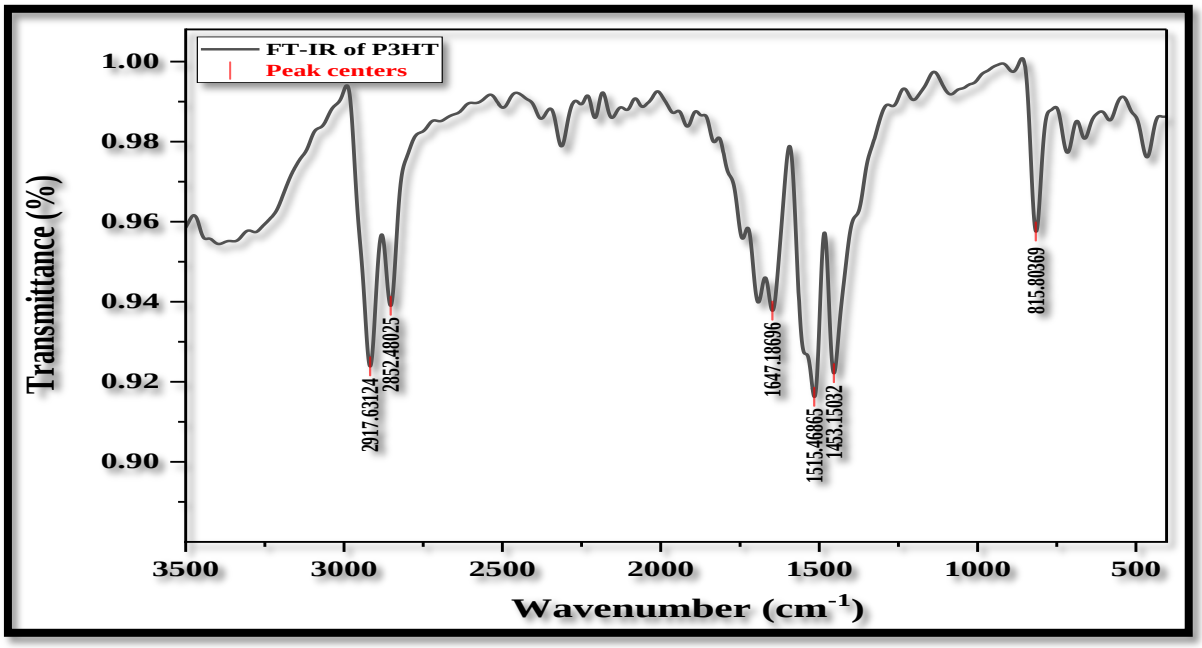


**Figure (4.2): FTIR spectra for $P_3HT$.**

### 4.2.2 Atomic Force Microscope (AFM) Analysis

To study the surfaces of film materials deposited important to recognize how the distribution and arrangement of atoms on surfaces, and get to know the differences or homogeneity properties or attributes relating to each atom separately, can through microscopic analysis AFM to study the effect of the parameters (thickness, concentration,

method of preparation,...etc.) on the properties of film material deposited. As well as analysis of the AFM can calculate the thickness of film, roughness and grain size, and gives an illustrative picture of the distribution of the particle size of the crystal on the surface rate [90].

The atomic force microscope (AFM) scan's graphic scanning range has dimensions (5µm × 5µm). To give a detailed and comprehensive description of the topography of the prepared membrane surfaces, the vertical and horizontal

dimensions of the cover provide a complete description of the Nano-geometric structure of the films [91,92]. The vertical surface dimensions were described from the three-dimensional (3D) images of the surface topography represented by Figures (4.3- 4.7) of PMMA films and $P_3HT$ films at concentrations (0.02, 0.04, 0.06), respectively, where we note topographic surface and appearance of grains formed on the surface of the films, and from these images, we found that surface thickness equal (83.540) for pure PMMA, (116.860) for pure $P_3HT$, (21.3029, 19.05161, and 70.645) nm for concentrations (0.02, 0.04, 0.06)% of $P_3HT$, this values represents the thickness of the films surface roughness, which account for the highest crystalline granular tops on the surface, also we note regularity in the grow film and we note that granules with a vertical arrangement on the crystal axis and equal heights. According to the following parameters:

- **Root Mean Square:** The surface roughness factor is essential because it provides an idea of the surface quality and grain growth. The value of the mean square root represents the ratio of surface roughness, which is equal to the root square of the sum of the Height and depression of the surface divided by their sum. and can take advantage of that in how to get the morphology of the surface the films according to the required applications. From the AFM assays, the average roughness was (1.58nm) for pure PMMA, (2.538) for pure $P_3HT$ films and (1.178, 2.287, 4.47)nm for PMMA\ $P_3HT$ films with concentrations (2, 4, 6)%, respectively.
- **Maximum Height:** This Height represents the amount of growth of nanoparticles. The peak values were (45.62nm) for pure PMMA, (20.763) for pure $P_3HT$ films and (14.29, 17.55, 28.88) nm for $P_3HT$ films at concentrations (2, 4, 6) % respectively.

As for the horizontal dimensions of the surface, they were determined from the three-dimensional (3D) images of the total surface topography and the appearance of the formation of grains formed on the surfaces of the membranes and represented in Figures (4.3- 4.7) according to the following parameters:

- **Skewness:** The deflection amounts were (-0.361580) for pure PMMA films, (-0.190833) for pure $P_3HT$ films, and (1.02184, 0.597299, 1.2961) for PMMA: $P_3HT$ films at concentrations (0.02, 0.04, 0.06)% respectively.
- **Surface Area:** It is known that increasing the surface area of nanoparticles gives them distinctive properties. The increase in the surface area was 5.62nm) for pure PMMA films, (2.569) for pure $P_3HT$, and (2.789nm, 3.011nm, 4.446nm) for PMMA\$P_3HT$ films at concentrations (0.02, 0.04, 0.06)%, respectively. These results are a good approximation with the results of the researcher [92].

Figures (4.3 - 4.7) shows the typical surface AFM images of pure PMMA, pure $P_3HT$ and PMMA:$P_3HT$ thin films, and results show that:

The root mean square, roughness average and the surface thickness increasing with increasing of PMMA: $P_3HT$ wt.%. As we note regularity in the grow film and note that granules with a vertical arrangement on the crystal axis and equal heights.

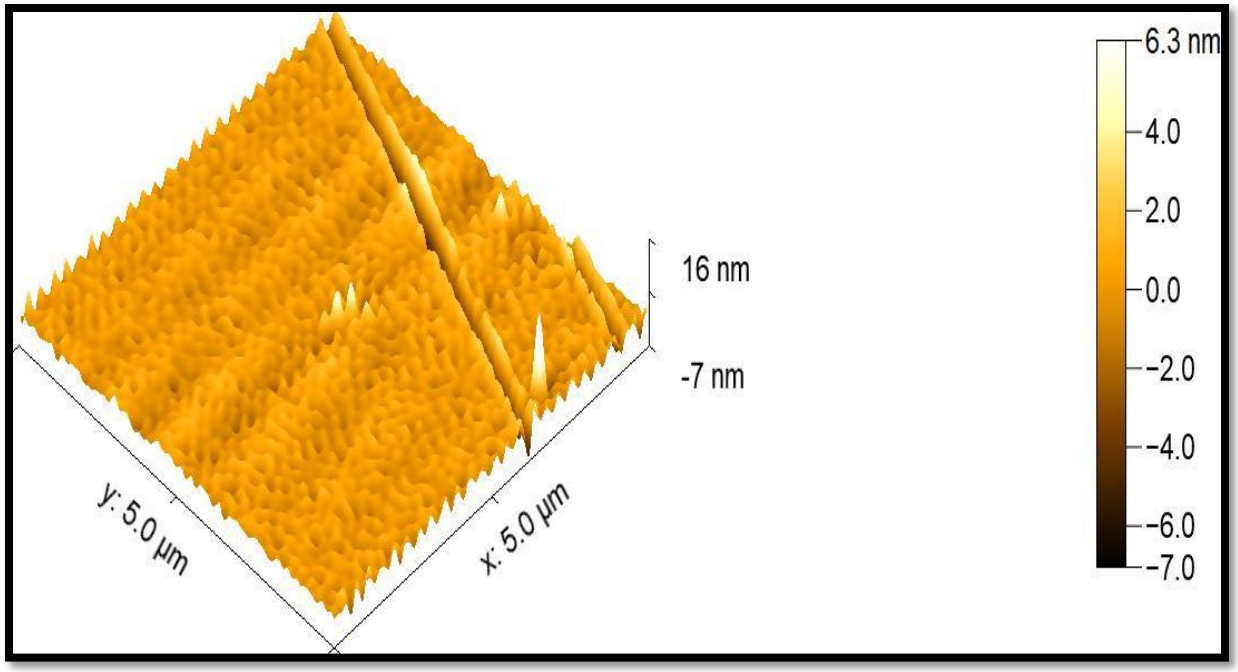


Figure (4.3): 3-D images of the prepared thin films for pure PMMA.

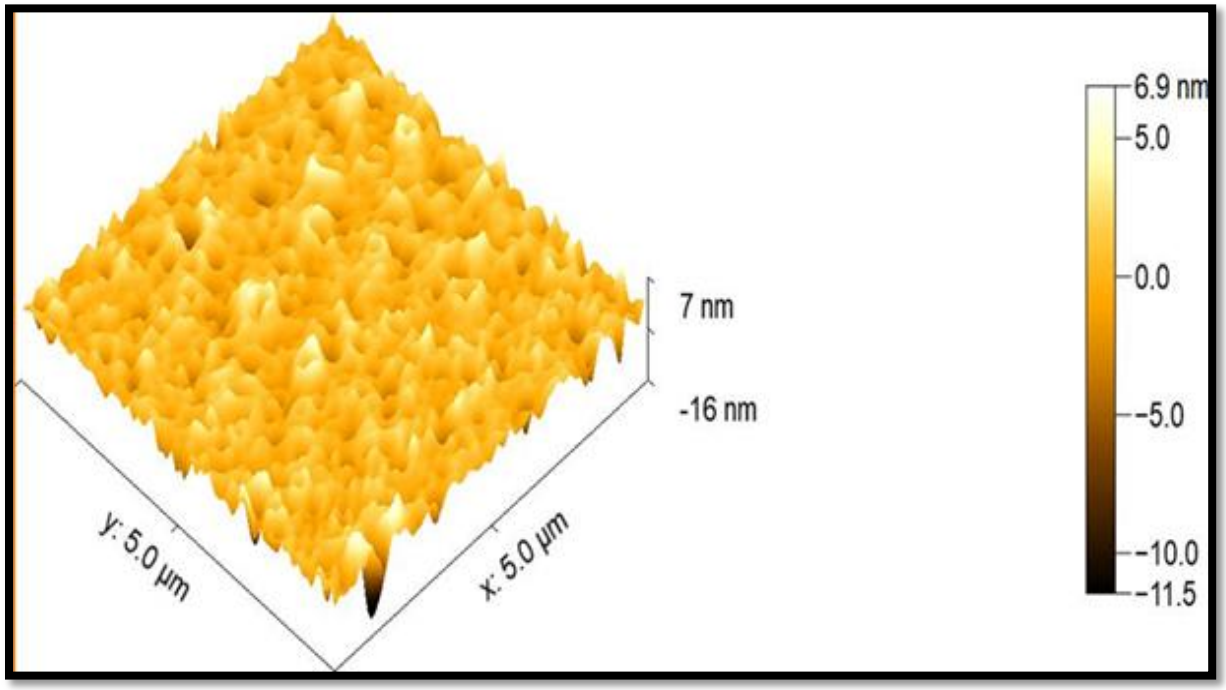


Figure(4.4): 3-D images of the prepared thin films for cons.(0.02)$P_3HT$.

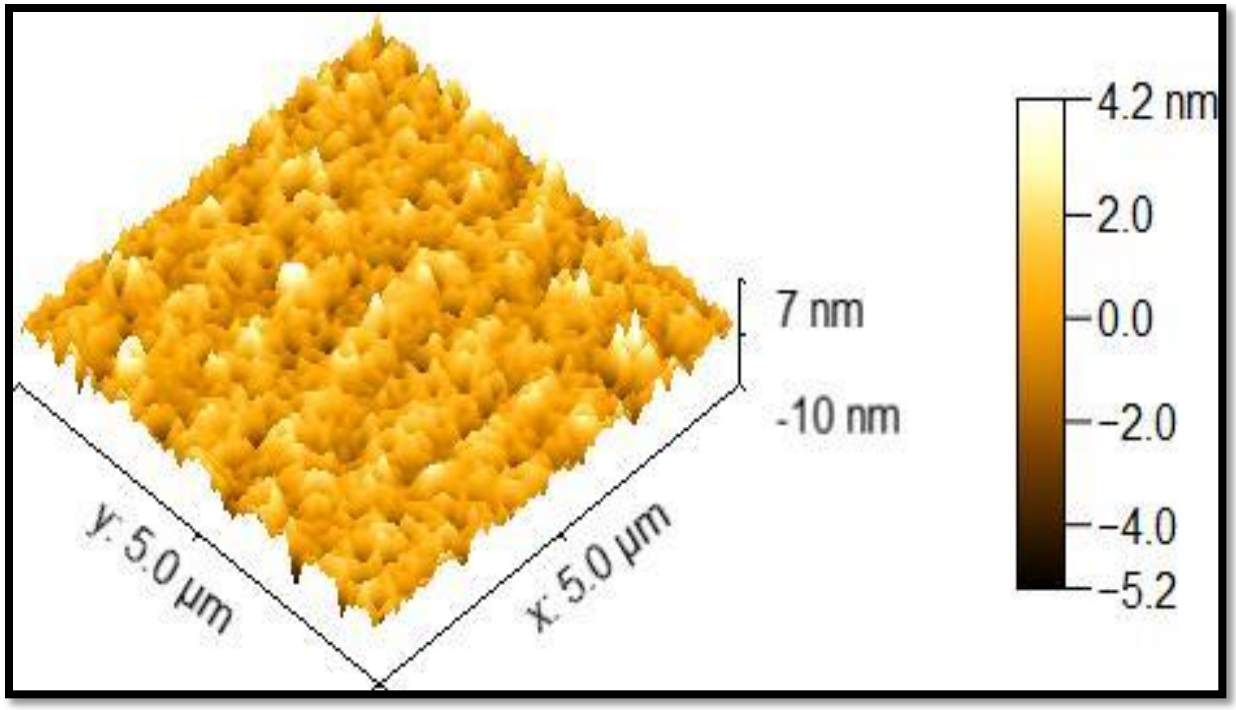


Figure(4.5): 3-D images of the prepared thin films for cons.(0.04)$P_3HT$.

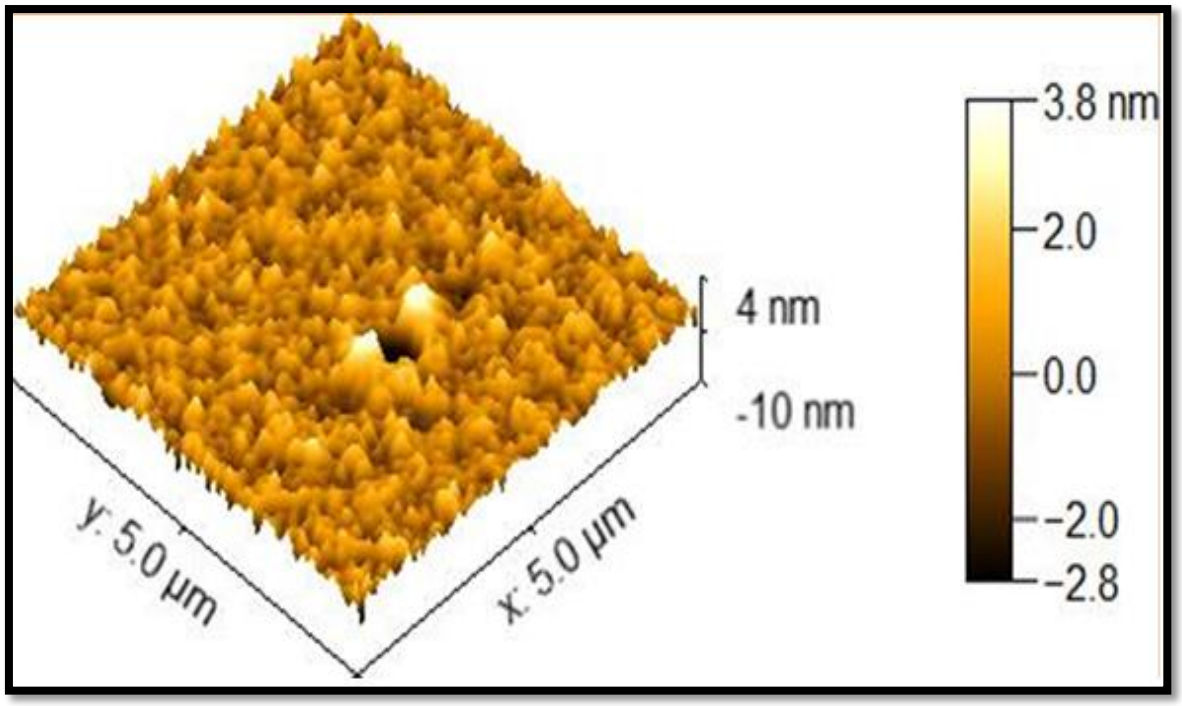


Figure(4.6): 3-D images of the prepared thin films for cons.(0.06)$P_3HT$.

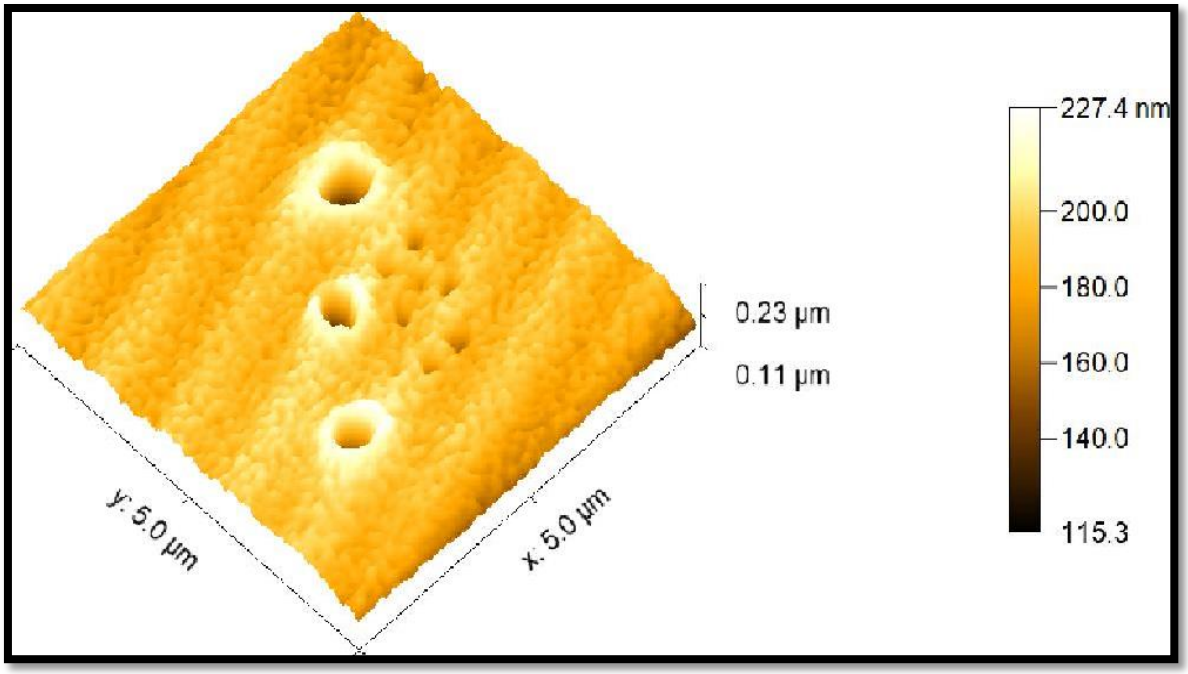


Figure(4.7): 3-D images of the prepared thin films for pure $P_3HT$.

**Table (4.1): Results of AFM assays for pure PMMA and PMMA\$P_3HT$ films.**

| Sample | | Root Mean Seqaure (nm) | Roughness average (nm) | Skewness | Surface Area (nm) | Surface Thickness (nm) |
|---|---|---|---|---|---|---|
| **Pure PMMA** | | **1.580** | **2.70** | **– 0.361580** | **5.620** | **83.540** |
| **Pure $P_3HT$** | | **2.538** | **5.03** | **–0.190833** | **2.569** | **116.860** |
| **$P_3HT$** | Con. | **1.178** | **1.29** | **1.02184** | **2.789** | **21.3029** |
| | **0.02** | | | | | |
| | **0.04** | **2.287** | **1.63** | **0.597299** | **3.011** | **19.0516** |
| | **0.06** | **4.470** | **2.81** | **1.2961** | **4.446** | **70.645** |

### 4.2.3 X– Ray Diffraction (XRD) Analysis

The structural information and crystallinity of PMMA and its doping can be deduced from XRD of the samples. The XRD patterns of, PMMA and PMMA:$P_3HT$ at different doping ratio (0.02, 0.04 and 0.06)% are shown in figures (4.8 – 4.10) respectively.

The results of XRD assays using Cu - 0.15406 nm laser source showed the purity and perfect amorphous of the pure PMMA, but pure $P_3HT$ were polycrystalline thin films. For the sample pure PMMA, four distinct peaks appeared at (2θ° = 13.24, 15.95, 31.05, and 35.11) at the levels, (111), (002), (112), and (221) respectively and the prevailing trend of growth is (111) as shown in the figure (4.8). And these results are an agreement with the results of the researcher [93,94].

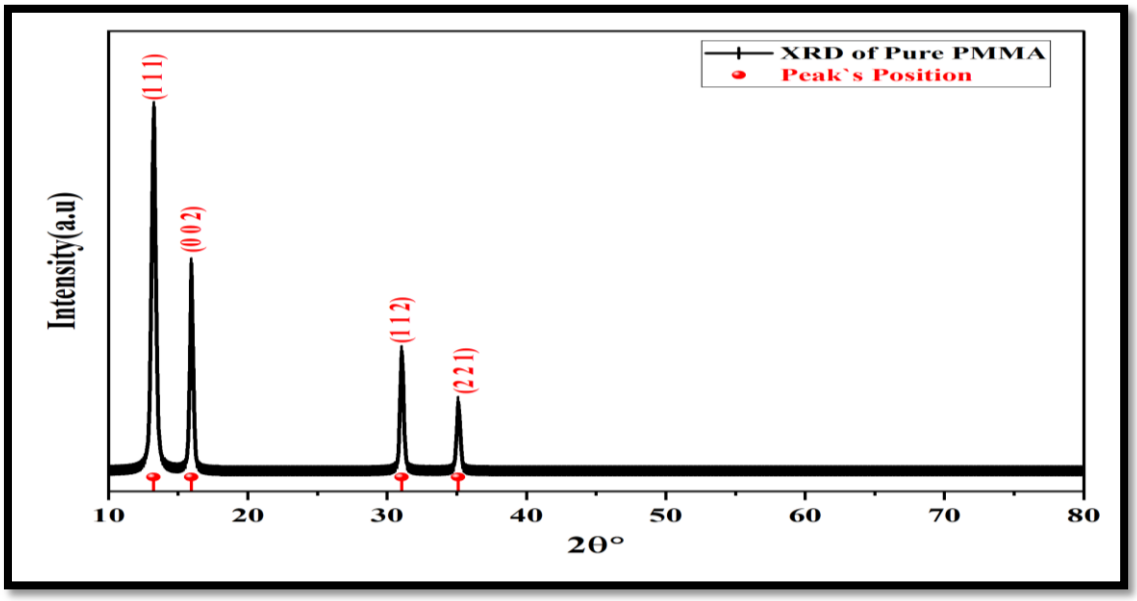


**Figure (4.8): XRD Pattern of Pure PMMA.**

So, for the sample pure $P_3HT$, four distinct peaks appeared at (2θ°= 13.67, 19.46, 25.11 and 36.02) at the levels, (100), (200), (300), and (020), respectively and the prevailing trend of growth is (100) as shown in the figure (4.9). And these results are an agreement with the results of the researcher [95].

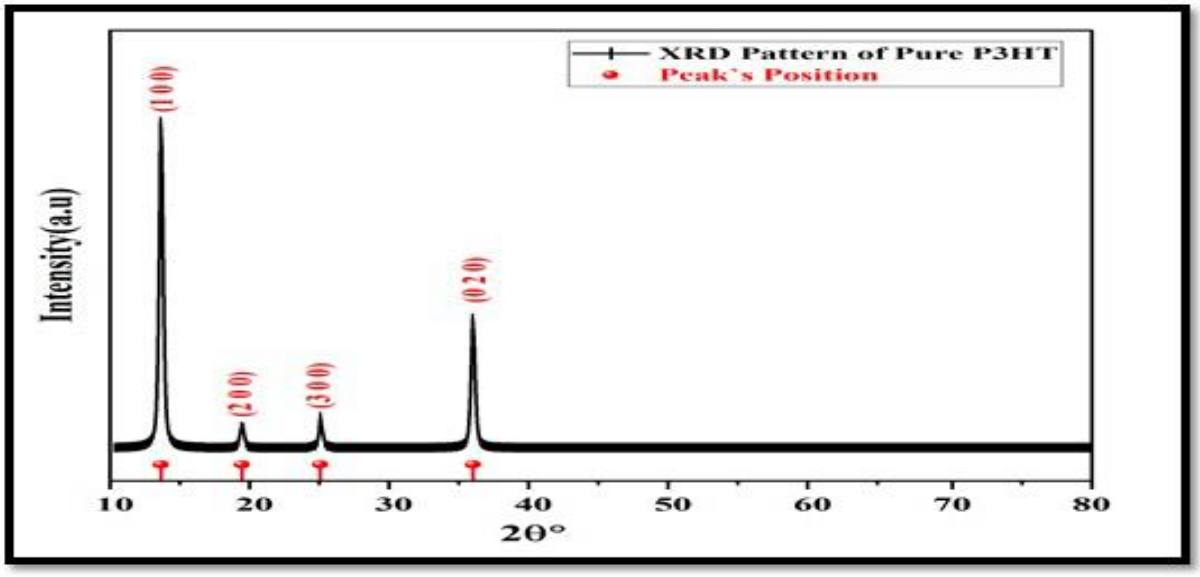


**Figure (4.9): XRD Pattern of Pure $P_3HT$.**

So, for the sample mixture of PMMA and $P_3HT$ by weight (0.02,0.04 and 0.06), three distinct peaks appeared at ($2\theta° = 13.03,25.05$, and 26.04) at the plans, (011), (110, and (121), respectively and the prevailing trend of growth is (011) as shown in the figure (4.10). And these results are an agreement with the results of the researcher [96].

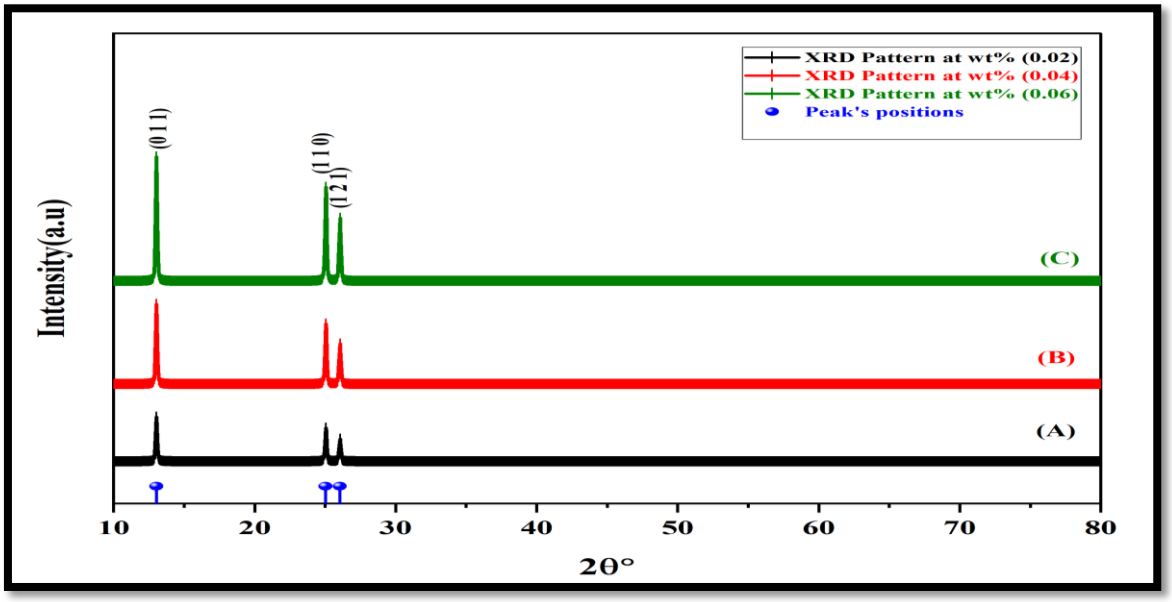


**Figure (4.10): XRD Pattern of PMMA : $P_3HT$.**

**(A) Wt: 0.02% (B) Wt: 0.04% (C) Wt: 0.06%.**

The crystal size of the prepared samples was estimated using equation (2.2), as well as the d- spacing were calculated using Bragg's law of diffraction, and full width at half maximum (FWHM) and other parameters shown in the table (4.2):

**Table (4.2): XRD parameter for prepared films.**

| Sample | (hkl) | 2θ° | θ° | FWHM (rad) | d-spacing (nm) | Crys. Size D (nm) |
|---|---|---|---|---|---|---|
| 0.02 | (011) | 13.03469 | 6.517345 | 0.13515 | 6.786545568 | 59.16361522 |
| | (110) | 25.05016 | 12.52508 | 0.15093 | 3.551947472 | 53.91879014 |
| | (121) | 26.04648 | 13.02324 | 0.15964 | 3.418295111 | 51.0775538 |
| 0.04 | (011) | 13.06469 | 6.532345 | 0.14515 | 6.771029204 | 55.08923201 |
| | (110) | 25.07016 | 12.53508 | 0.13093 | 3.549159166 | 62.15747855 |
| | (121) | 26.06648 | 13.03324 | 0.13964 | 3.415717702 | 58.395517 |
| 0.06 | (011) | 13.02469 | 6.512345 | 0.15515 | 6.791733608 | 51.53646737 |
| | (110) | 25.04016 | 12.52008 | 0.14093 | 3.553343309 | 57.74359798 |
| | (121) | 26.03648 | 13.01824 | 0.16964 | 3.419585314 | 48.06564572 |
| Pure PMMA | (111) | 13.24719 | 6.623595 | 0.36777 | 6.67815544 | 21.74639224 |
| | (002) | 15.95581 | 7.977905 | 0.26819 | 5.550063171 | 29.91136106 |
| | (112) | 31.05672 | 15.52836 | 0.29477 | 2.877310158 | 27.97183192 |
| | (221) | 35.11887 | 17.559435 | 0.29756 | 2.55324117 | 28.00291782 |
| Pure $P_3HT$ | (100) | 3.67409 | 1.837045 | 0.3790 | 4.02908022 | 20.97196343 |
| | (200) | 9.46142 | 4.73071 | 0.37094 | 9.340062093 | 21.48985047 |
| | (300) | 15.11738 | 7.55869 | 0.30736 | 5.855937967 | 26.07341521 |
| | (020) | 26.02172 | 13.01086 | 0.38401 | 3.421491482 | 21.23281527 |

## 4.3 Optical Properties of PMMA-$P_3HT$

In studying the variation of absorbance spectrum, transmittance and reflectance is used UV-Vis spectrophotometer in the region of (200–600) nm for these films, we can calculate absorption coefficient and allowed and forbidden energy gap for direct and indirect transitions. Optical constants, which including refractive index, excitation coefficient and dielectric constant were calculated.

### 4.3.1 Absorbance Spectrum

Optical absorption spectra depend on the chemical composition, crystal structure, energy of the incident photon, film thickness, and film surface morphology. Figures (4.11 - 4.12) displays the variation of absorbance spectra with wavelength from (200-600) nm of the PMMA and PMMA-$P_3HT$ thin films. It can be noticed from the figure that the absorbance for all films have a high values at wavelength in the neighborhood of the fundamental absorption edge (380nm), then the absorbance decreases with increasing of wavelength.

From the Figures (4.11, 4.12) the absorbance of films has medium values in the visible and UV-VIS region. This behavior can be explained as follows: at large wavelength the incident photons do not have enough energy to interact with atoms, the photon will be transmitted. When the wavelength decreases, the interaction between incident photon and material will occur, and then the absorbance will increase [40]. In other words, the incident light is absorbed by the free electrons. Consequently, by the increase of the weight percentages of $P_3HT$, absorbance is increased. These results are in agreement with [25, 31].

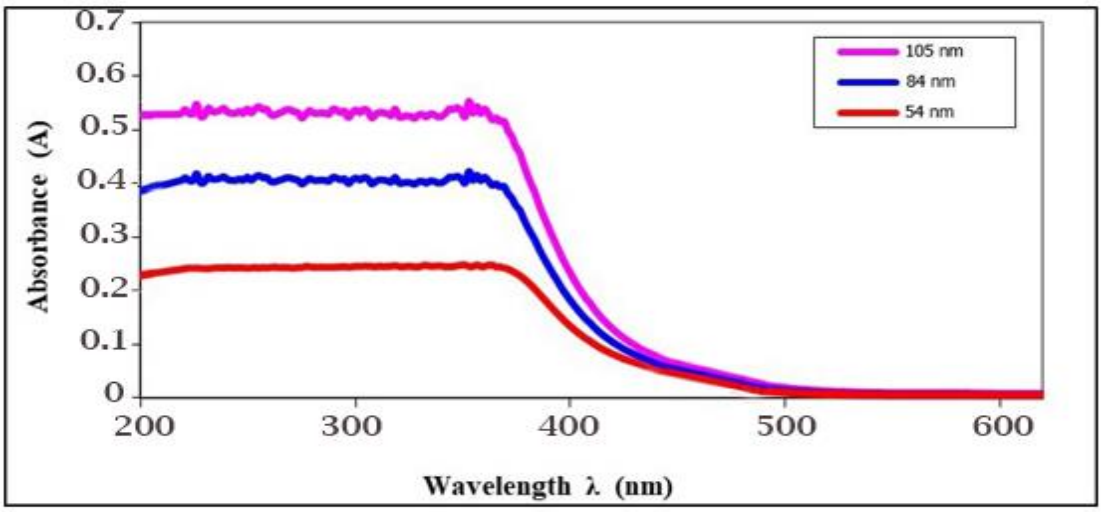


**Figure (4.11): Absorbance spectrum as a function of wavelength for PMMA thin films.**

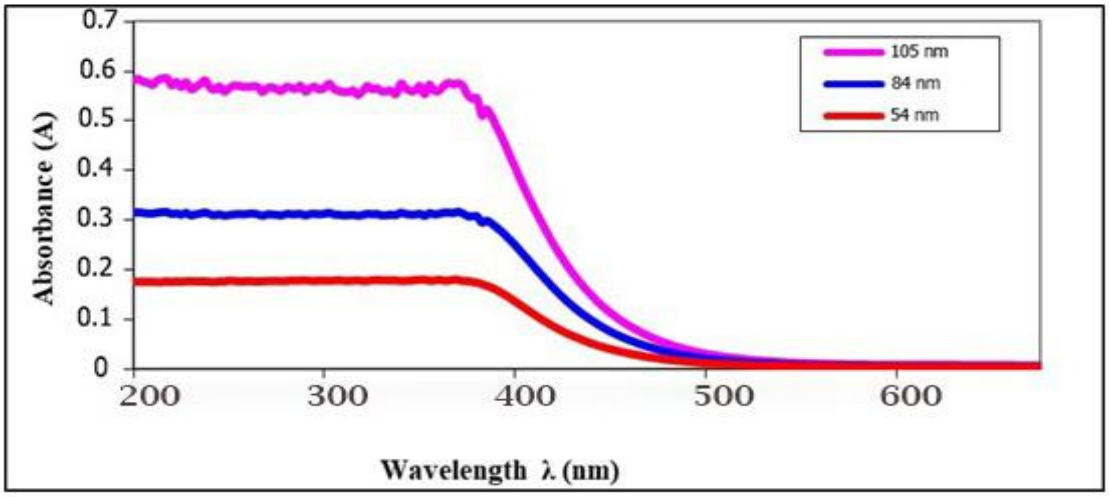


**Figure (4.12): Absorbance spectrum as a function of wavelength for PMMA:$P_3HT$ thin films.**

### 4.3.2 Transmittance Spectrum

The transmittance of the PMMA and PMMA-$P_3HT$ thin films are shown in Figures (4.13 - 4.14). It is clear from this figure that the transmittance spectrum of all thin films increases with the increasing of wavelength (λ). On the other hand, the transmittance spectrum decreases with the increasing thickness and this

is due to the decrease of the surface roughness promoting the decrease of the surface scattering of the light. These results are in agreement with [31,97].

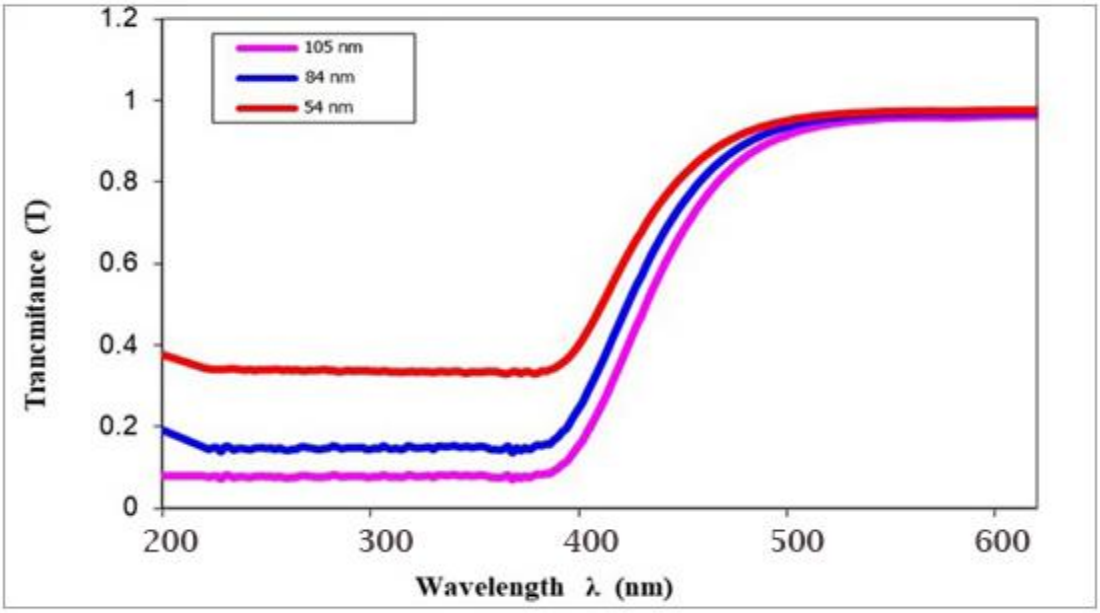


**Figure (4.13): Transmittance spectrum as a function of wavelength for PMMA thin films.**

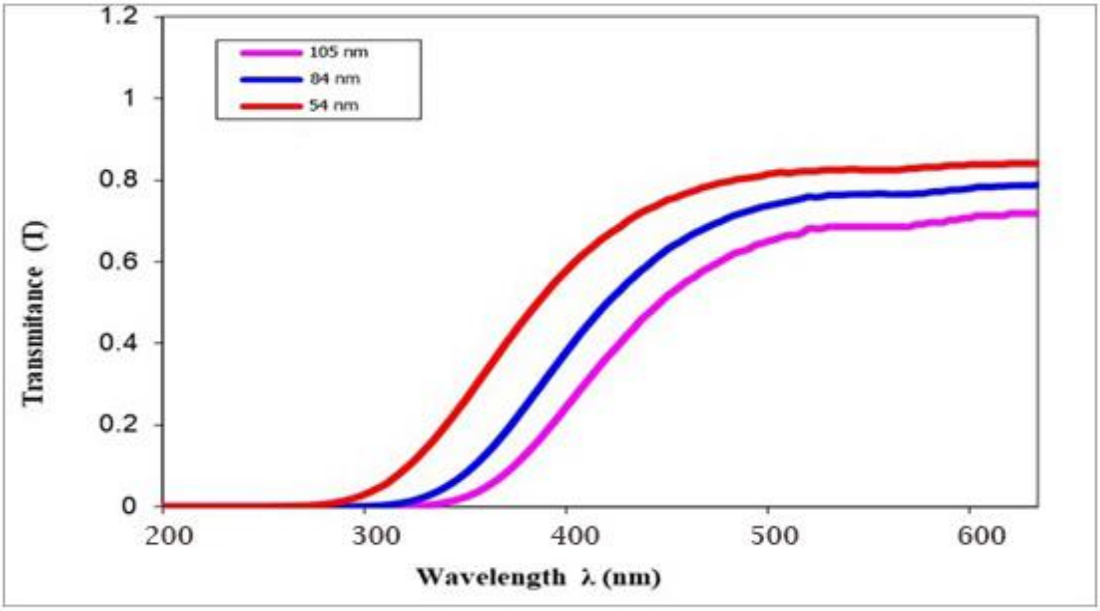


**Figure (4.14): Transmittance spectrum as a function of wavelength for PMMA:$P_3HT$thin films.**

### 4.3.3 Reflectance Spectrum

Figures (4.15 - 4.16) show the reflectance as a function of wavelength of the PMMA and PMMA-$P_3HT$ thin films, the incident photon with the variation of different thickness. The reflectance's has rapidly decreases with the increase of incident photon wavelength of all films and reach the maximum reflectance value at the wavelength corresponding to the film energy gap and it can be an indicator to the material absorption edge. These results are in agreement with [97,98].

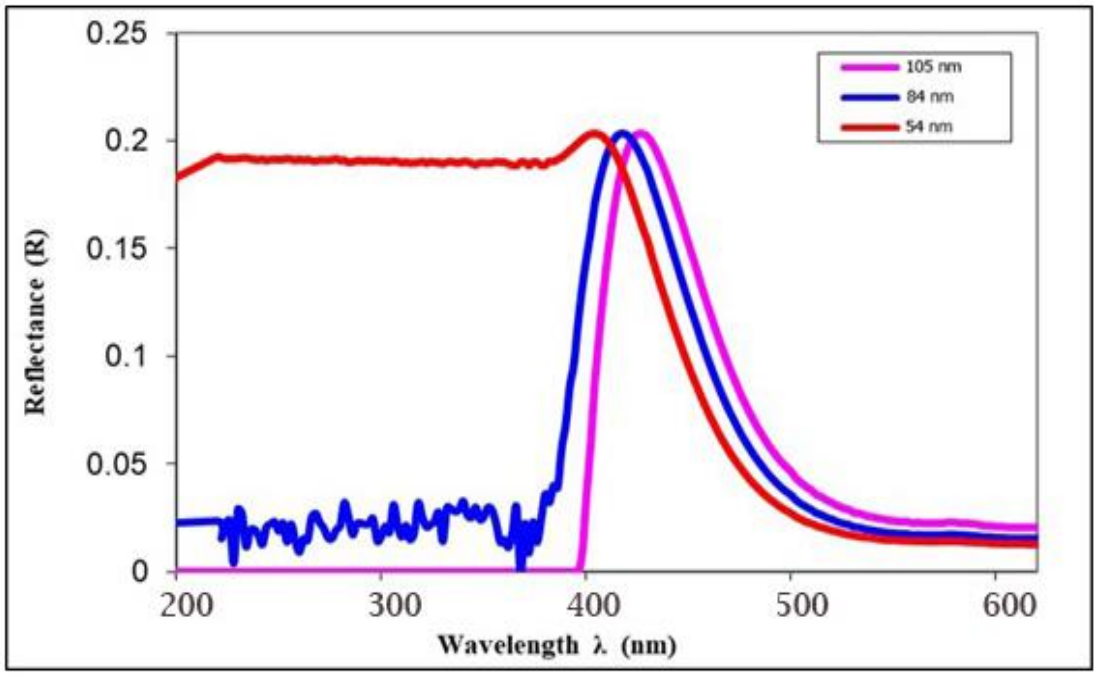


**Figure (4.15): Reflectance spectrum as a function of wavelength for PMMA thin films.**

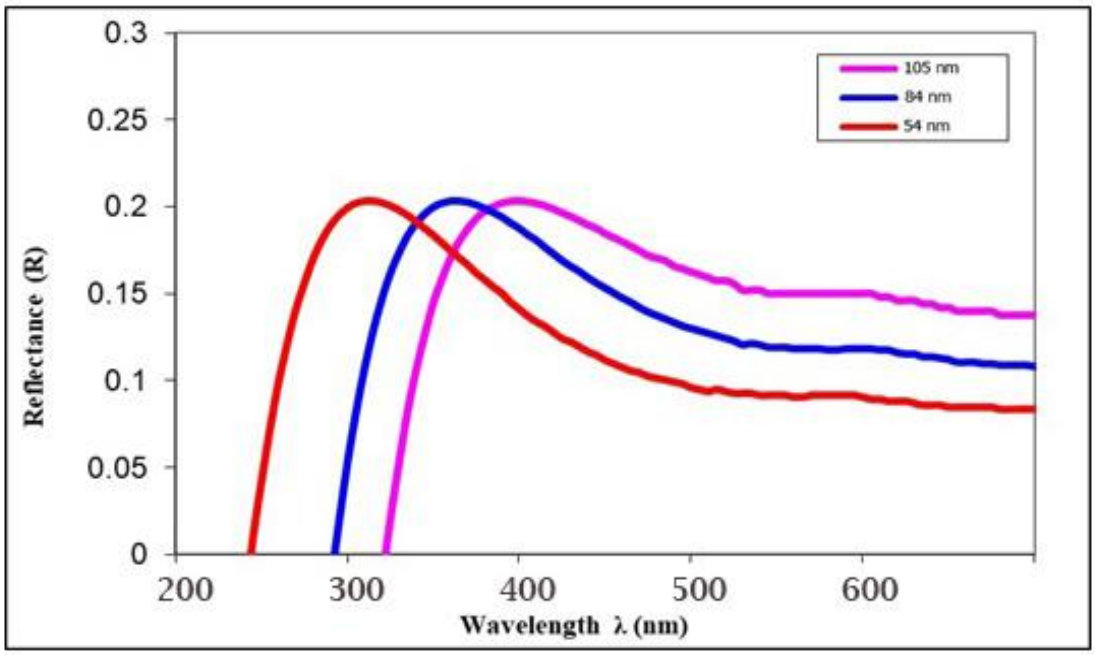


**Figure (4.16): Reflectance spectrum as a function of wavelength for PMMA: $P_3HT$thin films.**

### 4.3.4 Absorption Coefficient

The absorption coefficient α ($cm^{-1}$) is calculated by using equation (2.8). Figures (4.17 - 4.18) shows the absorption coefficient α ($cm^{-1}$)as a function of wavelength for the PMMA and PMMA:$P_3HT$ thin films. It can be seen that the absorption coefficient the smallest at large wavelength and low energy, this means that the possibility of electron transition is little because the energy of the incident photon is not sufficient to move the electron from the valence band to the conduction band.

From Figures (4.17 - 4.18) at high energies, absorption is bigger, this means that there is a great possibility for electron transitions. Consequently, the energy of incident photon is enough to move the electron from the valence band to the conduction band, the energy of the incident photon is greater than the forbidden energy gap, it is expected that indirect transition of electron occurs, and the electronic momentum is maintained with the assistance of the phonon, among

other results is that the coefficient of absorption is less than ($10^4$ $cm^{-1}$) at low concentrations. These results are in agreement with [99,100].

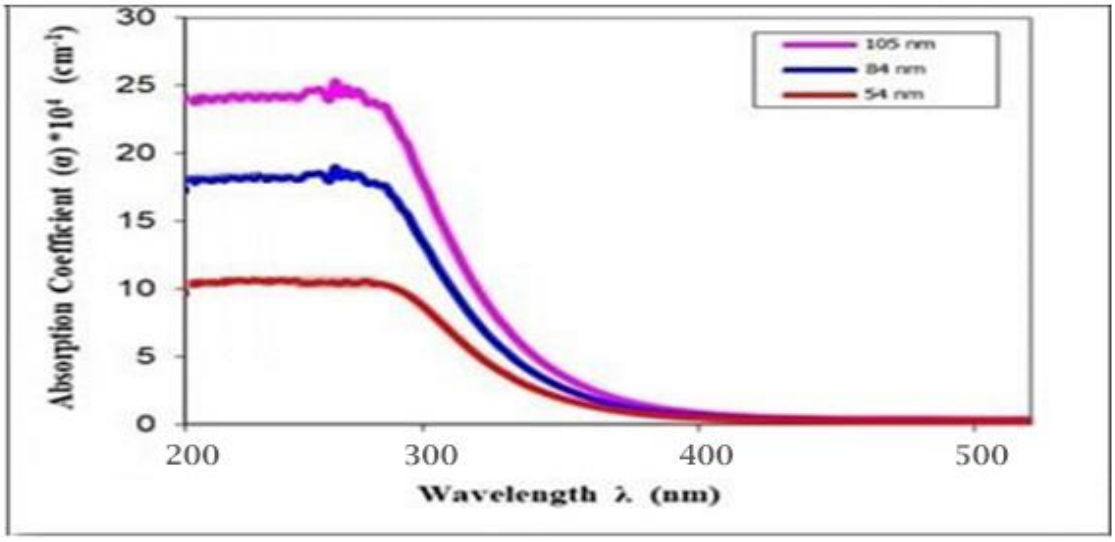


**Figure (4.17): Absorption coefficients as a function of wavelength for PMMA thin films.**

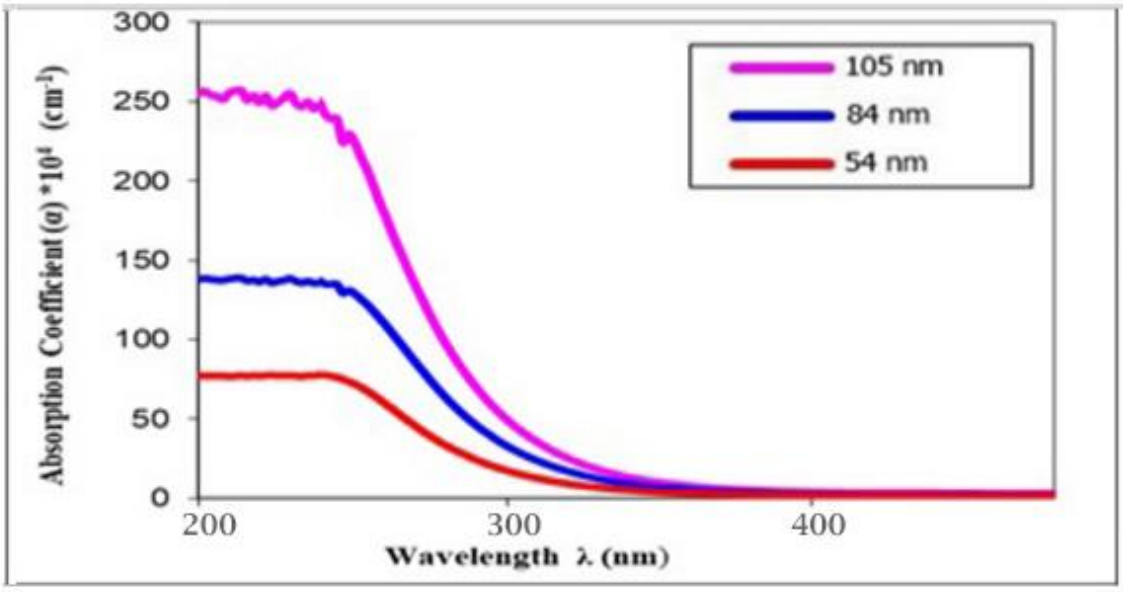


**Figure (4.18): Absorption coefficients as a function of wavelength for PMMA:$P_3$HT thin films.**

### 4.3.5 Optical Energy Gaps of the (Allowed and Forbidden) Indirect Transition

Both the allowed and forbidden indirect transition band optical energy gap have been calculated by using equation (2.18).When the value of r = 1/2, the allowed indirect transition band optical energy gap is calculated, but when the value of r =2/3, the forbidden indirect transition band optical energy gap is calculated. Figures (4.19- 4.20) show the relation between absorption edge $(\alpha h\nu)^{1/2}$ for PMMA and PMMA-$P_3HT$ thin films as a function of photon energy, on drawing straight line from the upper part of the curve toward the (x) axis at the value $(\alpha h\nu)^{1/2}$ =0 we get the optical energy gap for the allowed indirect transition. The obtained values are shown in table (4.3).We can see that the values of optical energy gap decrease with the increasing of the weight percentages. This attributed to the creation of site levels in the forbidden optical energy gap; the transition in this case is conducted in two stages that involve the transition of electron from the valence band to the local levels to the conduction band as a result of increasing the weight percentage. This behavior is attributed to the fact that films are of heterogeneous type (i.e. the electronic conduction depends on added concentration), the increase of the weight percentage provides electronic paths in the polymer which facilitates the crossing of electron from the valance band to the conduction band, which explains the decrease of optical energy gap with the increase of the weight percentage of PMMA and PMMA:$P_3HT$. These results are in agreement with [30, 101].

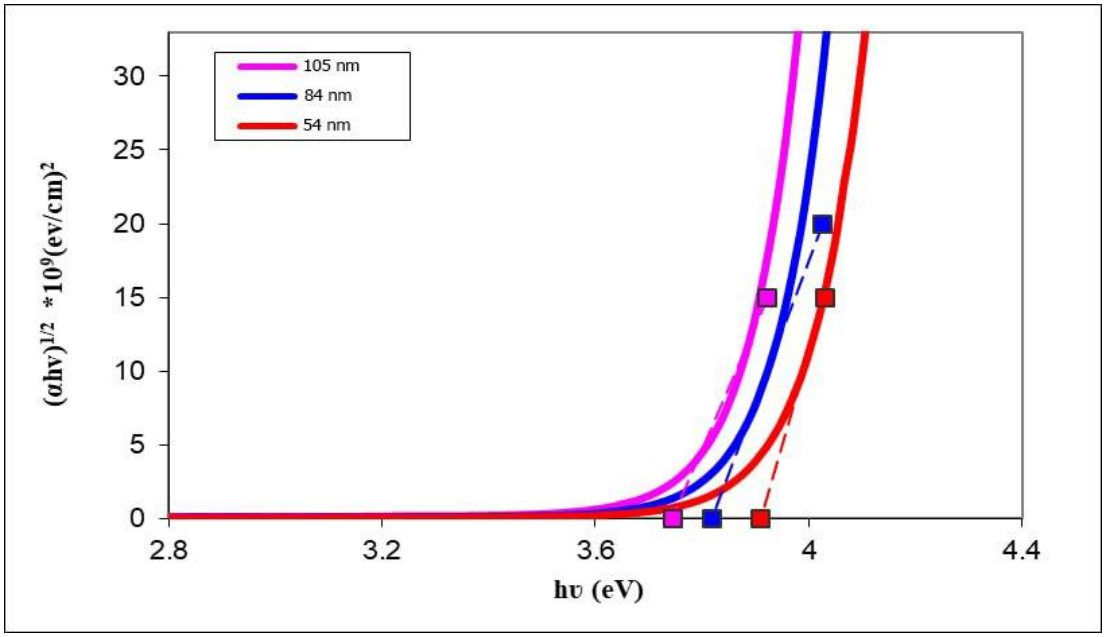


**Figure (4.19): $(\alpha h\upsilon)^{1/2}$ as a function of hυ for PMMA thin films.**

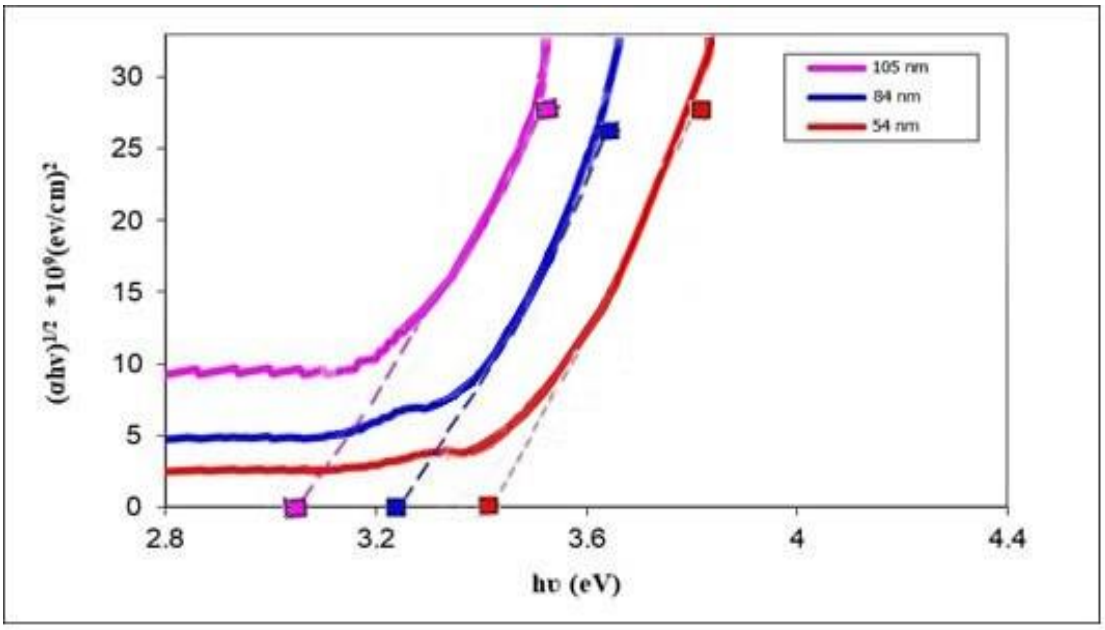


**Figure (4.20): $(\alpha h\upsilon)^{1/2}$ as a function of hυ for PMMA-$P_3$HT thin films.**

**Table (4.3): The values of optical energy gap for the allowed and forbidden indirect transition for PMMA thin films.**

| Thickness nm | $E_g$(eV) allowed | $E_g$(eV) forbidden |
|---|---|---|
| 105 | 3.745 | 3.213 |
| 84 | 3.818 | 3.514 |
| 54 | 3.91 | 3.708 |

**Table (4.4): The values of optical energy gap for the allowed and forbidden indirect transition for PMMA:$P_3$HT thin films.**

| Thickness nm | $E_g$(eV) allowed | $E_g$(eV) forbidden |
|---|---|---|
| 105 | 2.699 | 2.554 |
| 84 | 3.211 | 2.921 |
| 54 | 3.325 | 3.112 |

### 4.3.6 Refractive Index

The refractive index depends on many parameters of the type material and crystalline structure, the variation of the refractive index versus wavelength in the range of (200–600) nm for PMMA and PMMA:$P_3$HT thin films at different thickness are shown in Figures (4.21-4.22). It can be noticed from this figure the refractive index (n) value increases when thickness increases. This behavior can be explained on the basic of that increases thickness leads to make prepared samples less dense (decreasing the packing density) and the change in crystalline structure, which in turn increases propagation velocity of light through the sample which results decreasing of the refractive index (n) values. The shape of the refraction index curve for different parameters is similar to the reflectivity curve

because the reflectance is associated with refraction index according to the same relationship. These results are in agreement with [102].

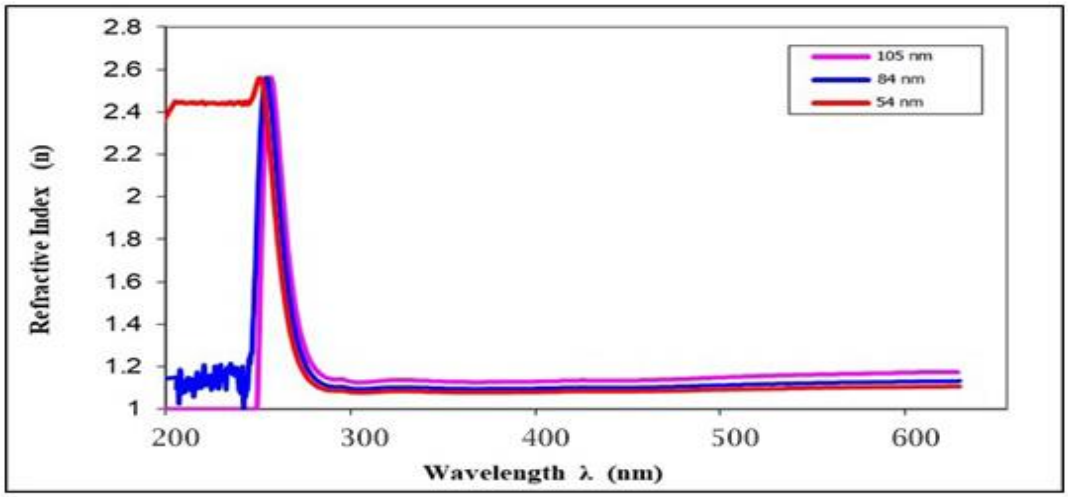


**Figure (4.21): Variation of refractive index as a function of wavelength for PMMA thin films.**

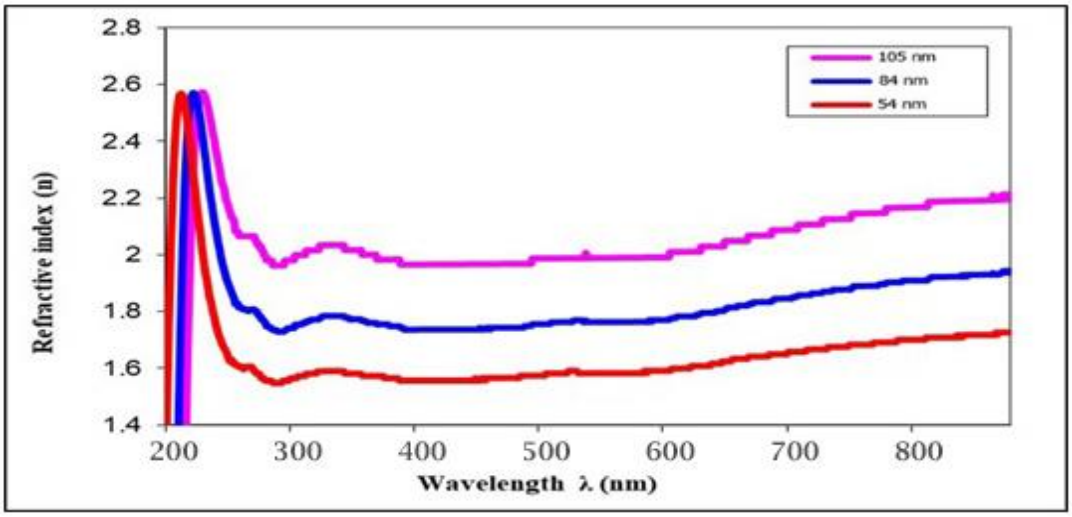


**Figure (4.22): Variation of refractive index as a function iof wavelength for PMMA:$P_3HT$ thin films.**

### 4.3.7 Extinction Coefficient

The extinction coefficient ($k_o$) is calculated by using equation (2.11), represents the amount of absorption energy in the thin film material, which means the attenuation of an electromagnetic wave that is traveling in a material. The

values of ($k_o$) depends on the density of free electrons in the material and also on the structure defects. The relationship between extinction coefficient and wavelength of deposited PMMA and PMMA:$P_3HT$ thin films is shown in Figures (4.23, 4.24). In general, it is clear that the extinction coefficient ($k_o$) change with the increasing of wavelength (λ) for all prepared samples. The extinction coefficient ($k_o$) decreases with the decreasing of thickness for all prepared samples. In general, the behavior of ($k_o$) similar to the behavior of α. This is attributed to the same reason mentioned previously, since the increasing of thickness decreases the optical energy gap as a result of absorbance increment. These results are in agreement with [103,104].

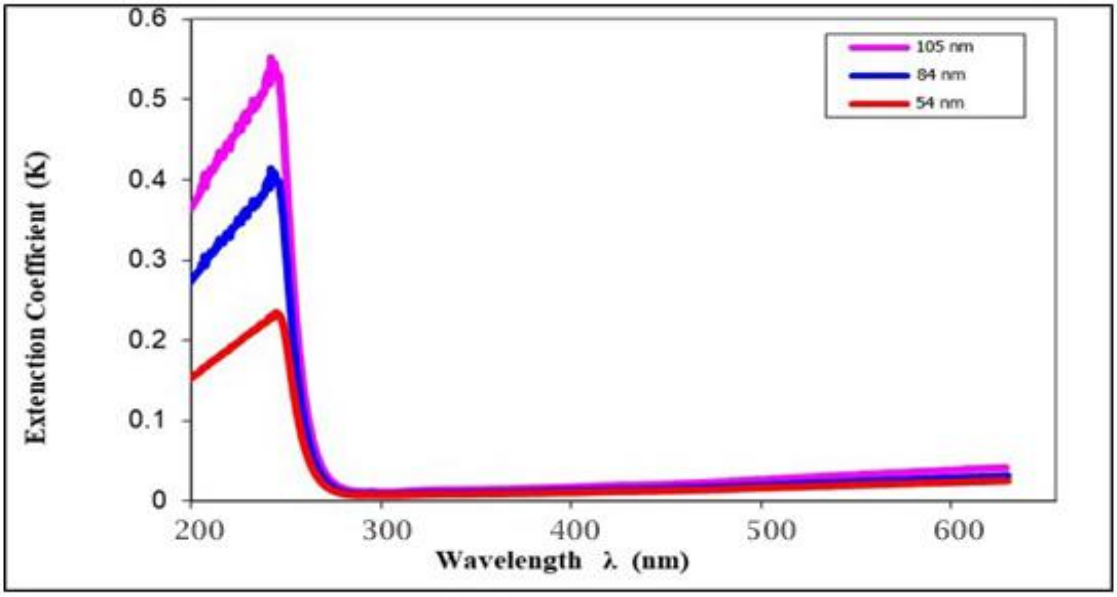


**Figure (4.23): Extinction coefficient as a function of wavelength for PMMA thin films.**

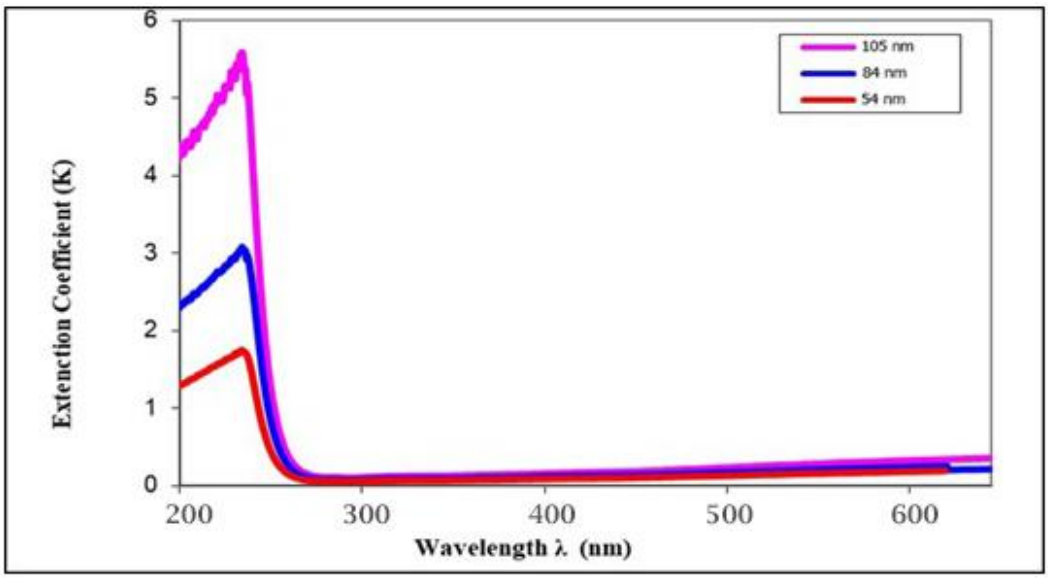


**Figure (4.24): Extinction coefficient as a function of wavelength for PMMA:$P_3HT$ thin films.**

### 4.3.8 Real and Imaginary Part of Dielectric constant

The real and imaginary complex dielectric constant ($\varepsilon_1$, $\varepsilon_2$) for PMMA and PMMA-$P_3HT$ thin films have been calculated from equations (2.15) and (2.16), respectively. The Figures (4.25, 4.26) show the change of ($\varepsilon_1$) as a function of the wavelength. It can be seen that ($\varepsilon_1$) considerably depends on ($n^2$) due to low value of ($k_o^2$) so, the real dielectric constant increased with the increase of the thickness and it is smallest at high wavelength. Figures (4.27, 4.28) show the change of ($\varepsilon_2$) as a function of the wavelength. It can be seen that ($\varepsilon_2$) is dependent on ($k_o$) values that change with the change of the absorption coefficient due to the relation between ($\alpha$) and ($k_o$). These results are in agreement with [104, 105].

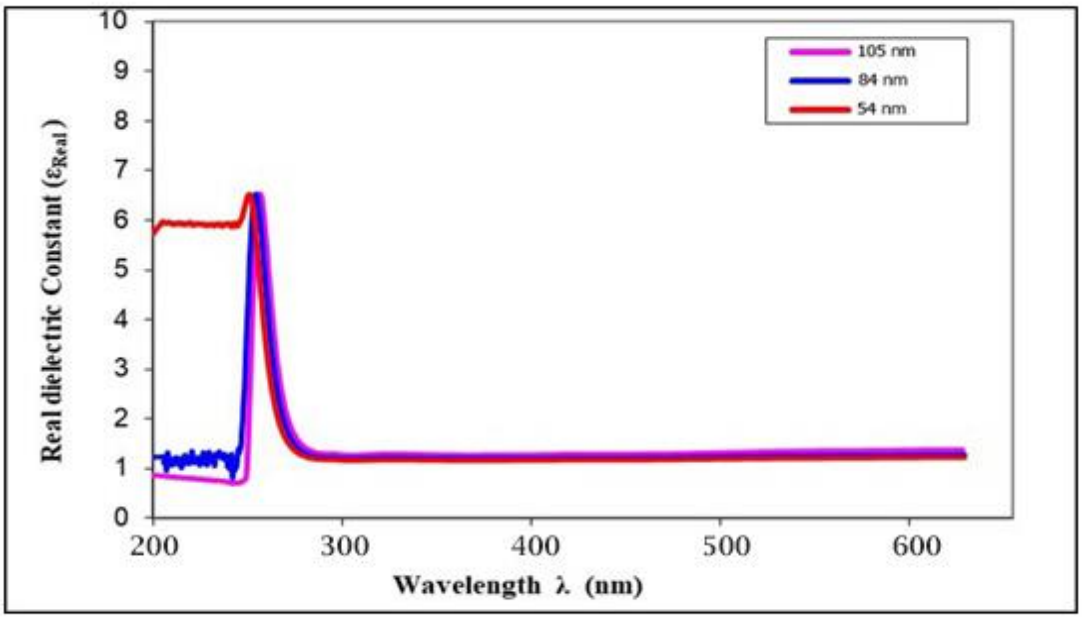


**Figure (4.25): Real dielectric constant as a function of wavelength for PMMA thin films.**

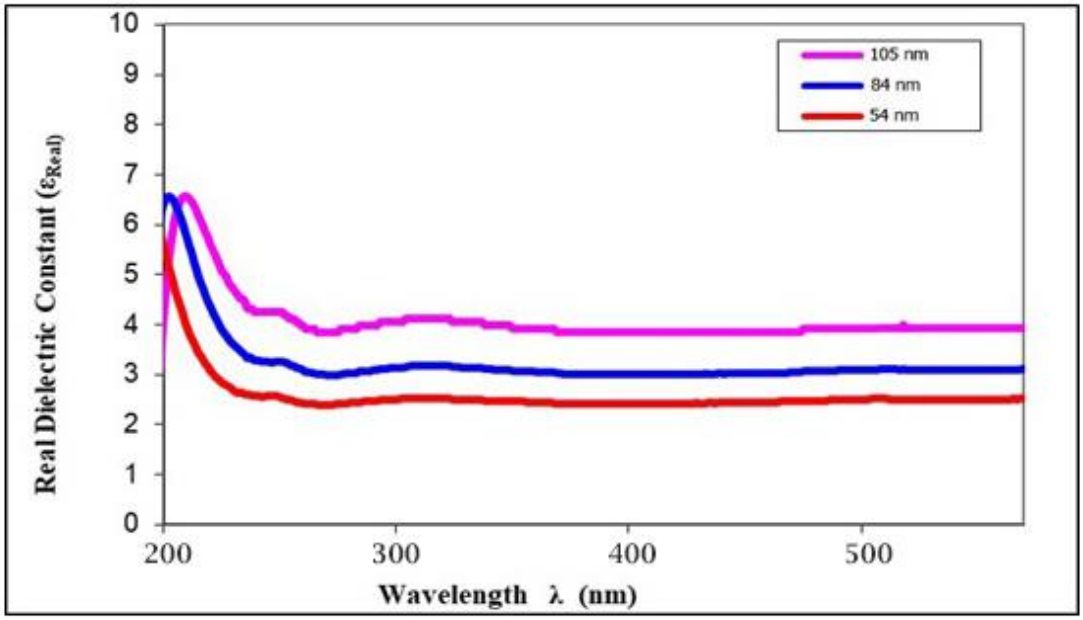


**Figure (4.26): Real dielectric constant as a function of wavelength for PMMA:$P_3HT$ thin films.**

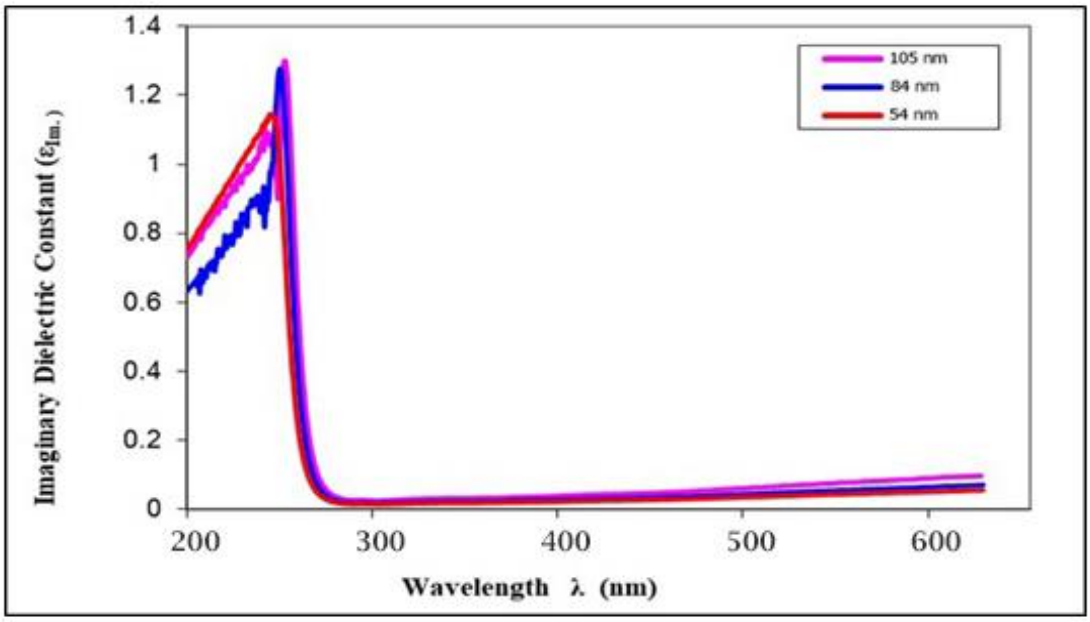


**Figure (4.27): Imaginary dielectric constant as a function of wavelength for PMMA thin films.**

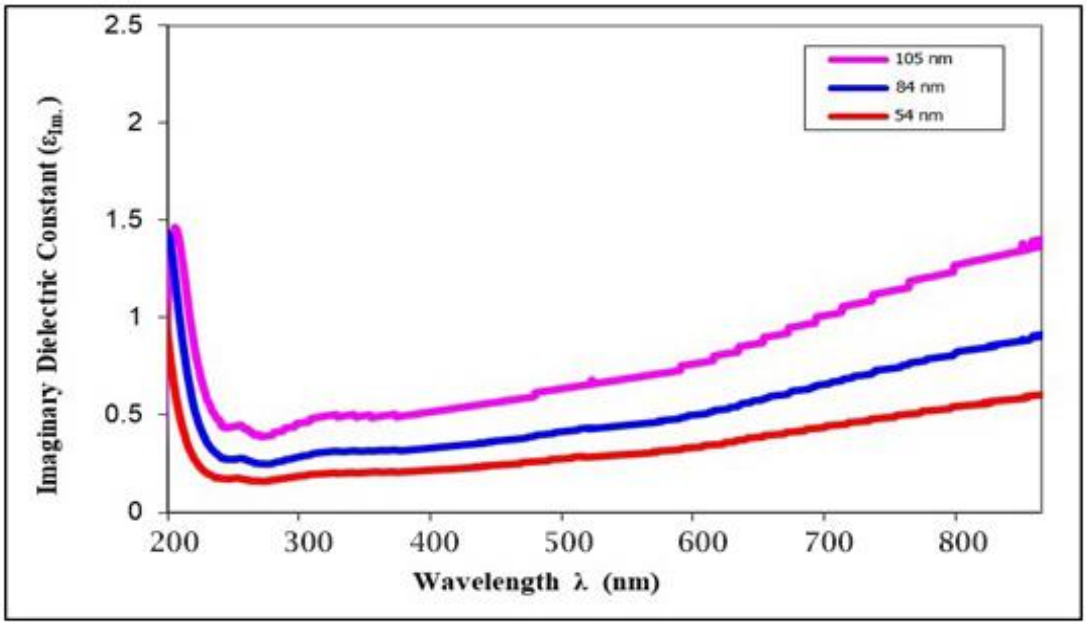


**Figure (4.28): Imaginary dielectric constant as a function of wavelength for PMMA:$P_3$HT thin films.**

## 4.4 Electrical Properties of PMMA and PMMA-$P_3HT$

The bulk electrical conductivity $\sigma_{d.c}$ is calculated for the prepared films by using equation (2-20). The detailed results of these properties are:

### 4.4.1 The D.C Conductivity and Activation Energy

In Figure (4-29) show us the behavior of electrical conductivity of the samples with the temperature. We note that the electrical conductivity increase with increasing temperature that means has a negative thermal coefficient of resistance .the interpretation of this is that the polymeric chains and $P_3HT$ particles act as traps the charge carriers which transited by hopping process. On increasing the temperature, segments of the polymer being to move, releasing the trapped charges. The released of trapped charges is intimately associated with molecular motion. The increase of current with temperature is attributed to two main parameters, charge carriers and mobility of these charges, and therefore the increase of temperature will increase the number of charge carriers exponentially. The mobility depends on the structure and the temperature these results are in agreement with [27,106]. The conductivity increases with increasing the proportion of doped as shown in Table (4-4).

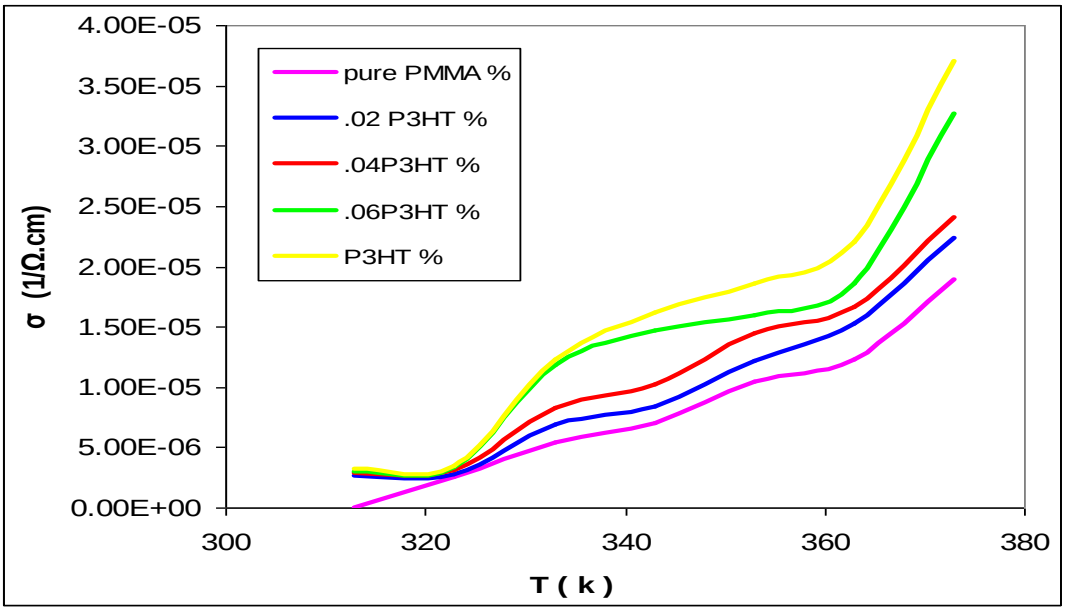


**Figure (4.29): Variation of D.C electrical conductivity with temperature for PMMA:$P_3HT$.**

**Table (4.5) Values of conductivity with concentration of PMMA:$P_3HT$ wt.% .**

| PMMA/$P_3HT$ wt.% | $\sigma_{d.c}$ $(\Omega . cm)^{-1}$ |
|---|---|
| Pure PMMA | 0.547 |
| 0.02 $P_3HT$ | 0.690 |
| 0.04 $P_3HT$ | 0.835 |
| 0.06 $P_3HT$ | 1.190 |
| Pure $P_3HT$ | 1.253 |

Figure (4.30) show the relation between lnσ and the inverse absolute temperature for PMMA-$P_3HT$. The activation energy was calculated by using

equation (2.25), and from these calculation, it can be seen that the high value existence for the activation energy in state of pure(PMMA) , and by adding weight ratios ($P_3HT$) the value of activation energy are decreasing for all (PMMA:$P_3HT$) Thin films as shown in Figure (4-30). The activation energy decreases with increasing the proportion of doped as shown in Table (4.5) , This can be explained that increasing the proportion of impurities led to the approach of the Fermi level more towards the conduction band. This is consistent with the findings of the researcher [107,108].

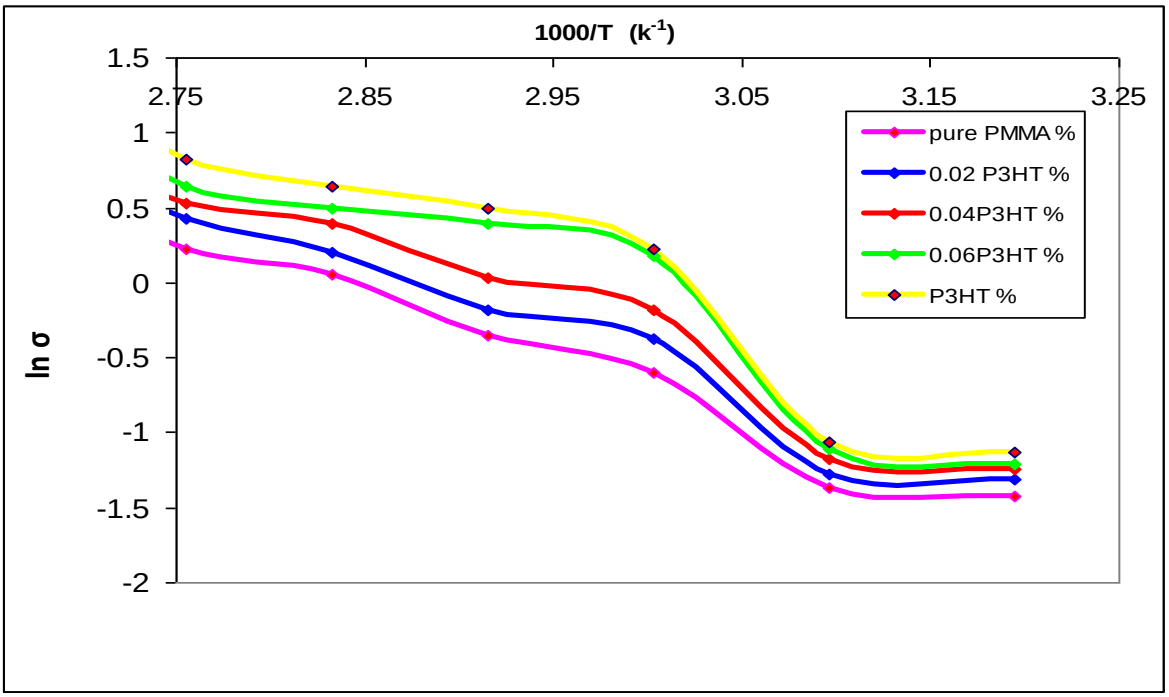


**Figure (4.30):Variation of D.C electrical conductivity with inverse absolute temperature for PMMA:$P_3HT$.**

**Table (4.6): Values of activation energy with concentration of PMMA:$P_3HT$.**

| (PMMA:$P_3HT$) wt.% | $E_a$ (eV) |
|---|---|
| **Pure PMMA** | **0.747** |
| **0.02 $P_3HT$** | **0.439** |
| **0.04 $P_3HT$** | **0.964** |
| **0.06 $P_3HT$** | **0.839** |
| **Pure $P_3HT$** | **1.142** |

## 4.5 J-V Characteristic of PMMA-$P_3HT$ Heterojunction Under Dark and Illuminated Conditions

Poly (methyl methacrylate) (PMMA) is one of the organic polymer that are widely using because of their applications in solar cells. It was obtained anisotype n-p heterojunction (HJ) by (PMMA: $P_3HT$/n- Si ) where (PMMA: $P_3HT$) are p-type and (Si) is n-type. The (J-V) Characteristics of (pure PMMA) solar cell devices in dark and Xenon illumination with intensity of 100mW/$cm^2$, is shown in Figures (4-31).The open circuit voltage $V_{oc}$ is about (0.36V) at short circuit current $J_{sc}$ about (11.6mA/cm). The fill factor (F.F) is about (0.62) and the efficiency (η) is about(2.6%).

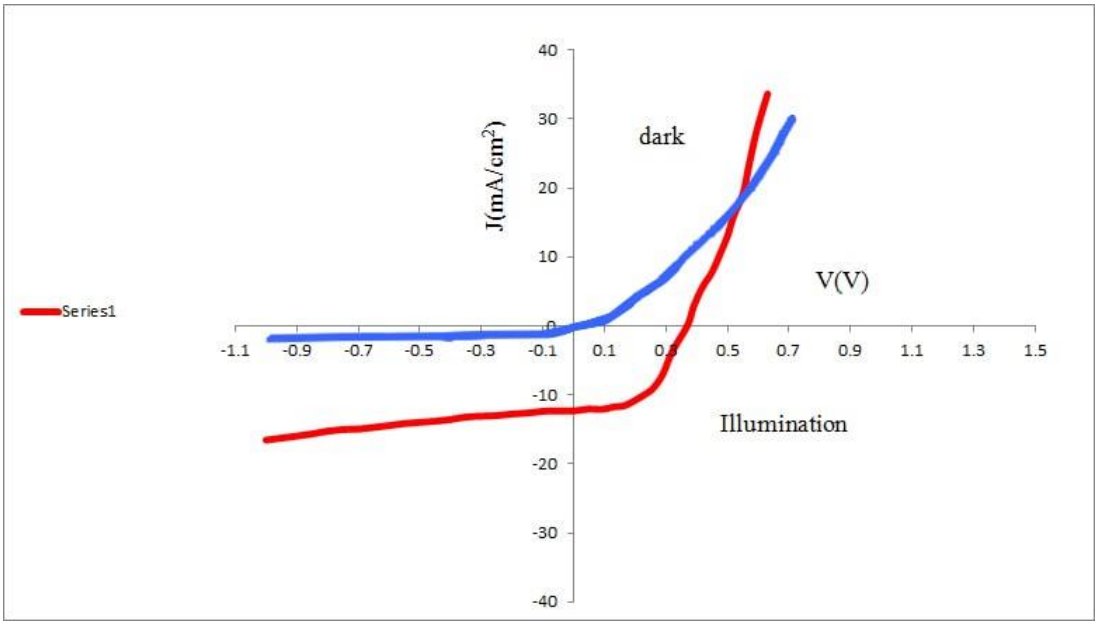


**Figure (4.31): J- V characteristic for PMMA/ Si solar cell.**

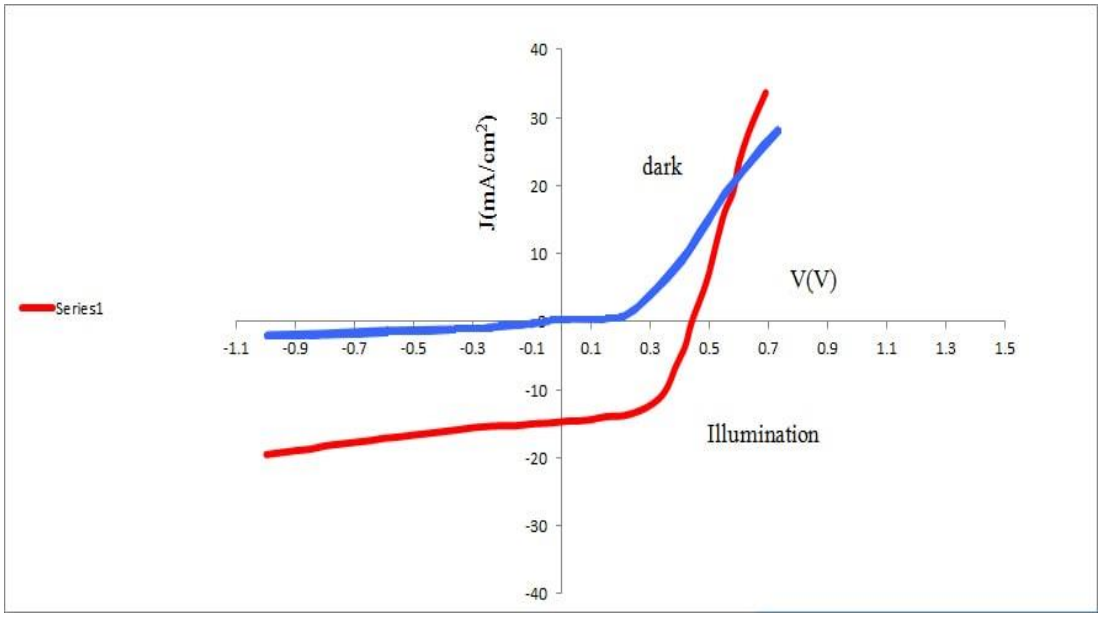


**Figure (4.32): J- V characteristic for $P_3HT$/ Si solar cell.**

When doping with( $P_3HT$) , the results showed an increasing in the value of the efficiency with an increasing in the ratio of doped , as in Figures(4.32 – 4.35). Where the efficiency increases from (3.58) with the ratio of doping (0.02) to (6.1)

by the ratio of doping (0.06) as in Table (4.6). This is consistent with the findings of the researchers [109].

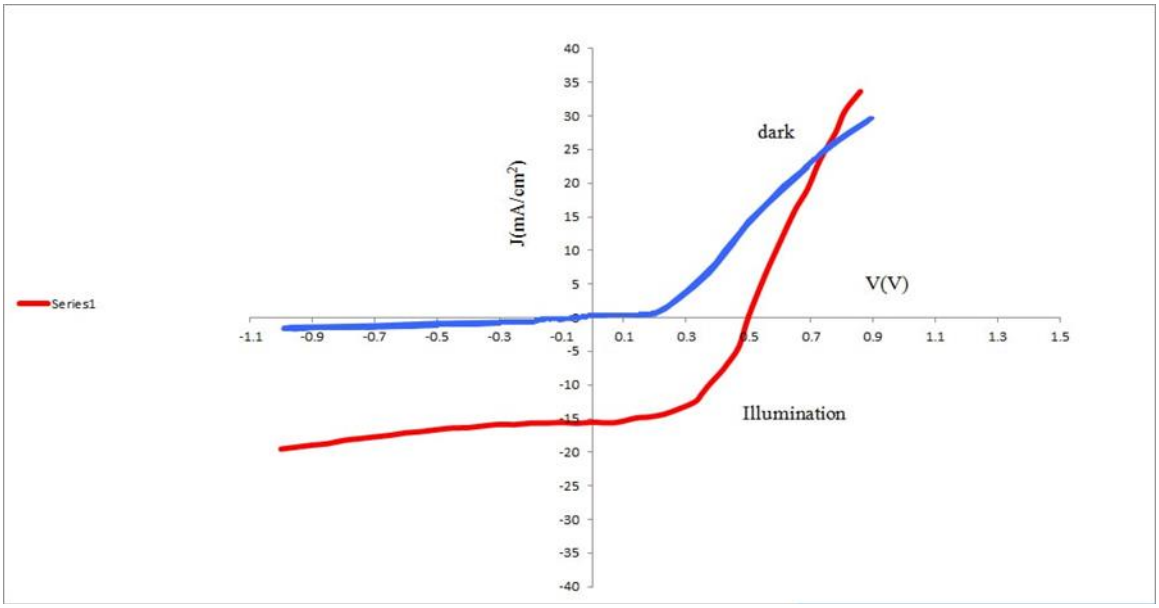


**Figure (4.33): J- V characteristic for PMMA: 0.02 $P_3HT$ / Si solar cell.**

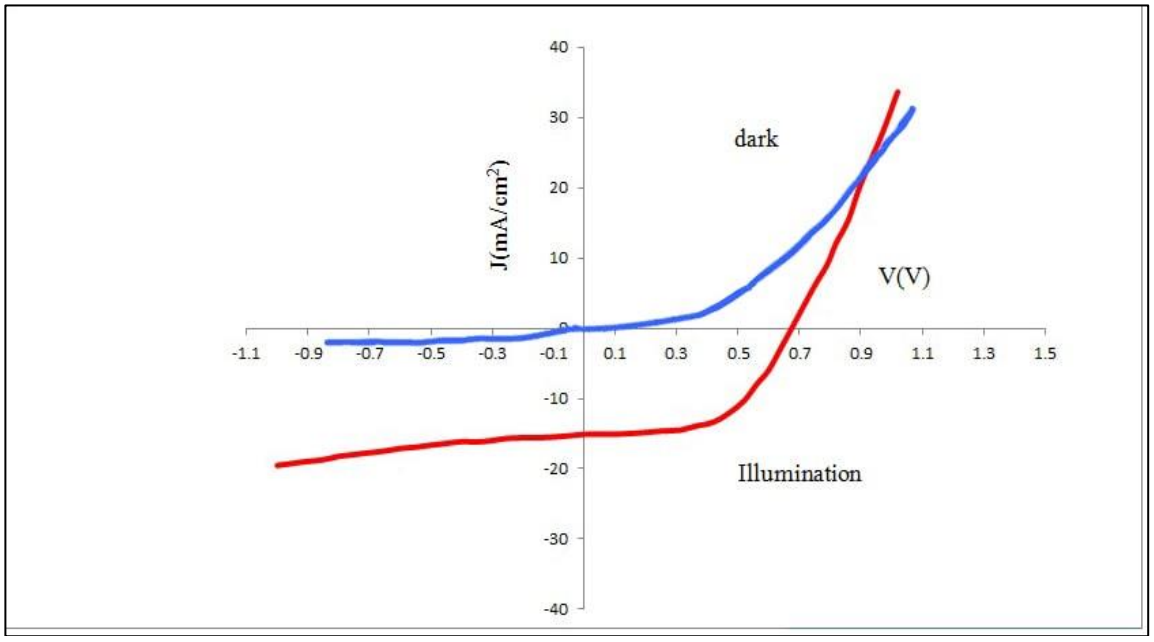


**Figure (4.34): J- V characteristic for PMMA: 0.04 $P_3HT$ / Si solar cell.**

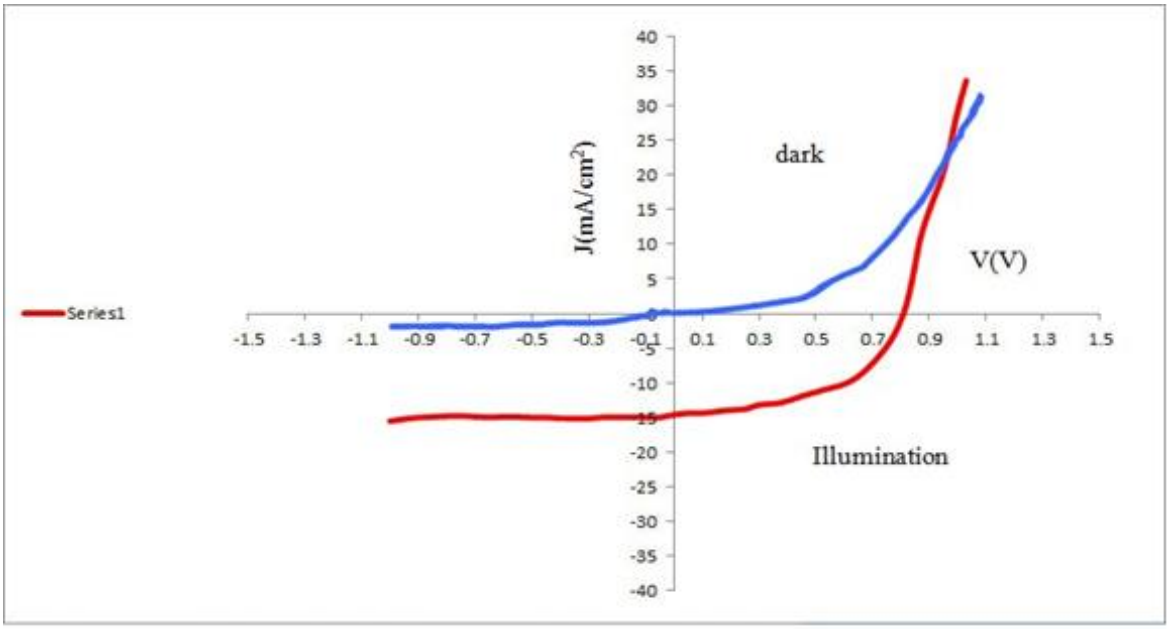


**Figure (4.35): J- V characteristic for PMMA: 0.06 $P_3HT$ / Si solar cell.**

**Table (4.7) The results of the J-V for PMMA-$P_3HT$ thin films at different concentration.**

| Devices based on con. | Jsc ($mA/cm^2$) | Voc (V) | $J_{max}$ (mA) | $V_{max}$ (V) | F.F (%) | η (%) |
|---|---|---|---|---|---|---|
| **Pure PMMA** | 11.6 | 0.36 | 10 | 0.26 | 0.62 | 2.6 |
| **Pure $P_3HT$** | 14.9 | 0.44 | 11.2 | 0.32 | 0.54 | 3.58 |
| **0.02% $P_3HT$** | 15.5 | 0.5 | 12 | 0.35 | 0.54 | 4.2 |
| **0.04% $P_3HT$** | 14.9 | 0.68 | 11 | 0.49 | 0.52 | 5.3 |
| **0.06% $P_3HT$** | 15.5 | 0.88 | 10 | 0.61 | 0.44 | 6.1 |

## 4.6 Stability of Cell Efficiency with Change of Time

For the purpose of proving the stability of cell efficiency with the change of time, the efficiency was measured for two months November in 2021 and March in 2022 for ten days measure it the results were identical for these two months with less different ratios, as shown in Figures (4.35and 4.36) .

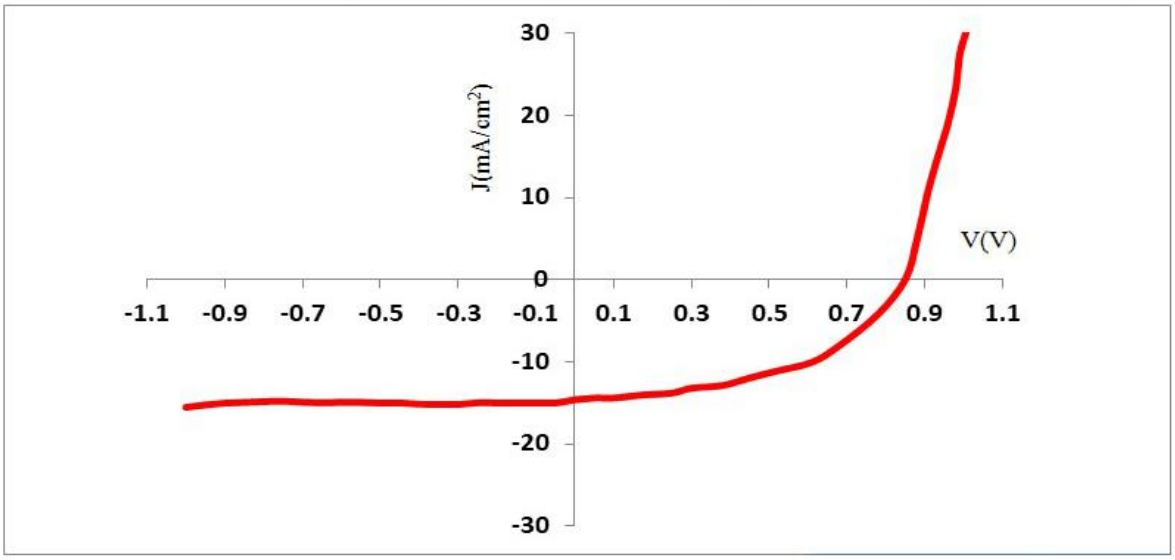


**Figure(4-36): J-V characteristic for PMMA: 0.06 $P_3HT$/ Si solar cell in 1st ten days in November.**

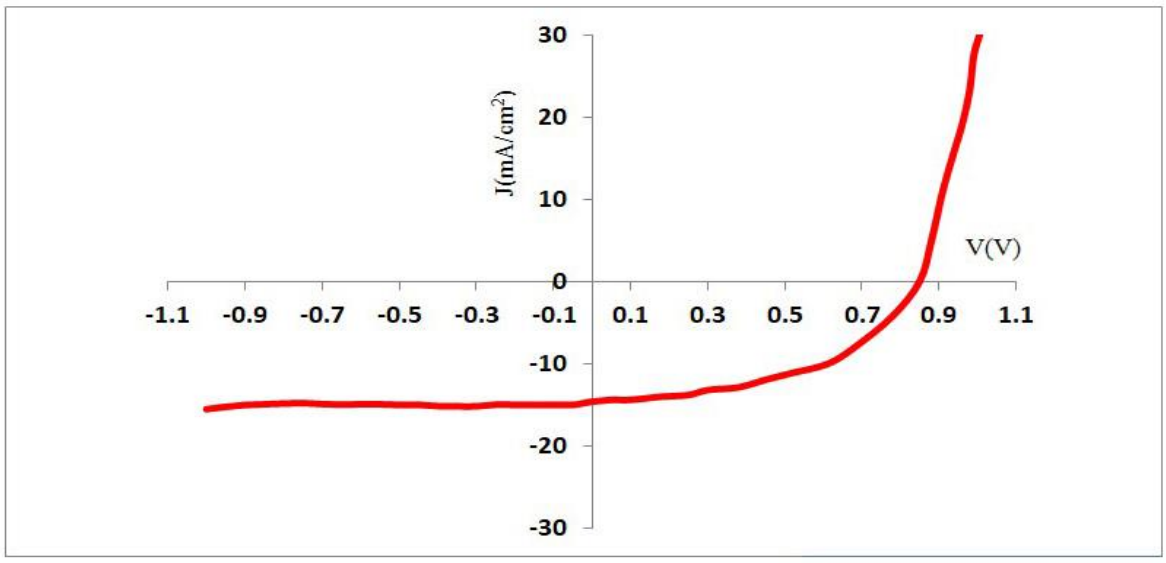


**Figure (4-37): J-V characteristic for PMMA : 0.06 $P_3HT$/Si solar cell in 1st ten days in March.**

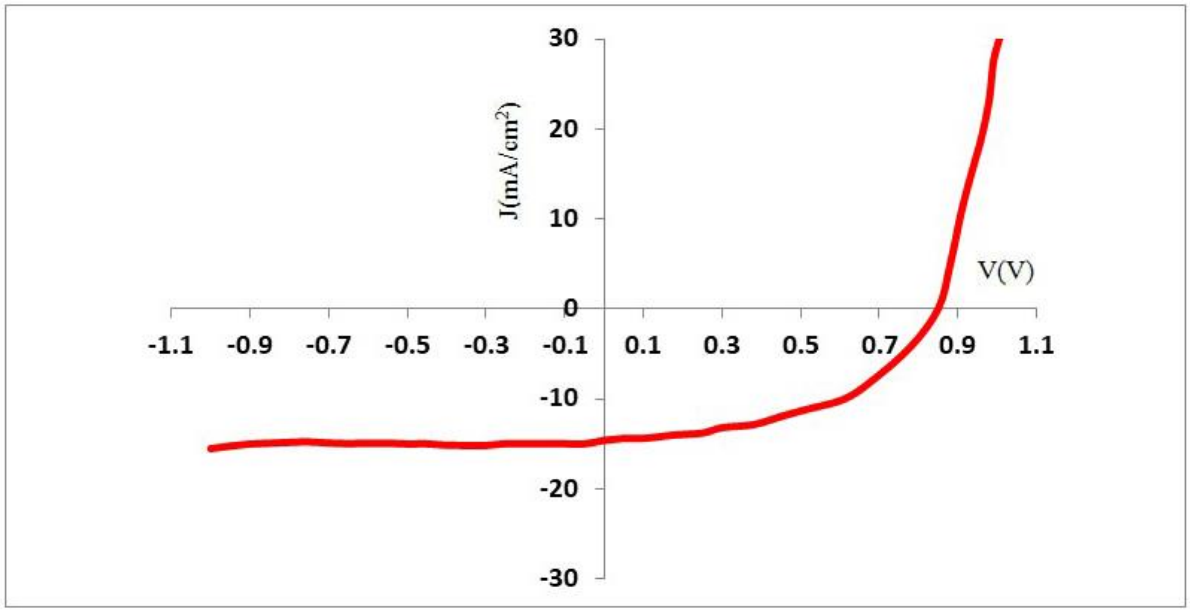


**Figure(4-38): J-V characteristic for PMMA: 0.06 $P_3HT$/Si solar cell in 2nd ten days in March.**

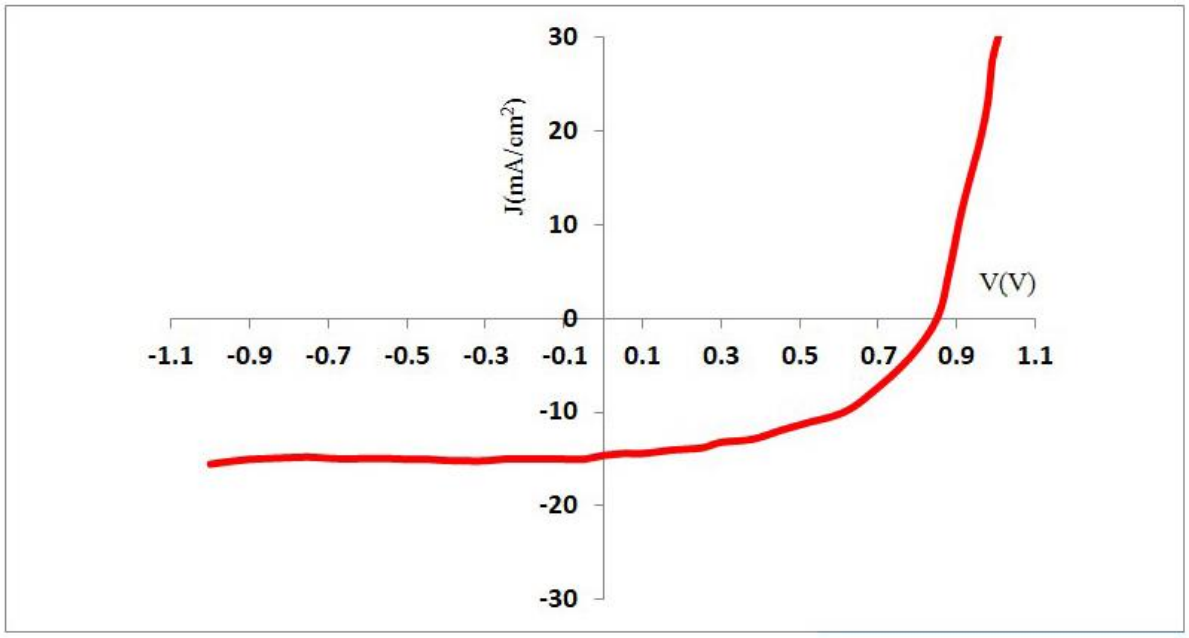


**Figure (4-39): J-V characteristic for PMMA:0.06 $P_3HT$/Si solar cell in 3ed ten days in March.**

## 4.7 Conclusions

In the light of these results and facts which have been mentioned previously in this work, adding process is very useful and important to enhance applications characteristics. Based on results presented in this work, we conclude the following points:

**1.** Spin coating technique is a good technique in the preparation of thin films and a preferred method in polymers with low molecular weights.

**2.** It is found through a study of XRD that these polymers polycrystallinity.

**3.** Study showed of AFM all films the roughness increased with increasing the ratio of doped a for the films surface morphology.

**4.** The addition of poly (3-hexylthiophene) to (PMMA) led to the improvement optical properties, these led to wide used in devices.

**5.** The optical study appear that the PMMA:$P_3HT$ thin films were highly absorbed with an indirect type of transition. The value of optical energy gap ($E_g$) was found decreased with increasing of doping ratio.

**6.** The results of the electrical properties showed that the electrical conductivity increases with increasing of doping ratio.

**7.** The prepared of thin films has one activation energy and this energy decreased with increasing of doping ratio.

**8.** Efficiency increases with increasing the rate of concentration PMMA:$P_3HT$ and the change in the time factor does not effect on the efficiency of the solar cell.

## 4.8 Suggestion for Future Works

Based on the data and the results obtained, we must mention some of the proposals for future work that could serve as future research:

1. Study the effect of poly (3-hexylthiophene) on the mechanical and thermal properties of poly (methyl methacrylate) and used as pyroelectric materials.
2. Irradiation of the pure and doped poly (methyl methacrylate) by γ- Ray and study the change in their properties.
3. Using the produced poly (methyl methacrylate) in practical application such as: cancer treatment and antibacterial reagent.
4. Study the effect of frequency and relative humidity on the capacitance of PMMA and PMMA-$P_3$HT thin film as humidity sensors application.

# REFERENCES

# References


**1-** R.W. Berry, P.M. Hall and T. Harris "Thin Film Technology", New York, (1979).

**2-** O.R. Ebewele , " Polymer Science and Technology " ,University of Benin City, Nigeria , (2000) .

**3-** J. Poortmans and V. Arkipov, "Thin Film Solar Cells", John Wiley and Sons publications, (2006).

**4-** L. Eckertova," Physics of Thin Films", Springer Science and Business Media, (2012).

**5-** R.F. Bunshaw, "Handbook of Deposition Technologies for Films and Coatings", 2nd ed., Noyes Publications, (1994).

**6-** I. D. Bower , " An Introduction to Polymer Physics", Published in the United States of America by Cambridge University Press, New York, (2002) .

**7-** C. christopher ibeh, "Thermoplastic Materials Properties, Manufacturing Methods, and Applications", CRC Press Taylor and Francis Group, pp.(391-402), (2011).

**8-** S. M. Sze, "Semiconductor Devices: Physics and Technology", John wiley and sons, (2008).

**9-** M. Adriana Forte, R. Manuel Silva, C. José Tavares, and R. Ferreira e Silva," Is Poly(Methyl Methacrylate) (PMMA) a Suitable Substrate for ALD?: A Review", Journal of Polymer, Vol.(13). No.(8), p.(1346) (2021).

**10-** A. Kiriy, V. Senkovsky, and M. Sommer Kumada," Catalyst-Transfer Polycondensation: Mechanism, Opportunities, and Challenges", Macromolecular rapid communications, Vol.(32), No.(19), pp.(1503-1517), (2011).

**11-** P. Bisi, Jr. dos Santos, H. Jorge da Silva Ribeiro , A. Costa Ferreira, Caio Campos Ferreira, L. Pinto Bernar , F. Paula da Costa Assunção, D. Alberto

# References

Rocha de Castro, M. Costa Santos, S. Duvoisin, Jr. Luiz Eduardo Pizarro Borges and N. Teixeira Machado," Process Analysis of PMMA-Based Dental Resins Residues Depolymerization: Optimization of Reaction Time and Temperature", Journal of Energies, Vol.(15), No. (1), (2021).

**12-** Y.G. Suu," Studies on Mechanical Properties of Poly ( Methyl Methacrylate) and Poly( Pethyl Methacrylate)- Modified Natural Rubber Blend ", MSc. Thesis, Semantic Scholar, (2008).

**13-** C. E. Carraher Jr., "Introduction to polymer chemistry", 4th Edition , CRC press (Taylor and Francis group), (2017).

**14-** J. Hwan Park, J. Soo Kim, J. Hwang Lee, W. Hyoung Lee, and K. Cho," Effect of Annealing Solvent Solubility on the Performance of Poly (3-Hexylthiophene)/Methanofullerene Solar Cells", The Journal of Physical Chemistry C, Vol.(113), No.(40), pp. (17579-17584), (2009).

**15-** K. Tremel and S. Ludwigs," Morphology of $P_3HT$ in Thin Films in Relation to Optical and Electrical Properties", Journal of Adv Polym Sci, (2014).

**16-** D.W Vankreven, P.J. Hoftyzer," Properties of polymers", Elsevier Scientific publishing Company, (1976).

**17-** A. M. Yasser Ismail, T. Soga , and T. Jimbo," Effect of Composition on Conjugation Structure and Energy Gap of $P_3HT$:PCBM Organic Solar Cell", International Journal of New Horizons in Physics, Vol. (2), No. (2), pp.(87-93), (2015).

**18-** A. Abbass Hashim, " Polymer Thin Films", Published by In-The, published April, (2010).

**19-** T. Anna, "Physical Chemistry of Polymers", translated by Akram Aziz Mohammed, University of Mosul, (1984).

# References


**20-** J. Roncali," Synthetic Principles for Bandgap Control in Linear π-Conjugated Systems", Chemical Reviews, Vol. (97), No. (1), 1997.

**21-** F. M. Smits, "History of silicon solar cell", IEEE Trans-Electron Devices, Vol( ED-23), (1976).

**22-** M. S. Abd Ali Khudair," Preparation of PANI – MWCNTs composite for Solar Cells Applications", Ph.D. Thesis, College of Science, University of Babylon, ( 2017).

**23-** B. Hussien , M. Abdul-Muhsien, A. Hashim," Study of Some Electrical Properties for PMMA-$TiO_2$ Composites", The Journal of Fondazione Giorgio Ronchi, Vol.(66), No. (1), (2010).

**24-** A. Jaipean, Ph. Suriyakiat, and K. Wasapinyokul," Transmittance of Baked Spin-Coated Poly(methyl methacrylate) Films", Published by the American Institute of Physics, Vol. (2010), No.(1), p.(020001), (2010).

**25-** L.N Ismail, Z. Habibah, M.H Abdullah, S.H. Herman, M. Rusop, "Electrical Properties of Spin Coated PMMA for OFETs Applications", International Conference on Electronic Devices, Systems and Applications (ICEDSA), pp.(333-338), (2011).

**26-** L. Nyl Ismail, H. Zulkefle, S. Hana Herman, and M. Rusop Mahmood," Influence of Doping Concentration on Dielectric, Optical, and Morphological Properties of PMMA Thin Films", Advances in Materials Science and Engineering, (2012).

**27-** A. Hassan Rasan," Dopping Effect on Optical Constant of Poly Methylacrelate (PMMA) Dopping With Phenolphthalein", Journal of Babylon University, Pure and Applied Sciences, Vol. (21), No.(4), (2013).

**28-** H. Neama Najeeb, A. Alaa Balakit, G. Abdul Wahab, A. Kadem Kodeary," Study of the Optical Properties of Poly (Methly Methaacrylate) (PMMA)

Doped with a New Diarylethen Compound", Academic Research International, Vol. (5), No.(1), (2014).

**29-** R. G. Kadhim," Study the Electrical and Structural Properties of (PMMA-$TiO_2$) Nanocomposites", Chemistry and Materials Research, Vol.(7), No. (9), (2015).

**30-** P. Maji, R.B. Choudhary, and M. Majhi," Structural, Optical and Dielectric Properties of $ZrO_2$ Reinforced Polymeric Nanocomposite Films of Polymethylmethacrylate (PMMA)" , Optik - International Journal for Light and Electron Optics, Vol.(127), No.(11), pp.(4848-4853), (2016).

**31-** Z. Shi, L. Song, and T. Zhang," Optical and Electrical Characterization of Pure PMMA for Terahertz Wide-band Metamaterial Absorbers", Optik - International Journal for Light and Electron Optics, Vol.(40), No.(1), pp.(80-91), (2018).

**32-** Ö. Bahadır Mergen, E. Arda , S. Kara, and O. Pekcan," Effects of GNP Addition on Optical Properties and Band Gap Energies of PMMA Films", International Conference on Society of Plastics Engineers, Vol.(40), No.(5),PP.(1862-1869), (2019).

**33-** A. Shaker Hussein, M. Hadi Shinen, and M. Sami Abdali," Study the Effect of Thickness on Optical Properties of Polymer PMMA Thin Films Preparated by Spin CoatingMethod", Journal of University of Babylon for Pure and Applied Sciences, Vol. (27), No.(4), (2019).

**34-** A. A. Hasan, and A. A. Mohammed," Optical and A.C. Electrical Properties of PMMA/CB, PMMA/G and PMMA/(CB+G) Composite", Journal of Nanomaterials and Biostructures, Vol.(15), No.(3), (2020).

**35-** M. Qais Al-Bataineh , A. Ahmad , A.M. Alsaad , D. Ahmad Telfah, "Optical Characterizations of PMMA/ Metal Oxide Nanoparticles Thin

Films: Bandgap Engineering Using a Novel Derived Model", Journal of Heliyon, Vol.(7), No.(1), (2021).

**36-** A. Hazim, A. Hashim, and H. Abduljalil," Fabrication of Novel (PMMA-$Al_2O_3$/Ag) Nanocomposites and its Structural and Optical Properties for Lightweight and Low Cost Electronics Applications", Egyptian Journal of Chemistry, Vol. (64), No.(1), pp.(359–374), (2021).

**37-** A. Areen Bani-Salameh , A. A. Ahmad , A. M. Alsaad , I. A. Qattan, and A. Ihsan Aljarrah," Synthesis, Optical, Chemical and Thermal Characterizations of PMMA-PS/$CeO_2$ Nanoparticles Thin Film", Journal of Polymer, Vol. (13), No.(7), (2021).

**38-** S. Sarid," Scanning Force Microscopy", Oxford, U.K., Oxford University Press, (1994).

**39-** Sh. Ahmad, A. Sharif, and S. Agnihotry," Synthesis and Characterization of in Situ Prepared Poly (Methyl Methacrylate) Nanocomposites", Bulletin of Materials Science, Vol.(30), No.(1), pp. (31-35), (2007).

**40-** H. H. Abbas," Study Structural and Optical Properties of CdSe: Al Thin Films as a Function of Doping Ratio and Annealing Temperature", MSc. Thesis, University of Baghdad, (2015).

**41-** S. M. Sze, "Physics of Semiconductor Devices", John Wiley and Sons, (1981).

**42-** S. Giridharan, and P. Shankar,"Optical Charastrazation of PMMA Doped With an Organic Polymer", ISSUE: Engineering and Technolohy, IIOAB Journal, Vol.( 9), pp.(18-25), (2018).

**43-** G. S. Roland Goh, R. Eric Waclawik , N. Motta , M. John Bell," Influence of Dispersed Carbon Nanotubes on the Optical and Structural Properties of a

Conjugated Polymer", Device and Process Technologies for Microelectronics, Vol. (6037), pp. (264-270), (2005).

**44-** K. Tagreed Hamad," Refractive Index Dispersion and Analysis of the Optical Parameters of (PMMA/PVA) Thin Film", Journal of Al-Nahrain University, Vol. (16), No.(3), (2013).

**45-** K. Ahmad, and M. Shaikh Mobin, "Graphene Oxide Based Planar Heterojunction Perovskite Solar Cell Under Ambient Condition", The Royal Society of Chemistry and the Centre National de la Recherche Scientifique, Vol.(41), No.(23), pp.(14253-14258),(2017).

**46-** Z. Sahhib Obaid," Physical Properties of PMMA/ZnO Composite Material", MSc. Thesis, AL-Nahrain University, (2017).

**47-** R. Balen, W. Vidotto da Costa, J. de Lara Andrade, J. Francis Piai, E. Curti Muniz, M. Vianna Companhoni, T. Ueda Nakamura, S. Marcio Lima , L. Humberto da Cunha Andrade , P. Rodrigo Stival Bittencourt, A. Adelina Winkler Hechenleitner, E. Alfonso Gómez Pineda, and D. Martins Fernandes," Structural, Thermal, Optical Properties and Cytotoxicity of PMMA/ZnO Fibers and Films: Potential Application in Tissue Engineering", Journal of applied surface science, Vol.(385), pp.(257-267), (2016).

**48-** P. Custodio, P. A. Ribeiro, M. Raposo and S. Sério, "Development of Graphene Oxide and $TiO_2$ Heterojunctions for Hybrid Solar Cells", Science and Technology Publications, Vol. (2), pp. (386-390), (2018).

**49-** L. Hrostea, M. Girtan , R. Mallet, and L. Leontie," Optical and Morphological Properties of $P_3HT$ and $P_3HT$: PCBM Thin Films Used in Photovoltaic Applications", IOP Conf. Series: Materials Science and Engineering, Vol. (374), No.(1), p. (012015), (2018).

# References


**50-** G. S. Roland Goh, R. Eric Waclawik, N. Motta, M. John Bell," Influence of Dispersed Carbon Nanotubes on the Optical and Structural Properties of a Conjugated Polymer", The International Society for Optical Engineering, Vol. (6037), pp. (264-270), (2005).

**51-** J. I. Pankove, "Optical Process in Semiconductors", Dover Publishing, Inc., New York. (1971).

**52-** S. M. Sze, "Semiconductor Devices Physics and Technology", Prentice-Hall of India private Limited ,(1985) .

**53-** Mohammed J.," Preparation of some Organic Nanocomposites for Solar Cells and Sensing Applications", Ph.D. Thesis, College of Science, University of Babylon, ( 2017).

**54-** C. Kittel, "Introduction to Solid State Physics", 5th Ed., Willy, New York, (1981).

**55-** S. Mustafa," Engineering Chemistry", Lib. of Arab Society for Publication and Distribution, Jordan, (2008).

**56-** A. N. Donald, "Semiconductor Physics and Devices", Irwin, USA, (1992).

**57-** L. Hrostea, M. Girtan, R. Mallet, and L. Leontie," Optical and Morphological Properties of P3HT and P3HT: PCBM Thin Films Used in Photovoltaic Applications", In IOP Conference Series: Materials Science and Engineering, Vol. (374), No.(1), (2015).

**58-** J. Oras," Study Some of Physical Properties of Conductive Polyaniline: Polyamide Blends as Gas Sensor", Ph.D. Thesis , College of Science, University of Babylon, ( 2020).

**59-** M. Hashem, M. Fayez AL-Rez, H. Fouad, T. Elsarnagawy, M. A. Elsharawy, A. Umar, M. Assery, and S. G. Ansari, " Influence of Titanium Oxide Nanoparticles on the Physical and Thermomechanical Behavior of

Poly Methyl Methacrylate (PMMA): A Denture Base Resin", Journal of Science of Advanced Materials, Vol. (9), pp. (938–944), (2017).

**60-** W. Wang and E. A. Schiff, "Polyaniline on Crystalline Silicon Heterojunction Solar Cells", Applied Physics Letters, Vol.(91), No. (13), p. (133504), (2007).

**61-** A. Al.maamori ," Characterizations of Nanostructure $(SnO_2)1\text{-}x(ZnO)x$ Thin Films and their Applications", Ph. D. thesis, College of Science, University of Babylon, (2017).

**62-** H. Q. Zhang, Y. Jin, and Y. Qiu," The Optical and Electrical Characteristics of PMMA Film Prepared by Spin Coating Method", In IOP Conference Series: Materials Science and Engineering, Vol.(87), No.(1), p.(012032). IOP Publishing, (2015).

**63-** N. F. Mott and E. A. Davis, "Electronic Process in Non-Crystalline Materials", 2nd ed., Clarendon Press, Oxford, (1979).

**64-** A. R. Siekkinen, J. M. McLellan, J. Chen and Y. Xia, "Rapid Synthesis of Small Silver Nanocubes by Mediating Polyol Reduction With a Trace Amount of Sodium Sulfide or Sodium Hydrosulfide", Chem. Phys. Lett., Vol. (43), pp. ( 491–496), (2006).

**65-** A. N. Abd, "Quantum dots CdSe/PSi/Si photodetector", Ph.D. thesis, University of Mustansiriyah, (2015).

**66-** M. B. Chorin , F. Moller and F. Koch, "Band Alignment and Carrier Injection at the Porous-Silicon Crystalline-Silicon Interface", J. Appl. Phys., Vol. (77), No.(9), pp. ( 4482–4488) , (1995).

**67-** H. Ito, S. Tagawa, and K. Horie," Polymeric Materials for Microelectronic Applications", Science and Technology, American Chemical Society, (1995).

# References


**68-** S. S. Hegedus, and B. E. McCandless," CdTe Contacts for CdTe/CdS Solar Cells: Effect of Cu Thickness, Surface Preparation and Recontacting on Device Performance and Stability", Solar Energy Materials and Solar Cells, Vol.(88), No.(1), pp.(75-95), (2005).

**69-** M. Green, "Limits on the Open-Circuit Voltage and Efficiency of Silicon Solar Cells Imposed by Intrinsic Auger Processes", IEEE Trans. Electron. Dev., Vol.(31), pp.(671–678), (1984).

**70-** S Azizi, MB Ahmad, MZ Hussein, NA Ibrahim, F. Namvar," Preparation and Properties of Poly (Vinyl Alcohol)/Chitosan Blend Bionanocomposites Reinforced With Cellulose Nanocrystals/ZnO-Ag Multifunctional Nanosized Filler", International journal of nanomedicine, Vol.(9), No.(1909), ( 2014).

**71-** M.K. Mohammed, "Fabrication and Study the Effect of AL-doping on Efficiency of ZnO:Al/Si Solar Cell Prepared by Thermal Evaporation Technique", M.Sc. Thesis, University of Babylon, (2016).

**72-** H. F. H. Al-Luaibi , "Preparation of Conducting Poly (O-Toluidine) and Study of its Electrical and Optical Properties For Application as a Solar Cells", Ph. D. Thesis Basrah University, (2010).

**73-** W. M. Abdulridha, "Fabrication and Characterization Study of CNTs/PSi Photodetector", Ph.D. Thesis ,University of Babylon , College of Science , Department of Physics, (2015).

**74-** M.D. Uplane, Kshirsagar P.N., Lokhande B.J. and Bhosale C.H., "Characteristic Analysis of Spray Deposited Cadmium Oxide Thin Films", Materials Chemistry and Physics, Vol.(64), pp. (75–78), (2000).

**75-** M.A. Islam and M.S. Hossain, "Comparison of Structural and Optical Properties of CdS Thin Films Grown by CSVT, CBD and Sputtering

Techniques", Solar Energy Research Institute, The National University of Malaysia, Vol.(33) , pp.( 203-213),(2013).

**76-** S. Ali Shawai ," Preparation and Study of the Physical (Dopant, Temperature and Band Gap) and Electrical Properties on Conducting (PANI-Cu) Composites", M.Sc. Thesis, University of Wasit, College of Science, (2021).

**77-** H. S. Abdulla, and I. A. Abdullah, "Optical and Electrical Properties of Thin Films of Polyaniline and Polypyrrole", Int. J. Electrochem. Sci Vol.(7), No. (11), pp.( 10666-10678), (2012).

**78-** S. Sriram, A. Balu and A. Thayumanavan , "Design and Development of Automated Liquid Flow Deposition Method for Thin Film Formation", Applied Science Research, Vol.(3), pp. (438-447), (2011).

**79-** P. R. Berger and M. Kim," Polymer solar cells: $P_3$HT:PCBM and beyond", Journal of Renewable and Sustainable Energy, Vol. (10), No. (013508), (2018).

**80-** F. Timothy O'Connor, V. Aliaksandr Zaretski, S. Savagatrup, D. Adam Printz," Wearable Organic Solar Cells With High Cyclic Bending Stability: Materials Selection Criteria", Journal of Solar Energy Materials and Solar Cells, Vol.(144), PP.( 438-444), (2016).

**81-** S. Lizin, J. Leroy, C. Delvenne, M. Dijk, E. D. Schepper, and S. Van Passel, "A patent landscape Analysis For Organic Photovoltaic Solar Cells: Identifying the Technology's Development Phase," Journal of Renewable Energy, Vol.(57), PP.(5–11), (2013).

**82-** Sh. Ma, Sh. Pang, H. Dong, X. Xie, G. Liu, P. Dong, D. Liu, W. Zhu, H. Xi, D. Chen, Ch. Zhang, and Y. Hao," Stability Improvement of Perovskite

Solar Cells by the Moisture-Resistant PMMA: Spiro-OMeTAD Hole Transport Layer", Journal of Polymer, Vol.(14), No.(343), (2022).

**83-** B. Kadem, M. Göksel, A. Şenocak, E. Demirbaş, D. Atilla, M. Durmuş, T. Basova, K. Shanmugasundaram, A. Hassan," Effect of Covalent and Non-Covalent Linking on the Structure, Optical and Electrical Properties of Novel Zinc(II) Phthalocyanine Functionalized Carbon NanoMaterials", Journal of Polyhedron, Vol. (110), PP.( 37-45), (2016).

**84-** A. Raheem, K. AbidAli, A. Hashim, and A. Ali," The D.C and A.C Electrical Properties of Polymer Filled with Metal Powder", The Iraqi Journal For Mechanical and Material Engineering, Vol.(13), No.(2), (2013).

**85-** M. ChungWu, H. ChungLiao, H. singLo, Sh. Chen, Y. YueLin, W. CheYen, T. WeiZeng, Ch. WeiChen, Y. FangChen, and W. FangSu, "Nanostructured Polymer Blends ($P_3HT$/PMMA): Inorganic Titania Hybrid Photovoltaic Devices", Solar energy materials and solar cells, Vol.(93), Issues (6-7), pp.(961-965), (2009).

**86-** A. Kumar Mishra," Conducting Polymers: Concepts and Applications", Journal of Atomic, Molecular, Condensate and Nano Physics Vol.(5), No.(2), pp. (159–193), (2018).

**87-** N. S. Alghunaim, "Spectroscopic Analysis of PMMA/PVC Blends Containing $CoCl_2$", Journal of Results in Physics, Vol.(5), pp.( 331-336), (2015).

**88-** G. Kalonga, G. K. Chinyama, M. O. Munyati, and M. Maaza. "Characterization and Optimization of Poly (3-Hexylthiophene-2,5-diyl)($P_3HT$) and [6,6] Phenyl-C61-Butyric Acid Methyl Ester (PCBM)

blends for optical absorption," Journal of Chemical Engineering and Materials Science, Vol. (4), No. (7), pp.(93-102), (2013).

**89-** V. Shrotriya, J. Ouyang, R. J. Tseng, G. Li, and Y. Yang, "Absorption Spectra Modification in Poly (3-Hexylthiophene): Methanofullerene Blend Thin Films", Chemical physics letters, Vol.(411), No.( 3), pp.(138-143), (2005).

**90-** K. Hayden Webb, V. Truong, J. Hasan, Ch. Fluke, J. Russell Crawford, and P. Elena Ivanova," Roughness Parameters for Standard Description of Surface Nanoarchitecture." Scanning, Vol.(34), No. (4), pp.( 257-263), (2012).

**91-** R. Bkakri, N. Chehata , A. Ltaief ,O. Kusma , E. Rtseva , F. Kusmartsev , M. Songc , and A. Bouazizia , " Effects of the Graphene Content on the Conversion Efficiency of $P_3HT$: Graphene Based References 96 Organic Solar Cells", Journal of Physics and Chemistry of Solids, Vol.(85),pp. (206-211), (2015).

**92-** F. James Tommasini, L. da Cunha Ferreira, L. Galhardo Pimenta Tienne, V. de Oliveira Aguiar, M. Henrique Prado da Silva, L. Felipe da Mota Rocha, and M. de Fátima Vieira Marques," Poly (Methyl Methacrylate)-SiC Nanocomposites Prepared Through in Situ Polymerization", Materials Research, Vol. (21), (2018).

**93-** C. Rameshkumar, S. Sarojini, K. Naresh, and R. Subalakshmi, "Preparation and Characterization of Pristine PMMA and PVDF Thin Film Using Solution Casting Process for Optoelectronic Devices", Vol. (33), Issue (1-2), pp.(12–18), (2017).

**94-** H. T. Nguyen, T. N. Trung, T. N. Le-Thu, V.L. Thang, Q. N.Viet, A. N. Thu, and T. L. Anh,"Synthesis and Characterization of Three-Arm

Star-Shaped Conjugated Poly (3-Hexylthiophene)s: Impact of the Core Structure on Optical Properties", Polymer International Vol.(64), No. (11), pp.( 1649-1659), (2015).

**95-** Z. Lin, and M. Wei," Morphology Optimization in Ternary Organic Solar Cells", Chinese Journal of Polymer Science Vol.(35), No.(2), (2017).

**96-** L. H. Joseph, H. Ching-Chang, L. Yu-Ming, and L. Ai-Kang, "Preparation of Transparent Silica–PMMA Nanocomposite Hard Coatings." Progress in Organic Coatings, Vol.(62), No.(4), pp.(436-439), (2008).

**97-** Sh. Mohammed," Preparation of Nano-Thin Films of ZnO by Sol–Gel Method and Applications of Solar Cells Hetrojunction." Journal Nat. Sci. Res., Vol.(4), No.(1), pp.( 98-106), (2014).

**98-** F. A. Tuma," The Optical Constants of Poly Methyl Methacrylate PMMA Polymer Doped by Alizarin Red Dye", Am. Int. J. Res. Form. Appl. Nat. Sci, Vol.(16), pp.(13-18), (2016).

**99-** E. Rouaramadan, and A.A. Hasan," Study of the Optical Constants of the PVC/PMMA Blends", International Journal of Application or Innovation in Engineering and Management (IJAIEM),Vol.(2), Issue (11), pp.(240-5), (2013).

**100-** T. K. Ziad, H. A. Muhammad, H. S. Mustafa," Study of Optical Properties of (PMMA) Doped by Methyl Red and Methyl Blue Films", Iraqi Journal of Physics (IJP), Vol.(12), No(24), pp.(47-51), (2014).

**101-** M. Khairy, N. H. Amin, and R. Kamal," Optical and Kinetics of Thermal Decomposition of PMMA/ZnO Nanocomposites", Journal of Thermal Analysis and Calorimetry, Vol.(128), No. (3), PP. (1811-1824), (2017).

**102-** H. Hakim, A. Hashim, S. Sabah, and N. Mohammad," Preparation of (PMMA-$Y_2O_3$) Nanocomposites and Study their Optical

Properties", Journal of Industrial Engineering Research, Vol.(1), No.(3), (2015).

**103-** S. Agarwal, Y.K. Saraswat, and V. K. Saraswat," Study of Optical Constants of ZnO Dispersed PC/PMMA Blend Nanocomposites," Open Physics Journal, Vol.(3), No.(1), (2016).

**104-** H. M. Shanshool, M. Yahahya, W.M.M. Yunus, and I. Y. Abdullah, "Optical Properties of PMMA/ZnO Nanocomposites as Foils Prepared by Casting Method", Australian Journal of Basic and Applied Sciences, Vol.(9), pp.(401-409), (2015).

**105-** S. Tekin, A. Karatay, E. A. Yildiz, Y. O. Donar, A. Sınağ, H. Dulkadir, and A. Elmali," Tuning the Energy Bandgap and Nonlinear Absorption Coefficients of WOx/$ZrO_2$ Nanocomposite Thin Films With the Role of Weight and Doping Concentration", Journal of Luminescence, Vol.(247), No.(118869), (2022).

**106-** Z. Al-Ramadhan," Effect of Nickel Salt on Electrical Properties of Poly Methylmethacrylate", Journal of College of Education, Vol. (3),(2008).

**107-** A. Abid, A. Hashim, and A. Ali," The D.C and A.C Electrical Properties of Polymer Filled With Metal Powder", The Iraqi Journal For Mechanical and Material Engineering, Vol.(13),No.(2), (2013).

**108-** M. Dixit, V. Mathur, S. Gupta, K. Sharma," Activation energy of α- and β-relaxation process of pmma and CdS-pmma nanocomposite", Journal of Nanostructured Polymers and Nanocomposites, Vol. ( 6), No.(1), pp.(28-35), (2010).

**109-** S. Ma, S. Pang, H. Dong, X. Xie, G. Liu, P. Dong, and Y. Hao, "Stability Improvement of Perovskite Solar Cells by the Moisture-Resistant

# References

PMMA: Spiro-OMeTAD Hole Transport Layer," Polymers, Vol.(14), No.(2), p.(343), (2022).

# الخلاصـــــــة


في هذه الدراسة تم تشويب البولي مثيل ميثااكريلايت بـ (3- هكساثيوفين) بالنسب ( 2، 4 ، 6) % وتم تحضير اغشية رقيقة بواسطة تقنية الطلاء البرمي ، على قواعد من الزجاج والسليكون عند درجة حرارة الغرفة .

تم تحليل مسحوق البوليمرات (PMMA وP$_3$HT) بواسطة (FT-IR) لتحديد المجاميع الوظيفية الفعالة للروابط الكيميائية. أظهرت نتائج التحليل أن البوليمر هو PMMA و P$_3$HT وتمت مقارنة النتائج ومطابقتها للمادة الأصلية.

ظهرت نتائج حيود الأشعة السينية (XRD) أن أغشية PMMA المحضرة غير متبلورة بطبيعتها ، وأغشية PMMA: P$_3$HT المدروسة هي أغشية متعددة التبلور بطبيعتها ، ولم يؤثر التشويب على الخواص التركيبية لمادة PMMA.

كما تم فحص التشكل السطحي للأغشية الرقيقة باستخدام تقنية مجهر القوة الذرية (AFM) ، وأظهرت النتائج أن جميع الأغشية المحضرة ذات تجانس جيد وان معدل الخشونة و قيم مربع معـدل الجـذر(RMS) ومعدل الحجم الحبيبي تزداد مع زيادة التشويب بـ P$_3$HT .

تم دراسة الخصائص البصرية من خلال قياس طيف الامتصاصية كدالة للطول الموجي في مدى الاشعة الفوق بنفسجية عند الطول الموجي ( 200 – 600) نانومتر. أظهرت النتائج أن قيم الامتصاصية ومعامل الانكسار ومعامل الامتصاص للأغشية النقية والمشوبة تزداد مع زيادة نسبة التشويب ، وان فجوة الطاقة تقل مع زيادة نسبة التشويب مما يجعل المادة مناسبة لاستخدامها في تطبيقات الخلايا الشمسية.

بالإضافة إلى ذلك تم دراسة الخصائص الكهربائية والمتضمنة التوصيلية الكهربائية المستمرة. أظهرت النتائج أن التوصيلية الكهربائية تزداد مع زيادة نسبة التشويب ، وان المادة تمتلك طاقة تنشيط واحدة تقل مع زيادة نسبة التشويب .

تم تحضير المفرق الهجين ( PMMA:P$_3$HT/Si ) بتراكيز ( 0.02 ، 0.04 ، 0.06) % وكتطبيق عملي على استخدامات المادة في تصنيع خلية شمسية من أغشية المادة النقية والمشوبة. وأظهرت خصائص ( التيار – الجهد ) للخلية الشمسية بأن التشويب بـ (P$_3$HT) يزيد من كفاءة الخلية الشمسية بواسطة عرقلة اتحاد الإلكترون مع الفجوة كما أن تحسين أداء الجهاز ناتج عن تيار

الدائرة القصيرة ($I_{sc}$ ) وفولتية الدائرة المفتوحة ($V_{oc}$). وقد وجد أن أعظم كفاءة كانت عند نسبة التشويب (0.06% ) وكانت قيمتها ( 6.1%). أيضاً تمت دراسة كفاءة الخلية الشمسية مع تغير عامل الزمني لمعرفة مدى كفاءة الخلية الشمسية المحضرة. حيث تم قياس الكفاءة لمدة شهرين (نوفمبر ومارس) من عام 2021 ، 2022 لمدة عشرة أيام ، ووجد أن التغير في العامل الزمني لا يؤثر على كفاءة الخلية الشمسية المحضرة .

وزارة التعليم العالي والبحث العلمي

جامعة بابل / كلية العلوم

قسم الفيزياء

# تحضير وتوصيف أفلام PMMA - $P_3HT$ لتطبيقات الخلايـــــــــــا الشمســـــية

أطروحة مقدمة إلى

مجلس كلية العلوم في جامعة بابل

وهي جزء من متطلبات نيل درجة دكتوراه فلسفة في علوم الفيزياء

تقدمت بها

## لميـــس فائـــز ناصـــر مثنـــى

بكالوريوس علوم في الفيزياء / ٢٠٠٢

ماجستير علوم في الفيزياء / ٢٠١٦

إشراف

أ. د. محمد هادي شنين

١٤٤٤ هـ

٢٠٢٢ م